Exploration, modelling and management of groundwater-dependent ecosystems in karst – the Sian Ka'an case study, Yucatan, Mexico

Gondwe, Bibi Ruth Neuman

Publication date:
2010

Document Version
Publisher's PDF, also known as Version of record

Technical University of Denmark

Exploration, modelling and management of groundwater-dependent ecosystems in karst

– the Sian Ka'an case study, Yucatan, Mexico

Bibi R. N. Gondwe

DTU Environment
Department of Environmental Engineering

PhD Thesis
March 2010

Exploration, modelling and management of groundwater-dependent ecosystems in karst

– the Sian Ka'an case study, Yucatan, Mexico

Bibi R. N. Gondwe

PhD Thesis
March 2010

DTU Environment
Department of Environmental Engineering
Technical University of Denmark

Bibi R. N. Gondwe

Exploration, modelling and management of groundwater-dependent ecosystems in karst
– the Sian Ka'an case study, Yucatan, Mexico

PhD Thesis, March 2010

The thesis will be available as a pdf-file for downloading from the homepage of the department: www.env.dtu.dk

Address:	DTU Environment Department of Environmental Engineering Technical University of Denmark Miljoevej, building 113 DK-2800 Kgs. Lyngby Denmark
Phone reception:	+45 4525 1600
Phone library:	+45 4525 1610
Fax:	+45 4593 2850
Homepage:	http://www.env.dtu.dk
E-mail:	reception@env.dtu.dk

Printed by:	Vester Kopi Virum, March 2010
Cover:	Torben Dolin
ISBN:	978-87-91855-86-3

Preface

This PhD thesis is based on research undertaken from November 2006 to February 2010 at the Department of Environmental Engineering, Technical University of Denmark (DTU). The work was carried out under the supervision of Associate Professor Peter Bauer-Gottwein. Associate Professor Esben Auken, Department of Earth Sciences, Aarhus University, was co-supervisor. The work was primarily funded by DTU.

The research was primarily carried out at DTU, but included two field trips to the study area in Mexico (Feb–Apr 2007, Jan–Mar 2008), a short external stay at Geological Survey of Austria (Nov–Dec 2007) and a longer research stay at Rosenstiel School of Marine and Atmospheric Sciences, University of Miami, Florida, USA (Mar–Jun 2008).

The content of this thesis is based on five scientific journal papers. At the time of writing, two have been published:

I Gondwe, B.R.N., Hong, S.-H., Wdowinski, S., Bauer-Gottwein, P. (2010). Hydrologic dynamics of the ground-water-dependent Sian Ka'an wetlands, Mexico, derived from InSAR and SAR data. Wetlands 30 (1), 1–13. doi: 10.1007/s13157-009-0016-z.

II Supper, R., Motschka, K., Ahl, A., Bauer-Gottwein, P., Gondwe, B., Alonso, G.M., Romer, A., Ottowitz, D., Kinzelbach, W. (2009). Spatial mapping of submerged cave systems by means of airborne electromagnetics: an emerging technology to support protection of endangered karst aquifers. Near Surface Geophysics 7 (5–6), 613–327.

III Gondwe, B.R.N., Ottowitz, D., Supper, R., Motschka, K., Merediz-Alonso, G., Bauer-Gottwein, P. (submitted). Exploring regional-scale preferential flow paths in the karst aquifer of Southern Quintana Roo, Mexico. Manuscript submitted.

IV Gondwe, B.R.N., Lerer, S., Stisen, S., Marín, L., Rebolledo-Vieyra, M., Merediz-Alonso, G., Bauer-Gottwein, P. (in review). Hydrogeology of the south-eastern Yucatan Peninsula: New insights from water level measurements, geochemistry, geophysics and remote sensing. Manuscript submitted.

V Gondwe, B.R.N., Merediz-Alonso, G., Bauer-Gottwein, P. (submitted). The influence of conceptual model uncertainty on management decisions for a groundwater-dependent ecosystem in karst. Manuscript submitted.

In the thesis, these papers are referred to by author names and Roman numbers. Please note that the papers are not included in this web-version but may be obtained from the library at Department of Environmental Engineering, DTU, Miljoevej, Building 113, DK-2800 Kgs. Lyngby, Denmark, library@env.dtu.dk.

A technical note is included as an appendix, displaying maps and coordinates of field data points.

Additionally, the following publications, related to the topic of the thesis, have been co-authored during the PhD-study, but are not included in the thesis:

Bauer-Gottwein, P., Gondwe, B.N., Christiansen, L., Herckenrath, D., Kgotlhang, L., Zimmermann, S. (2010). Hydrogeophysical exploration of three-dimensional salinity anomalies with the time-domain electromagnetic method (TDEM). Journal of Hydrology 380 (3–4), 318–329. doi: 10.1016/j.jhydrol.2009.11.007.

Gondwe, B.N., Bauer-Gottwein, P., Merediz-Alonso, G., Fregoso, A., Supper, R. (2010). Groundwater resources management in Quintana Roo, Mexico: Problems, scientific tools and policy. In: Friedman, M.J. (Ed.): Global water issues. U.S. Department of State, Bureau of International Information Programs. In press.

Kgs. Lyngby, February 2010
Bibi Ruth Neuman Gondwe

Acknowledgements

First of all, I would like to extend a warm thank you to my supervisor, Peter Bauer-Gottwein. You have been an inspiring supervisor, always willing and ready to help, guide and discuss, and full of contagious enthusiasm and motivation.

I also owe a great thank you to Amigos de Sian Ka'an, for introducing me to this exciting topic and for a good cooperation throughout.

The field work could not have been possible without the extensive help, personnel- and equipment-wise, from Amigos de Sian Ka'an, especially Gonzalo, Miriam, Alejandra, Luis, Basilio, Valdemar and Albert; from Luis Marin and students from UNAM – Pépé, Gabriela, Alexander, José Antonio and Mario B. , and from Judith Morales. CICY-CEA staff, particularly Mario Rebolledo, is gratefully acknowledged for use of equipment and for chemical analyses. Global Vision International is kindly acknowledged for lodging in Tulum. I furthermore greatly appreciate the field work and project work carried out by the DTU M.Sc. students Chiara, Sara and Guillaume.

I thank Shimon Wdowinski and Sang-Hoon Hong from RSMAS/MGG, University of Miami, as well as Robert Supper, David Ottowitz and the rest of the staff from the Geophysics Department of Geological Survey of Austria for the cooperation on the work reported in three of the papers. I also thank Esben Auken and staff at Department of Earth Sciences, University of Aarhus, and Yusen Ley-Cooper, now Geoscience Australia, for help and discussions on ground-based and airborne EM data.

I am grateful to Jim Coke, Quintana Roo Speleological Survey, and Grupo de Exploracion Ox Bel Ha for permission to use cave maps. The principal explorers of the Ox Bel Ha system: B. Birnbach, S. Bogaerts, F. Devos, C. Le Maillot, S. Meacham, B. Philips, S. Richards, D. Riordan, S. Schnittger, G. Walten and K. Walten, and the principal explorers of the Sac Actun system: S. Bogaerts, K. Davidson, D. Jones, B. Phillips and R. Schmittner are gratefully acknowledged.

CONAGUA, especially Ing. José Luis Acosta, Ing. Iván Gamboa and Ing. Sergio Peña, are acknowledged for access to borehole and climate data. CAPA, especially Ing. Angel Huape and Ing. Dionné Rivas, are acknowledged for access to water supply wells and chemical data sets. I thank well operators, private ranch owners, subdelegados, commisariados ejidal, and private well owners for granting us access to sample water, measure water levels and log in wells. CONANP staff is acknowledged for reading surface water gauges inside Sian Ka'an.

I thank Sinh Hy Nguyen and Jens Schaarup Sørensen for lab analyses of water samples, and Centre for Ice and Climate, Niels Bohr Institute, University of Copenhagen, for oxygen isotope analyses. I appreciate the help with figures and printing of the thesis from Lisbet Brusendorff and Torben Dolin.

Funding from WWF Verdensnaturfonden/Aase & Ejnar Danielsens Fond 2006 and 2007, the COWIfoundation, Amigos de Sian Ka'an, the Austrian Science Fund (project L524-N10 'XPLORE'), The Nature Conservancy, UNESCO, Geological Survey of Austria, ETH Zürich, Otto Mønsted's foundation and the NASA Cooperative Agreement No. NNX08BA43A (WaterSCAPES: Science of Coupled Aquatic Processes in Ecosystems from Space) is gratefully acknowledged.

My family, both in Denmark, USA, Mexico, Botswana, Malawi and Israel, has been wonderful. A special thank you to my parents, Inger and Ouri, for your constant support, encouragement and love. Thanks to my colleagues at DTU and to my friends for fun times and good chats.

Most especially, a huge and warm thank you to my husband, Tiyezge. You turn difficult days in to fun ones, and make happy days even happier. Also thanks to our li'l "+" for kicks of encouragement.

Abstract

Sian Ka'an is a nature reserve of international importance, located on one of the world's largest and most spectacular karst aquifers – the Yucatan Peninsula in Mexico. The vast wetlands in Sian Ka'an are fed by groundwater from the aquifer through both submerged caves and diffuse flow from the rock matrix. Groundwater-dependent ecosystems (GDEs) are increasingly the focus of environmental protection efforts worldwide. GDEs in karst, such as Sian Ka'an, are particularly sensitive and susceptible to pollution, because of fast water flow and pollution transport in karst. Stress on the quality and quantity of groundwater resources is increasing on the Yucatan Peninsula, making Sian Ka'an's wetlands vulnerable. Ensuring water for both the wetlands and human use has attracted regional and international attention. The Sian Ka'an wetlands and their catchment serve as the case study of this PhD study. With the ultimate aim of improving the management of the groundwater resources feeding the wetlands the following objectives were outlined:

1. To physically characterize the data-scarce groundwater catchment area of the Sian Ka'an wetlands
2. To develop conceptual hydrogeological models for the study area, based on the collected data
3. To develop numerical hydrological models of the groundwater catchment. The models should produce results relevant for groundwater and ecosystem management in the region

A multi-disciplinary approach working on scales from local to regional was applied to address the objectives. The approach is applicable to other catchment-scale studies of data-scarce karst regions.

The dynamics of Sian Ka'an's surface water wetlands were investigated using the backscattered amplitude of remotely sensed synthetic aperture radar (SAR) data, and interferometric processing of the SAR data (InSAR). Wetland extent ranged from 1067 km^2 in the dry season to 2588 km^2 at the end of the wet season. The flooding extent variations correlated with a 3-month backward moving average of the catchment precipitation. This highlighted the connection of the

wetlands to a much larger groundwater catchment. InSAR was used for determination of surface water flow directions and surface water divides in the extensive and complex wetlands. The usefulness of SAR and InSAR techniques for multi-purpose hydrodynamic investigations of vast data-scarce wetlands was documented.

Recharge was estimated to be ~17% of mean annual precipitation in the conjectural groundwater catchment, using remotely sensed thermal infrared imagery and vegetation indices. Aquifer salinity stratification was investigated using the time-domain electromagnetic method. The regional freshwater lens was found to be well described at the regional scale using the Dupuit-Ghyben-Herzberg principle. Inland the freshwater lens was up to 100 m thick.

On a local scale karstic caves were mapped using airborne electromagnetic (EM) measurements, and verified using cave maps produced by scuba divers. For the regional-scale, potential high-permeability zones were outlined using visual inspection of optical and near-infrared satellite imagery. In one case, exploration of the outlined structures with airborne EM confirmed a higher electrical conductivity within the structure compared to outside it. The structure is therefore likely a zone of higher permeability. The nature of the remaining structures could not be characterized using airborne EM, because of a shallow, highly conductive geological layer preventing deep penetration of the EM signals. Using airborne and borehole EM this layer, 200–800 mS/m and 3–8 m thick, was found to be present relatively close to the ground surface within the hilly inland areas, but apparently absent in surface-near sediments of the flat areas nearer to the coast. The high-conductive layer may locally be responsible for perched aquifers, seasonally inundated areas and ephemeral surface water runoff.

The nature of the regional structures was further investigated using inverse hydrological modelling. Hydrological models based on seven different conceptual models were developed and automatically calibrated. Models showed that model fit improved when structures were assigned a different hydraulic conductivity (K) than the bulk matrix. $K_{structures}$ was calibrated to be 1–2 orders of magnitude larger than K_{matrix}. However, a model with a lower coastal resistance assigned to the coastline north of Sian Ka'an than to the remaining coastline, and

with little difference between K_{matrix} and $K_{structures}$, gave an equally good fit to data, and could also be plausible.

Monte Carlo simulations based on the different plausible conceptual models illustrated the effect of model structure error on management decisions and gave first-order estimates of travel time zone distributions. The modelling highlighted that future research efforts should focus on determining the nature of the regional inland structures and on quantifying groundwater travel times within matrix and caves. The results of the case study are useful for land use zonation within the catchment of Sian Ka'an to protect groundwater resources. Restriction of polluting activities above highly permeable zones and critical recharge areas may be valuable tools in management. Vulnerability mapping, based on the results of this research, could provide a further way forward to ensure groundwater of good quality for both human beings and ecosystems in the region.

Sammenfatning

Sian Ka'an er et naturreservat af enestående international betydning, beliggende på en af verdens største og mest spektakulære karst-akviferer – Yucatan-halvøen i Mexico. Grundvand fra akviferen tilfører vand til Sian Ka'an's vidstrakte vådområder via både vandfyldte underjordiske huler og diffus tilstrømning fra akviferens bjergartsmatrix. Grundvandsafhængige økosystemer (GDE'er) er i stigende grad fokus for miljøbeskyttelsesindsatser verden over. GDE'er i karst, som f.eks. Sian Ka'an, er særligt følsomme og påvirkelige overfor forurening, fordi vand og forureninger transporteres hurtigt igennem karst-geologi. På Yucatan-halvøen er grundvandskvaliteten og -kvantiteten i stigende grad udsat for belastninger, hvilket gør Sian Ka'ans vådområder sårbare. At sikre vand både til vådområderne og til forbrug har fået regional og international bevågenhed. Sian Ka'ans vådområder og deres opland er valgt som case i nærværende PhD-studium. De følgende formål blev opstillet, med det ultimative mål for øje at forbedre forvaltningen af de grundvandsressourcer, der tilfører vand til vådområderne:

1. Fysisk at karakterisere Sian Ka'ans vådområders data-fattige grundvandsopland
2. At udvikle konceptuelle hydrogeologiske modeller for området, baseret på de indsamlede data
3. At udvikle numeriske hydrologiske modeller af grundvandsoplandet. Modellerne skal producere resultater, der er relevante for grundvands- og økosystemforvaltning i regionen

En multi-disciplinær tilgang, arbejdende på lokale til regionale skalaer, blev brugt til at adressere formålene. Denne tilgang er relevant også for andre studier på oplandsskala af data-fattige karst-regioner.

Dynamikken i Sian Ka'ans vådområder blev undersøgt vha. backscattered amplitude af satellit-bårne synthetic aperture radar (SAR) data samt interferometrisk processering af SAR-data (InSAR). Udstrækningen af vådområderne varierede fra 1067 km^2 i den tørre sæson til 2588 km^2 i slutningen af regnsæsonen. Variationerne i oversvømmelsernes udbredelse var korrelerede

med et 3-måneders bagud-rettet glidende gennemsnit af nedbøren i oplandet. Dette fremhævede forbindelsen mellem vådområderne, og et meget større grundvandsopland. InSAR blev brugt til at bestemme flow-retninger for overfladevand samt overfladevandsskel i de udstrakte og komplekse vådområder. Således blev nytteværdien af SAR- og InSAR-teknikker til hydrodynamiske undersøgelser af vidstrakte og data-fattige vådområder demonstreret.

Grundvandsdannelse blev estimeret til at være ~17% af gennemsnitlig årlig nedbør i det midlertidige grundvandsopland, ved brug af termisk infrarøde data fra satellit-bårne sensorer, samt vegetations-index fra samme. Salinitetslagdeling i akviferen blev undersøgt ved brug af den transiente elektromagnetiske geofysiske metode. Den regionale ferskvandslinse blev fundet godt beskrevet ved brug af Dupuit-Ghyben-Herzberg-princippet. Inde i landet var ferskvandslinsen op til 100 m tyk.

På lokal skala blev karst-hulerne kortlagt ved brug af luftbårne elektromagnetiske (EM) målinger, og blev verificeret ved brug af kort over huler produceret af dykkere. På regional skala blev potentielle høj-permeable zoner afgrænset via visuel inspektion af optiske og nær-infrarøde satellitbilleder. I et tilfælde bekræftede luftbårne EM-målinger, at der var en højere elektrisk ledningsevne over en af de afgrænsede strukturer, sammenlignet med udenfor strukturen. Strukturen er derfor sandsynligvis en zone med højere permeabilitet. De resterende strukturers karakter kunne ikke bestemmes vha. luftbåren EM, idet et overfladenært, højt-ledende geologisk lag forhindrede dybere indtrængning af EM-signalerne. Ved brug af luftbåren og borehuls-EM blev dette lag, 200–800 mS/m og 3–8 m tykt, fundet til stede i de bakkede områder inde i landet, relativt tæt på jordens overflade, men var tilsyneladende ikke til stede i overfladenære sedimenter i de kystnære flade områder. Det højt-ledende lag kan lokalt være årsagen til hængende grundvandsspejl, sæsonbetingede oversvømmede områder og efemeral afstrømning.

De regionale strukturers karakter blev yderligere undersøgt ved brug af invers hydrologisk modellering. Hydrologiske modeller baseret på syv forskellige konceptuelle modeller blev udviklet og automatisk kalibreret. Modellerne viste at model-fittet blev forbedret, når strukturerne blev tildelt en anden hydraulisk ledningsevne (K) end bulk matrix. $K_{strukturer}$ blev kalibreret til at være 1–2 størrelsesordner over K_{matrix}. En model med en lavere modstand mod outflow ved

kysten nord for Sian Ka'an end langs resten af kysten, og med begrænset forskel mellem K_{matrix} og $K_{strukturer}$ kunne dog give et lige så godt fit til data, og var derfor også sandsynlig.

Monte Carlo-simuleringer baseret på de forskellige sandsynlige konceptuelle modeller illustrerede indflydelsen af strukturelle fejl i modellerne på forvaltningsbeslutninger, og gav førsteordensestimater for udbredelsen af zoner med forskellige grundvandstransporttider til Sian Ka'an. Modelleringen fremhævede, at en fremtidig forskningsindsats bør fokusere på at fastslå karakteren af de regionale strukturer inde i landet, og på at kvantificere grundvandstransporttider i matrix og huler. Resultaterne af case-studiet er anvendelige i forbindelse med zonering af land i Sian Ka'ans opland for at beskytte grundvandsressourcerne. Indskrænkning af forurenende aktiviteter oven over høj-permeable zoner og kritiske grundvandsdannende områder kan være vigtige forvaltningsmæssige værktøjer. Sårbarhedskortlægning, baseret på resultaterne af nærværende forskning, kan være en yderligere vej fremad for at sikre grundvand af god kvalitet for både mennesker og økosystemer i regionen.

Table of contents

1 Introduction

1.1 Background and motivation

Groundwater and surface water can be viewed as one continuous water resource, given the high degree of interaction most often observed between these two categories of water. Groundwater consequently provides water for many wetlands, which commonly have a rich biodiversity and a high productivity. Worldwide, protection of groundwater-dependent ecosystems (GDEs) is receiving increasing focus, in recognition of their global and regional value (Eamus and Froend, 2006; Münch and Conrad, 2007; Krause et al., 2007; Rodríguez-Rodríguez et al., 2008). The need to ensure water both for human use and for ecosystems is becoming a priority within water management (e.g. Young et al., 2000; Acreman and Dunbar, 2004; Powell et al., 2008; Hinsby et al., 2008).

GDEs in karst are highly vulnerable. Karst aquifers are characterized by caves, sinkholes and other geological heterogeneities created by dissolution of the parent carbonate or evaporitic rock. Worldwide an estimated 20–25% of the population largely depends on groundwater from karst aquifers (Ford and Williams, 2007). However, karst water resources are highly susceptible and sensitive to pollution. Groundwater and contaminants are transported fast through these aquifers, and little filtration or retention of contaminants takes place in karst. Caves account for the majority of karst groundwater flow. In a section of the aquifer in the Caribbean Yucatan 99.7% of all groundwater flow was found to take place in caves (Worthington et al., 2000). Knowledge about the location and properties of submerged caves is therefore essential to understand groundwater flow in karst. However, it is a challenge to obtain data on the location and properties of the underground caves, particularly at the catchment scale on which many water management initiatives must be carried out.

Karst wetlands exist in many regions of the world, including Australia, Bulgaria, Ireland, Mexico, Slovenia and USA. The catchment of the Sian Ka'an Biosphere Reserve on the Yucatan Peninsula in Mexico provides an excellent case for

studying the regional scale water management problematic of protecting GDEs in karst. Fed by one of the world's largest karst aquifers, the wetlands of Sian Ka'an take up approximately ⅓ of the total 5280 km^2 area of the Reserve. They consist of a mosaic of freshwater sloughs, channels, floodplains, marshes and brackish tidally influenced areas (Fig. 1). Inflow of groundwater takes place through both underground cave systems and rock matrix, and is not directly observable. Sian Ka'an is one of Mexico's largest protected areas and is regionally and internationally valued. It hosts a rich biodiversity with both endemic and endangered species (Pozo de la Tijera and Escobedo Cabrera, 1999; Lopez-Ornat and Ramo, 1992). Besides the wetlands, tropical forests and part of the world's second largest coral reef system also constitute important ecosystem types within Sian Ka'an. Through the Ramsar Convention Sian Ka'an has been recognized as a 'Wetland of International Importance', and the Reserve has been designated a World Heritage site by UNESCO (www.ramsar.org; http://whc.unesco.org/en/list).

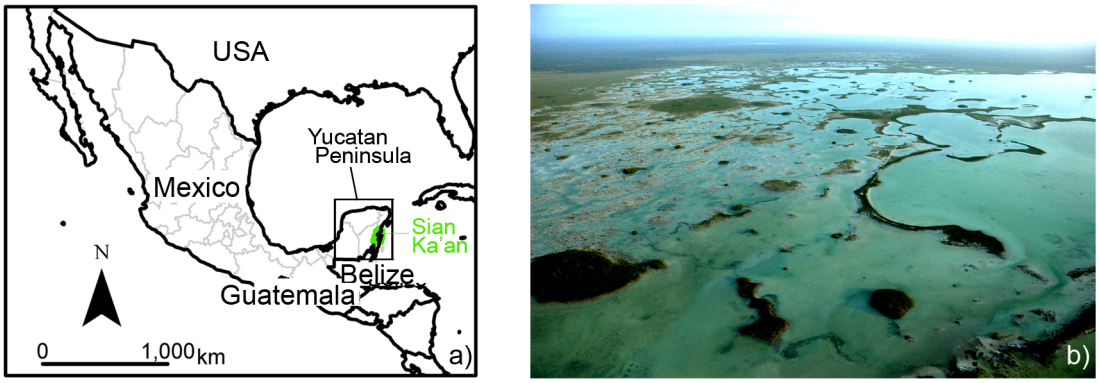

Fig. 1. a) Location of the Yucatan Peninsula and Sian Ka'an. In Fig. 10 an enlarged map of the Peninsula may be found. b) A brackish-water lagoon in Sian Ka'an with the vast vegetated wetlands stretching out behind it. Photo: Robert Supper.

Throughout the Peninsula, groundwater demands and groundwater pollution problems are growing. In northwestern Yucatan Peninsula and along the eastern coast, significant and rapid increases in population and water demands are taking place, partly due to an increasing tourism industry in the east (Escolero et al., 2000; Fideicomiso, 2006) (Fig. 2). Groundwater pollution in Yucatan State has been documented by Marin et al. (2000) and Pacheco et al. (2001). Wastewater on the Peninsula is often not treated, and is typically disposed into the Peninsular aquifer, e.g. through infiltration from septic tanks and direct injection into the saturated zone (ASK, 2003; Marin et al., 2000; Krekeler et al., 2007; Beddows,

2002; Beddows et al., 2007) (Fig. 3). Furthermore, agricultural activities are intensifying in the state of Quintana Roo (Mazzotti et al., 2005), potentially increasing the risk of groundwater contamination from agrichemicals. An illustration of the profound impact groundwater pollution may have in the region is seen in Merida, Yucatan State, where the upper 15 m of the 60 m thick freshwater lens have been rendered unfit for human consumption (Marin et al., 2000).

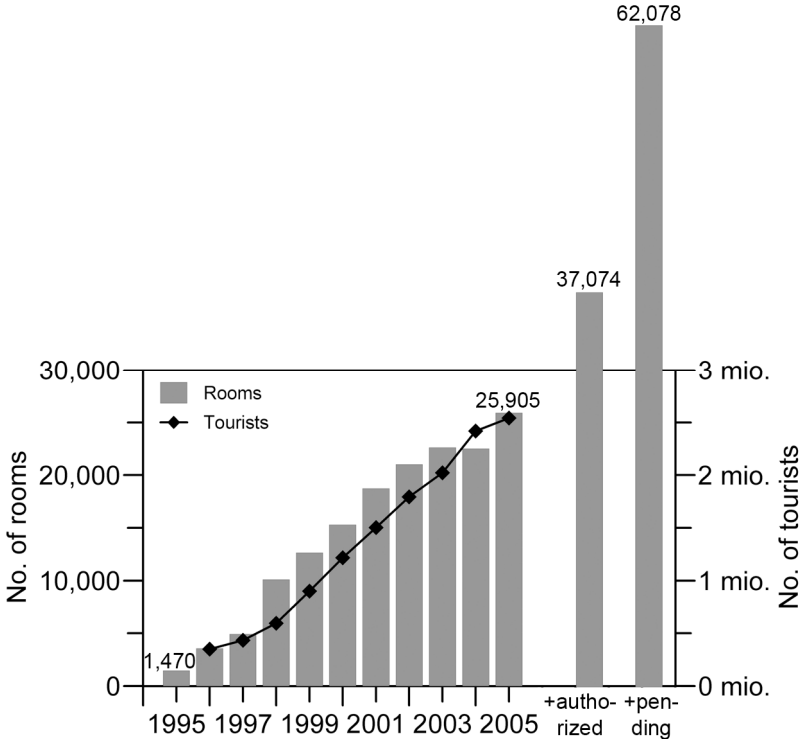

Fig. 2. Increase in number of hotel rooms and number of tourists from 1995 to 2005 in the Riviera Maya. Number of hotel rooms authorized, but not built, as well as number of rooms pending permission in 2003 is added to the last two columns. Sources: Fideicomiso (2006) and SEDUMA (2003).

Since 2003, regional stakeholders including non-governmental organizations (NGOs), research institutions, and governmental authorities for environment and water management have joined together in workshops and symposia to bring attention to and discuss how water management in the region can be improved (ASK, 2003; Holliday et al., 2007; Bautista et al., 2009). A basic prerequisite identified is the lack of knowledge on the area's hydrogeology and groundwater flow patterns (ASK, 2003). Previous research on the Peninsula hydrogeology has primarily concentrated on the Yucatan State (Back and Hanshaw, 1970; Lesser, 1976; Hanshaw and Back, 1980; Back and Lesser, 1981; Marin, 1990; Stoessell et al., 1993; Stoessell, 1995; Marin et al., 2000; 2004; Steinich and Marin, 1996;

1997; Perry et al., 1989; 1995; Escolero et al., 2000; 2002; Gonzalez-Herrera et al., 2002), whereas the eastern coast has received less attention. Primarily the regions north of Sian Ka'an have previously been studied (Back et al., 1986; Moore et al., 1992; Thomas, 1999; Beddows, 2003; 2004; Beddows et al. 2007; Stoessell et al., 1989; 2002). Perry et al. (2002; 2009) studied the Peninsula-wide hydrogeochemistry, but with relatively moderate contributions from the area west and south of Sian Ka'an. Thus, the need for scientific data to enable protection of the groundwater resources in the catchment of Sian Ka'an is clear (Merediz Alonso, 2007).

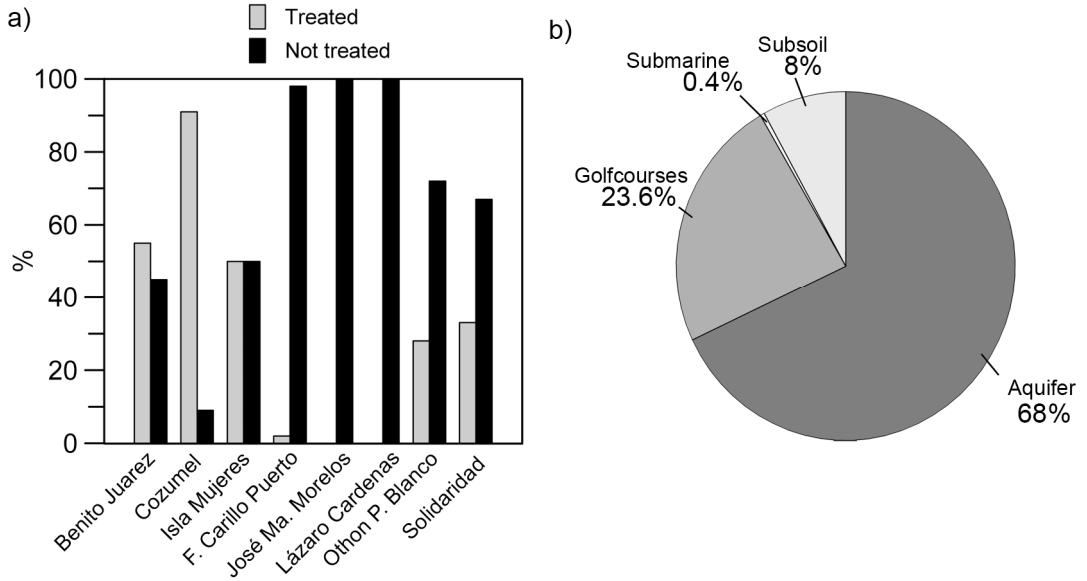

Fig. 3. a) Percentage of treated and untreated wastewater in the municipalities within the state of Quintana Roo. The municipalities Benito Juarez, Cozumel and Isla Mujeres lie outside the study area defined in Chapter 3. b) Recipient bodies of treated and untreated wastewater in Quintana Roo. In the municipalities of the study area 100% is lead into the aquifer. Source: Data from CONAGUA, distributed in ASK (2003).

1.2 Objectives and outline

To study the regional-scale hydrology of the study area, the following objectives were defined:

1. To physically characterize the conjectural groundwater catchment area of Sian Ka'an using data collected through field work and by remote sensors, on a local to regional scale – i.e. from individual cave systems, over the

whole wetland areas to the tentative groundwater catchment (Paper I, II, III, IV)
2. On the basis of the collected data to develop conceptual hydrogeological models for the study area (Paper IV, V)
3. To develop numerical hydrological models to describe the physical system with the aim of producing results relevant for groundwater and ecosystem management in the region (Paper V)

This thesis is based on the results from the five papers. First, a chapter is given on three main methodologies used in the research – synthetic aperture radar techniques, electromagnetic geophysics and numerical hydrological modelling. Subsequently an overall chapter on the study area follows. Main results from using each of the three main methodologies are then presented. The section on numerical hydrological modelling takes its point of departure in the findings from the previous sections. It utilizes the results from the site characterization in the model definition, calibration and validation. Thus, the hydrological modelling section, and Paper V, ties together the findings of the previous chapters, and elaborates upon them. In conclusion, perspectives for groundwater management are discussed based on the findings of the research, and possible future research directions are outlined.

2 Methodologies

2.1 Radar remote sensing for wetland hydrological monitoring

Remotely sensed data is increasingly being used to analyze the hydrology of the world's water bodies, including wetlands. Techniques yield direct or indirect information about water bodies and the hydrologic cycle. They utilize the visible, thermal or microwave bands of the electromagnetic spectrum, or gravity changes registered by remote sensors (Alsdorf et al., 2007a; Tang et al. 2009). Radars are active sensors that operate in the microwave spectrum (wavelengths (λ) = 0.1–100 cm). Their hydrological applications include measurement of rainfall (e.g. Grecu and Olson, 2006), soil moisture (e.g. Zribi et al., 2009), absolute water levels in rivers and lakes via radar altimetry (e.g. Berry et al., 2005), detection of flooded/non-flooded areas, and measurement of relative water level changes in wetlands via interferometry. The last two applications are described further in this section.

2.1.1 Synthetic Aperture Radar basics

As all electromagnetic radiation, the propagation of a radar pulse in the x-direction with time, t, can be described with the following expression, describing a planar harmonic wave in a plane perpendicular to the x-direction (e.g. Telford et al., 1990):

$$\psi(x,t) = A \cdot \cos\big(\kappa(x - V \cdot t)\big) = A \cdot \cos\left(\frac{2\pi}{\lambda} x - 2\pi \cdot ft\right) \quad (1)$$

where A is the amplitude [same dimensions as ψ, e.g. V/m for electric field strength or Tesla for magnetic induction], $\kappa/2\pi$ is the wave number i.e. number of wavelengths pr. unit length [1/m], V is the speed by which the wave travels (=speed of light for electromagnetic radiation) [m/s] and equals $V = f \cdot \lambda$, f is the frequency [1/s] and λ is the wavelength [m]. The term in the bracket of Eq.1 is known as the phase (φ), and describes the variation in angle of the wave with time and distance. The oscillations of the wave may be horizontally (H), vertically (V) (Fig. 4a) or circularly polarized. In radar detection, an antenna alternately transmits and receives electromagnetic pulses, thus imaging the target, in many cases while the sensor is moving. For a moving sensor, an object on the

ground remains within the radar footprint at several consecutive data acquisitions, because the footprints of the different acquisition times overlap. Therefore, the same object will be imaged several times, albeit at different angles at different times. Because the sensor is moving while the waves are returned to it from objects on the ground, a shift in frequency will occur, known as the Doppler effect. Objects approaching the sensor will, from the sensors point of view, reflect a higher frequency than that sent out by the sensor, and objects receding from the sensor will reflect waves with a lower frequency than that sent out by the sensor. Synthetic Aperture Radar (SAR) is a signal processing technique that utilizes the knowledge on the Doppler frequency shift to improve imaging resolution in the direction of flight. Details on the SAR processing technique is given in e.g. Hanssen (2001). SAR processing enables the use of short antennas while obtaining high resolution in the flight direction in the order of tens of meters (Bürgmann et al., 2000). That is a practical advantage. In contrast, for real aperture radars, resolution in flight direction can only be improved by using longer antennas.

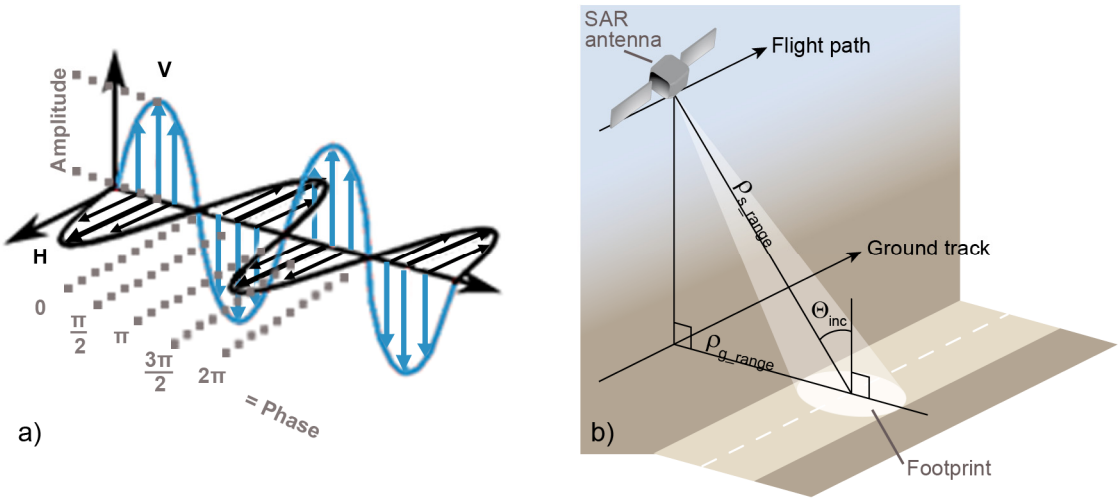

Fig. 4. a) V polarized and H polarized wave, shown in the same figure, with indications of amplitude and phase. b) Some definitions used within SAR.

SAR sensors measure the strength of the signal returned from the imaged object (amplitude, measured in decibels, dB) and the time it takes from a pulse is emitted till it is returned to the sensor (via the phase, measured in radians). Thereby, the distance from sensor to object in the sensor view direction, known

as the slant range, ρ_{s_range}, can be determined, using the following general formula (Fig. 4b):

$$\rho_{s\_range} = \frac{time\_delay \cdot c}{2} = \frac{\lambda \cdot (no.\_of\_full\_waves + phase)}{2} \quad (2)$$

where c is the velocity of light (= 299,792,458 m/s).

2.1.2 Utilizing radar backscatter for flooding extent mapping

As the radar pulse encounters other media, the wave is scattered by reflection or refraction. Through scattering some of the emitted radiation is returned to the sensor. Because scattering is determined by the dielectric constant of the surface, its roughness and its local slope, the amplitude of the signal which is backscattered to the sensor can be used to map surface properties (Ulaby et al., 1982; Topp et al., 1980, Dalton et al., 1984). Two overall types of scattering exist: surface scattering and volume scattering. The latter consist of the cumulative effect of different point scatterers. Specular scattering and double-bounce scattering (two times specular reflection) (Fig. 5) are special cases of surface scattering, and only take place when the surface is smooth compared to the wavelength of the pulse (criteria for evaluating smoothness are given in e.g. Ulaby et al., 1982). Radar imaging is independent of cloud cover because radar wavelengths are much larger than the size of the cloud droplets. Scattering by clouds is therefore minimal. Over wetlands, the radar pulses interact with the vegetation canopies, trunks/stalks and the water surface (Fig. 5). The amplitude of the signal returned to the sensor depends, among other factors, on the degree of inundation, vegetation type, canopy closure, and leaf on/leaf of condition of the vegetation (Lu and Kwoun, 2008; Borgeau-Chavez et al., 2005). Therefore the backscattered amplitude may be used to discriminate between flooded and non-flooded conditions, as well as to map vegetation and wetland types (Henderson and Lewis, 2008 and references herein). For SAR wetland imaging, typically L-band (15–30 cm), C-band (3.75–7.5 cm) and X-band (2.5–3.75 cm) wavelengths are used. Due to their different penetration capabilities, L-band radar is used to investigate flooded forests, whereas C-band radar is used to investigate herbaceous wetlands (Kasischke et al., 1997, and references herein).

SAR backscatter amplitude has been used to map flooded and non-flooded areas for more than twenty years (Hess et al., 1990). Greater classification accuracies have been found when using SAR to map flooded/non-flooded areas rather than more differentiated wetland vegetation and landcover types (Henderson and

Lewis, 2008). Over the years numerous studies have investigated the effect on flood mapping of using different wavelengths, incidence angles and polarizations (e.g. Hess et al., 1995; Kasischke et al., 1997 and references herein; Pope et al., 2001; Lang and Kasischke, 2008), the effect of using different processing algorithms (e.g. Oberstadler et al., 1997; Solbø et al., 2003; Shen et al., 2008) or the fusing of results obtained using different algorithms (Schumann et al., 2009). Most studies have focused on few instances in time, whereas investigations of multi-temporal flooding dynamics using SAR data are presently relatively limited (Henderson and Lewis, 2008; Martinez and Le Toan, 2007; Lang et al., 2008; Sass and Creed, 2008). The study of flooding dynamics in Sian Ka'an (Gondwe et al., I) is therefore one of few multi-temporal SAR flooding studies (see Chapter 4.1).

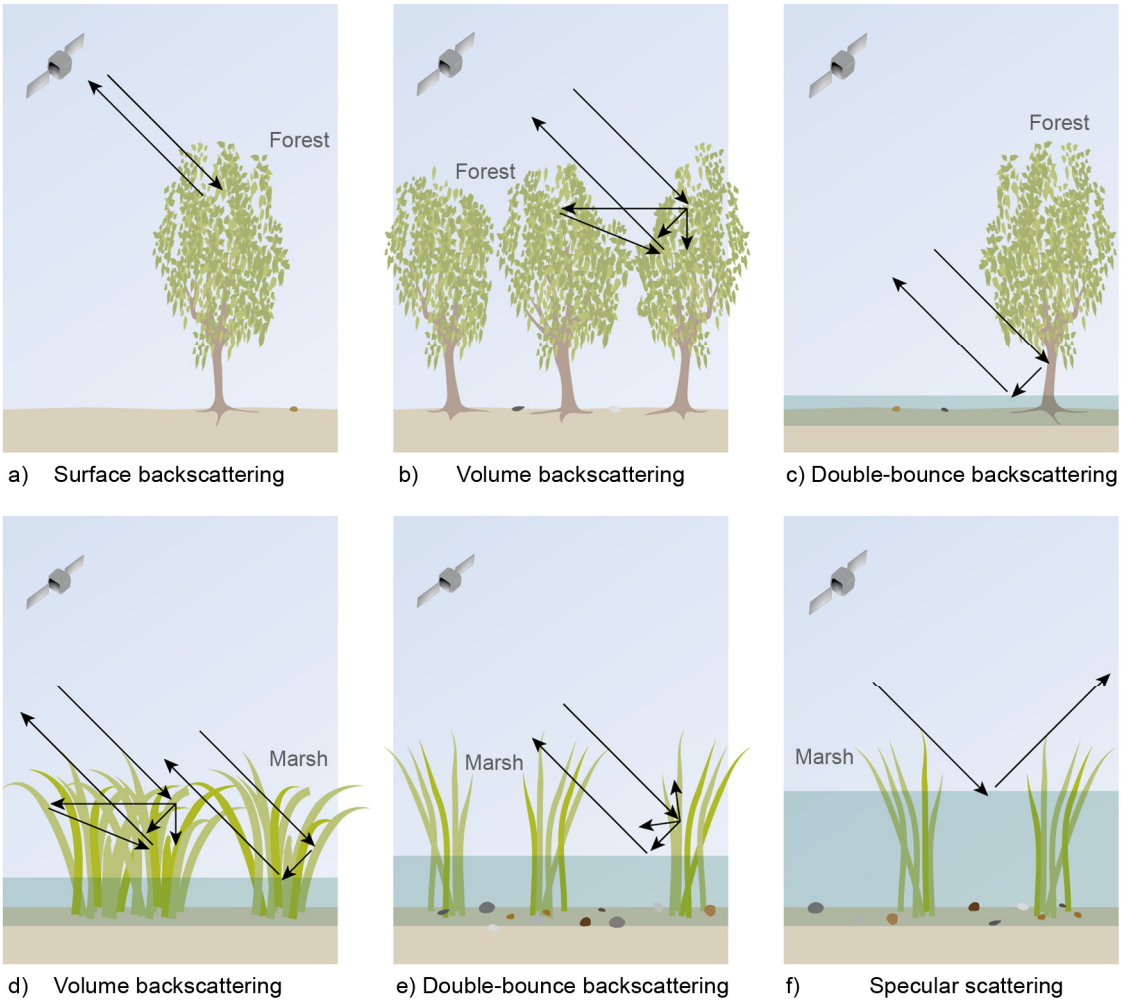

Fig. 5. Radar scattering mechanisms in different types of environments.

2.1.3 Utilizing InSAR for wetland hydrology

The measured distance from the sensor to an object is used in SAR interferometry (InSAR), through measurement of the phase of the returned signal. InSAR for derivation of glacial motion, topographic relief and topographic deformation is well established (e.g. Goldstein et al., 1993; Massonet et al., 1993; Amelung et al., 1999). In contrast, InSAR in wetlands is an emerging discipline. Primarily, wetland InSAR has been used to derive absolute water level changes. Wetland InSAR relies on double-bounce backscattering, and therefore is only useful in cases where double-bounce scattering dominates over surface- and volume scattering.

Interferometry uses measurement of the distance to an object from two (or more) different sensors at the same time or from one sensor located at approximately the same location at different instances in time (two-pass InSAR). The two (or more) images acquired are co-registered so they correspond exactly to each other, and the phases of the images (φ_1 and φ_2) are subtracted from on another, forming the so-called interferograms. An expression for the interferometric phase (ϕ_{int}) is found by first looking at the dependence of the phase on the distance travelled by the wave to the target and back again. This is expressed by $\varphi=-2\pi x/\lambda$, i.e. the distance-dependent term of the phase in Eq. 1, with a negative sign by convention (Rosen et al., 2000). The distance travelled by the wave can be expressed in terms of slant range as $x = 2\cdot\rho_{s\_range}$. An expression for the interferometric phase (ϕ_{int}) is then found by subtracting the two phases obtained at two different times (Rosen et al., 2000):

$$\phi_{\text{int}} = \varphi_1 - \varphi_2 = \frac{4\pi}{\lambda}(\rho_{s\_range,2} - \rho_{s\_range,1}) \quad (3)$$

This expression is valid for a system where each antenna alternately transmits and receives its own echoes, as in the case of two-pass InSAR. A different expression is valid for the interferometric phase obtained when one antenna transmits and two antennas receive the echoes (see Rosen et al., 2000).

The phase difference (or interferometric phase, ϕ_{int}) of a two-pass interferogram is influenced by topography, surface displacement, atmospheric effects and noise (e.g. Lu et al., 2009; Rosen et al., 2000; Massonnet and Feigl, 1998):

$$\phi_{int} = \phi_{topography} + \phi_{displacement} + \phi_{atmosphere} + \phi_{noise} \quad (4)$$

In order to obtain the surface displacement, the effect of topography is removed using a known digital elevation model. The effect of the approximately

ellipsoidal shape of the Earth is also removed, along with the effect of the slightly different position of the sensor at the different acquisition times. Phase noise may occur if the dielectric properties of the surface changes significantly between the two acquisition times. Phase noise is evaluated via the term coherence. It is the cross-correlation of images estimated within windows of a few pixels' size. Large changes in surface properties may cause decorrelation, and then differential InSAR cannot be used. The Earth's atmosphere is also an important source of phase error. In the latitudes of Sian Ka'an, presence of large amounts of water vapor (clouds) can cause delays in the radar pulse propagation, resulting in errors in the estimated distances. Mitigation of atmospheric delay errors may be carried out by using dense GPS networks (e.g. Hanssen, 2001) or high-resolution weather models (Massonnet and Feigl, 1998, Lu and Kwoun, 2008) to estimate the delay. At present the latter is rarely carried out in practice (Foster et al., 2006).

Once the other effects have been removed from the interferometric phase, the surface displacement can be evaluated. A change in surface location between the two acquisition times will appear as phase changes in interferograms. One cycle of phase change (0–2π) is called a 'fringe'. The fringes in the interferogram may then be converted from these cycles of 0–2π to continuous changes in phase; a process which is called 'unwrapping' (Fig. 6) (e.g. Goldstein et al., 1988; Ghiglia and Pritt, 1998; Chen and Zebker, 2001). Unwrapping is the process of adding an integer multiple of 2π to the fringes, because the actual change in distance measured by the sensor via the phase is in fact equal to an unknown integer number (the ambiguity) plus the phase difference. Filtering of the interferograms is often carried out before unwrapping, but was minimized in the Sian Ka'an interferogram processing, because it was found that important small-scale fringes, characteristic for these wetlands, were smoothed out by this process.

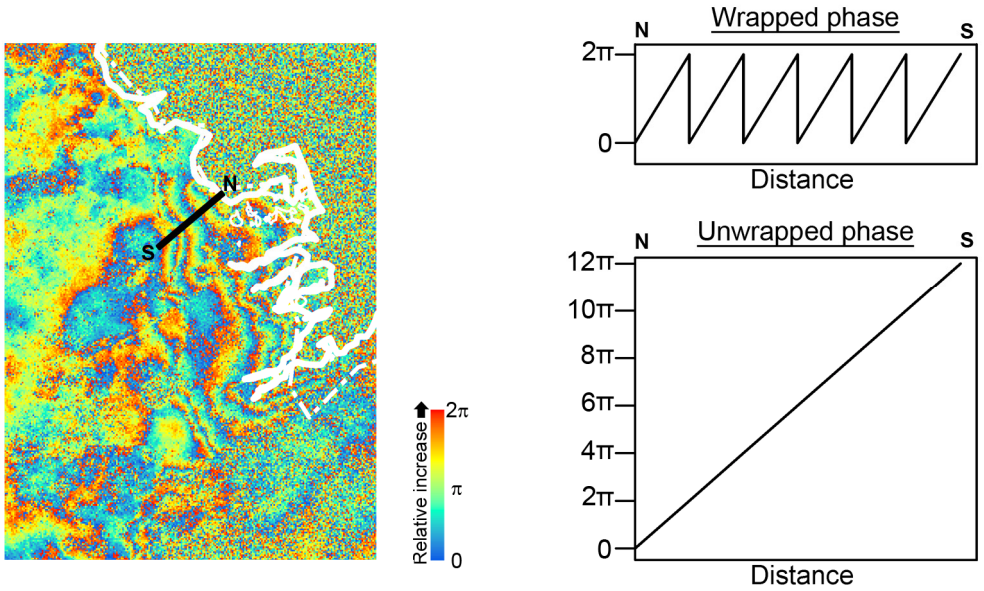

Fig. 6. Detail of interferogram over Sian Ka'an, showing principle of unwrapping.

If no other surface deformation (e.g. tectonic deformation) has taken place between acquisitions, and if only vertical movement between acquisition times is assumed, the phase change (ϕ_{int}) of the unwrapped interferograms can be recalculated to the water level change (Δh) using Eq. 3 together with the incidence angle (θ_{inc}, in radians, see Fig. 4b for definition) and the cosine relation:

$$\Delta h = \frac{\lambda \phi_{\text{int}}}{4\pi \cos(\theta_{inc})} \tag{5}$$

For the RADARSAT-1 SAR data used in the Sian Ka'an study, one phase cycle of 0–2π corresponded to 3.6 cm (FineBeam F1 data) and 3.9 cm (FineBeam F4 data) vertical displacement.

The number of previous studies using InSAR for wetlands is limited. Alsdorf et al. (2000; 2001) first described the utility of differential InSAR for mapping water level changes in wetlands, using the Amazon floodplains as a case study. Alsdorf et al. (2001) and Wdowinski et al. (2004; 2008) established that InSAR water level measurements using L-band data have an accuracy within centimeters. Lu et al. (2005) and Kim et al. (2005) were the first to show that also C-band data can be used for wetland InSAR. Previously C-band data were believed to bounce off the vegetation canopies in wetlands and therefore not provide the double-bounce backscatter necessary for the wetland InSAR

measurements. However the high coherence obtained with C-band data by Lu et al. (2005), Kim et al. (2005) and the later studies of Lu and Kwoun (2008), Kim et al. (2009) and Gondwe et al. (I) using C-band data confirmed the usefulness of C-band data for wetland InSAR. Lu et al. (2005) stated that C-band data may give higher accuracy than L-band data, due to the shorter wavelength. Accuracies using C-band data in wetland InSAR appears to be less than or equal to about 2 cm (Lu and Kwoun, 2008; Gondwe et al., I). Lu et al. (2009) and Kim et al., (2009) used radar altimetry data to convert the relative water level changes from InSAR into absolute water level changes. This is convenient for areas where gauge data are not available. It could have been a useful approach for the Sian Ka'an wetlands as well, as the installed gauges were limited in space and time; however radar altimetry of the required quality were not sufficient over Sian Ka'an to be used (Gondwe et al., I). Lu and Kwoun (2008) found that HH polarization (horizontal receive, horizontal transmit) was preferable to VV polarization for wetland InSAR, and Kim et al. (2009) found HH polarization to also be better than HV polarization. In the Sian Ka'an study, RADARSAT-1 data with HH polarization was used.

Only Alsdorf et al. (2007b) has previously used wetland InSAR to deduce hydrological information other than relative water level changes. They studied an Amazon flood plain during the passing of a flood wave, and showed that fringe directions may be used to evaluate surface water flow directions. In the Sian Ka'an study the utility of InSAR for evaluating surface water flow directions was also demonstrated, and it was found that the technique can be applied to evaluate local-scale surface water divides (Gondwe et al., I) (see Chapter 4.1).

2.2 Electromagnetic methods for exploration of karst geology

Geophysical methods measure physical properties of the geology indirectly or directly. By measuring how geophysical signals, such as electric, magnetic and electromagnetic fields, seismic waves and radioactive radiation, behave in space and time information about the properties of the subsurface can be obtained, deduced or estimated. Geophysical methods have been used throughout the second half of the 20th century for examining aquifer properties. However, in recent years there has been a new focus on the use of geophysics for hydrogeological applications (e.g. Ferré et al., 2009; Rubin and Hubbard, 2005; Auken et al., 2009; Pellerin et al., 2009). Geophysical fields or earth properties explored in geophysical surveys may occur naturally in the subsurface (i.e. be inherent or emitted passively from the ground, such as the case of natural gamma radiation, gravity fields and natural magnetic fields) or may be emitted actively from sensors, after which the earth's response to the signal is recorded. The present section describes the use of active electromagnetic induction methods for hydrogeophysical characterization, because these were the main methods used to investigate the subsurface of the study area. However, other methods reported in the literature for investigating karst geology will be briefly mentioned as well.

2.2.1 Basic concepts of electromagnetic induction methods

Electromagnetic methods can only give indirect information about hydrogeologic properties of the subsurface, specifically the electrical conductivity (σ [S/m]) or resistivity (ρ=1/σ [Ωm]) of the subsurface media. However, petrophysical relationships may be used to estimate the hydrologic properties from the geophysical parameters. An often used petrophysical relationship is Archie's Law (Archie, 1942), which relates measured formation conductivity or resistivity to formation porosity (φ_{por}[†]) and the pore fluid's conductivity or resistivity:

$$\rho = a\, \varphi_{por}^{-m} S^{n}\, \rho_w \qquad (6)$$

where a, m and n are empirical constants ($0.5 \leq a \leq 2.5$, $1.3 \leq m \leq 2.5$ and $n \approx 2$), S is the water-filled fraction of the pore space and ρ_w is the electrical resistivity of the pore-filling fluid (e.g. Telford et al., 1990). Archie's Law is valid for sediments and sedimentary rock, where the grains are non-conductive (e.g. do not contain clays or metals). When Archie's Law is valid, the electric conductivity of

[†] Subscript *por* used to differentiate this phi from that used to denote phase in the previous section.

the formation is dominated by the electrical conductivity of the pore-filling fluid. In other types of geologies the electrical conductivity of the formation may be dominated by ionic migration at the interface between soil grains and the pore fluid (details e.g. in review by Slater, 2007). Archie's Law may be used to estimate formation porosity from measured electrical conductivity or resistivity of the bulk formation. Other petrophysical relationships exist to recalculate porosity to an estimate of permeability (k) using grain size diameter (e.g. Berg, 1970; Revil and Cathles, 1999). k may then be recalculated to hydraulic conductivity (K) using the definition of K (e.g. Batu, 1998).

Maxwell's four equations govern electromagnetic phenomena. They describe the interaction between the vector functions of an electromagnetic field, namely **E**[‡]: the electrical field strength [V·s /m], **B**: the magnetic induction [Wb/m^2 or Tesla·s or V·s^2/m^2], **H**: the magnetic field intensity [A·s /m], **D**: the dielectric displacement [C·s /(m^2)] and **J**: the electric current density [A·s/m^2]. In the frequency-domain they are written as follows:

$$\nabla \times \mathbf{E} + i\omega\mathbf{B} = 0 \tag{7}$$

$$\nabla \times \mathbf{H} - i\omega\mathbf{D} = \mathbf{J} \tag{8}$$

$$\nabla \cdot \mathbf{B} = 0 \tag{9}$$

$$\nabla \cdot \mathbf{D} = \rho_{charge} \tag{10}$$

where i is the imaginary unit $\sqrt{-1}$, ω is the angular frequency [rad/s] (= $2\pi f$, where f is the frequency [1/s]). The angular frequency has the assumed time dependence $e^{-i\omega t}$. ρ_{charge} is the electric charge density [C·s /m^3][§].

The constitutive relations describe the relation between **J** and **E, D** and **E**, **B** and **H**:

$$\mathbf{J} = \sigma\mathbf{E} \tag{11}$$

$$\mathbf{D} = \varepsilon\mathbf{E} \tag{12}$$

$$\mathbf{B} = \mu_r \cdot \mu_0\mathbf{H} \tag{13}$$

[‡] Bold characters indicate that the parameter is a vector. Upper-case letters are used to represent the fields in frequency-domain; smaller-case letters to represent the fields in time-domain.

[§] Subscript *charge* used to distinguish this parameter from the ρ that indicates electrical resistivity in this section, and to distinguish this parameter from the the ρ_{s_range} used to indicate slant range in the previous section.

where ε is the dielectric permittivity [C/(Vm)], μ_0 is the magnetic permeability of free space, $\mu_0 = 4\pi \cdot 10^{-7}$ Vs/(A·m), and μ_r is the relative magnetic permeability [dimensionless]. σ, ε, and $(\mu_r \cdot \mu_0)$ are actually tensors, but σ and ε can, for applications with earth materials, be regarded as complex numbers, which are functions of the angular frequency ω. For hydrogeological applications μ_r=1 is typically a reasonable approximation and $(\mu_r \cdot \mu_0)$ is assumed a real number which is independent of frequency.

When applying the constitutive relations (Eq. 11, 12 and 13), Maxwell's inhomogeneous equations in frequency-domain can be written as (Ward and Hohmann, 1988):

$$\nabla \times \mathbf{E} + i\omega\mu_0 \cdot \mathbf{H} = -\mathbf{J}_m^S \tag{14}$$

$$\nabla \times \mathbf{H} - (\sigma + i\varepsilon\omega) \cdot \mathbf{E} = \mathbf{J}_e^S \tag{15}$$

where $\mathbf{J}_m^S$ and $\mathbf{J}_e^S$ are respectively the magnetic source current and the electric source current. In the absence of sources, the source terms are reduced to zero, and Eq. 14 and 15 become Maxwell's homogeneous equations.

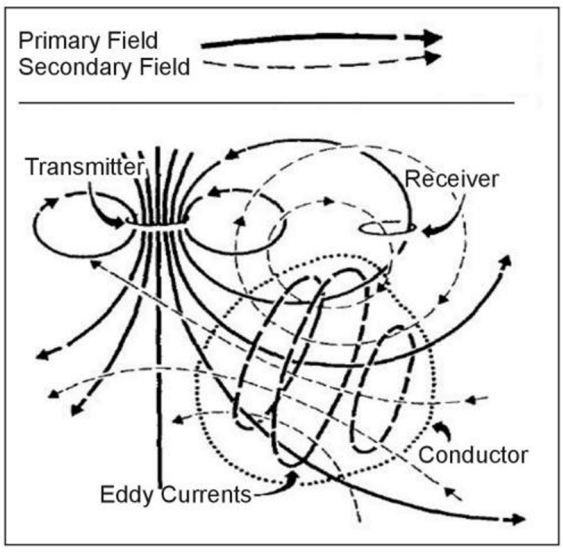

Fig. 7. Principle of EM induction methods, with generation of eddy currents in the subsurface. After Klein and Lajoie (1980), printed with permission from Northwest Mining Association.

The principle of induction is utilized in the electromagnetic methods. Ampere-Maxwell's Law (Eq. 8) explains that periodic variations in currents will generate periodically varying magnetic fields. Faraday's Law (Eq. 7) states that varying

magnetic fields will generate varying electric fields, which then again (according to Ampere-Maxwell's Law) generate varying magnetic fields. In active geophysical electromagnetic methods a time-varying magnetic field is generated by either switching off an electric current in a loop abruptly (time-domain methods) or using an alternating current in a loop (frequency-domain methods). The time-varying magnetic field generated by this process induces eddy currents in the subsurface (Fig. 7). Depending on the conductivity of the earth, the eddy currents may be larger or smaller. The response from the earth is then measured by voltage induction in receiver coils within the measurement instrumentation. In time-domain methods the response of the earth is measured in the absence of the primary field generated by the instrument transmitter. The response measured at different times after current switch-off is used to obtain information about the conductivity of the subsurface at different depths (e.g. Christiansen et al., 2006). In contrast, frequency-domain methods measure the response of the subsurface while the primary field is on. In the methods considered here, a magnetic dipole source is used, generated by an electric current oscillating at a frequency *f*. Frequencies used in EM methods are radio frequencies (e.g. 0–100 MHz; the upper range however being ground penetrating radar methods); in the present study frequencies were all below 30 kHz. The secondary field induced in the subsurface is measured compared to the strength of the primary field (as a ratio, in the unit parts per million – ppm), since the secondary field is much lower than the primary field. The primary field is calculated at the location of the receiver and compensated for in order to measure the much smaller secondary field. Due to induction processes in the subsurface, a small phase shift exists between the secondary and the primary field. The secondary field is therefore a complex number, and both the inphase and quadrature ($\frac{\pi}{2}$ radians out-of-phase with the primary field) components are recorded (e.g. Siemon, 2006). The conductivity at different depths is for frequency-domain methods measured using different frequencies. The penetration depth is controlled by the resistivity of the subsurface and by the frequency, as described in the expression for skin depth (δ), which is the depth at which the amplitude of the electromagnetic wave within the subsurface has been reduced to $\frac{1}{e}$ of the amplitude of the electromagnetic wave at the surface (Kirsch, 2006):

$$\delta = \sqrt{\frac{2\rho}{\omega\mu}} \tag{16}$$

where μ is assumed equal to the free-space value μ_0 for the earth materials discussed here.

Solutions to the EM field response (Eq. 14 and 15) may be found when the current source can be described. The equations become easier to solve if Schelkunoff potentials are introduced. Schelkunoff potentials are defined so that their differentiation yields the fields **E** and **H**. The potential **A** [V·s^2/m] is here defined as:

$$\mathbf{B} = \nabla \times \mathbf{A} \tag{17}$$

When an electric source type (denoted by subscript e) is assumed, the magnetic source current in Eq. 14 is assumed zero (Ward and Hohmann, 1988). Then, inserting Eq. 17, using the constitutive relationship of Eq. 13, and eliminating the curl operator on both sides of the equality sign, Eq. 14 becomes:

$$\mathbf{E}_e = -i\omega \cdot (\nabla \times \mathbf{A}) \tag{18}$$

Applying the quasi-static approximation that states that $\mu_0\varepsilon\omega^2 << \mu_0\sigma\omega$ for earth materials and frequencies less than 10 kHz (Ward and Hohmann, 1988), and inserting Eq. 18 into Eq. 15 yields:

$$\frac{1}{\mu_0}\nabla \times (\nabla \times \mathbf{A}) + i\sigma\omega \cdot \mathbf{A} = \mathbf{J}_e^S \tag{19}$$

which is the governing equation in frequency-domain for the propagation of EM fields expressed in terms of the vector potential **A**. In time-domain the solution is found by inverse Fourier transformation, yielding:

$$\frac{1}{\mu_0}\nabla \times (\nabla \times \mathbf{A}) + \sigma \cdot \frac{\partial \mathbf{A}}{\partial \mathrm{t}} = \mathbf{J}_e^S \tag{20}$$

These expressions are valid for heterogeneous as well as homogeneous subsurfaces. Likewise, expressions may be derived for magnetic source currents using the Schelkunoff potential **F**.

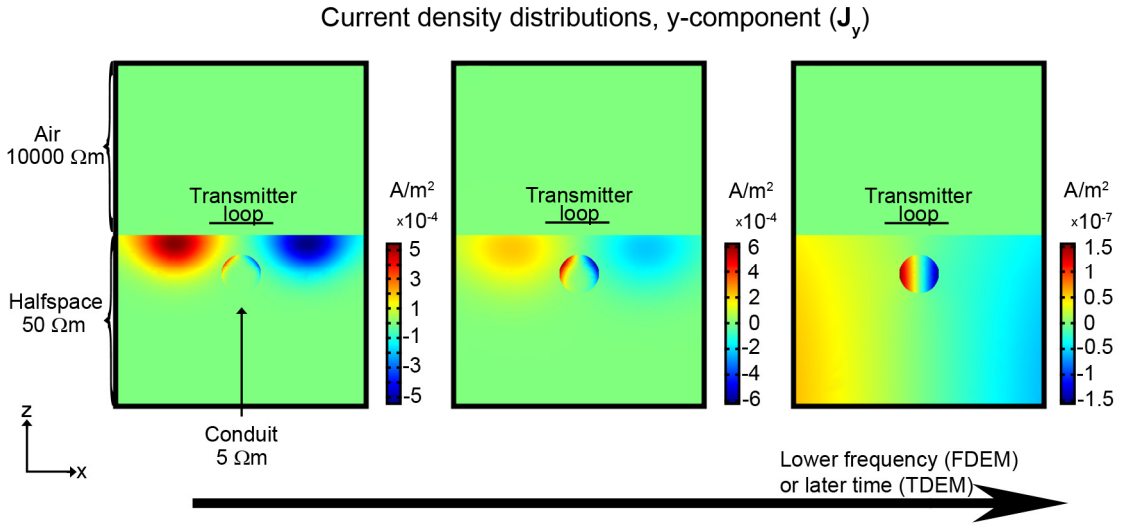

Fig. 8. Diffusion of current in halfspace with conduit, generated by simulation in COMSOL Multiphysics.

Solutions to the EM field response from the subsurface are given in Ward and Hohmann (1988) for homogeneous halfspace and layered earth (1D) configurations. Ward and Hohmann (1988) also present analytical solutions to simple geometries of anomalous 3D bodies in the ground. However, more advanced modelling of the propagation of the fields in the presence of 3D anomalous bodies requires numerical solutions. When an anomalous body exists in a layered halfspace both induction currents and galvanic currents form in the body. The latter is due to accumulation of charges at the interface between the body and the background medium. These processes are described further in West and Macnae (1991). Software exists for modelling the forward response of EM fields over a known 3D subsurface, e.g. EMIGMA (PetRos EiKon, 2003; Murray et al., 1999; Groom and Alvarez, 2002), AEM (Copyright © AKP Group 1994–1998; Pantrakov et al., 1997) and also general physical modelling software may be used to forward model EM fields in a 3D subsurface (e.g. Comsol Multiphysics; example in Bauer-Gottwein et al., 2010) (Fig. 8). Forward modelling codes are used in geophysical inversion routines, and although 1D inversion of frequency-domain EM is the most common way of interpretation (Siemon, 2006), 3D inversion methods are being developed and are the focus of recent research (for frequency-domain: e.g. Sasaki, 2001; Avdeev, 2005 and references herein; for time-domain: e.g. Newman and Commer, 2005).

Time-domain EM (TDEM) was in the present study used to map the depth to the freshwater-saltwater interface within the aquifer (Gondwe et al., IV and Chapter 3). Time-domain EM has been used for this purpose in many previous studies (e.g. Goldman et al., 1991; Kafri and Goldman, 2005; Nielsen et al., 2007). However, in the Yucatan Peninsula it had previously not been used at the regional-scale to examine the shape of the freshwater lens, as done by Gondwe et al. (IV). Christiansen et al. (2006) provide a detailed description of the technique.

Frequency-domain EM (FDEM) was in the present study used in the borehole logging carried out (Gondwe et al, IV and Chapter 3), and in the airborne EM exploration of caves and regional-scale structures described in Supper et al. (II), Gondwe et al. (III) and Chapter 4.2. Details on the technique are described in e.g. Siemon (2006) and Motschka (2001). Although the use of borehole logging as a method in this study is standard, borehole logging and airborne EM for mapping of a potential ejecta-layer (Gondwe et al., IV) had not previously been carried out at a regional scale. The successful use of the airborne frequency-domain EM technique for locating caves is unique to this study. To put the results into a context, previous work in this regard will be reviewed in detail in the following.

2.2.2 Geophysics and EM for karst cave exploration

Geophysical techniques have been applied to explore karst terrain for decades. However, detecting karst cavities (water- or air-filled) presents a particular challenge (e.g. Daniels, 1988), compared to detecting depths to karst bedrock, geological formations mapping and mapping of fault- and fracture zones with geophysical methods. Cavities in the subsurface may generate the following types of geophysical anomalies:

- Scattering of seismic and ground-penetrating radar (GPR) waves.
  For instance, acoustic velocity in water-filled cave is 1500 m/s, whereas it is 330 m/s in an air-filled cave, which is in both cases lower than what can generally be found in host rock (Daniels, 1988)
- Gravity anomalies, due to the lack of rock material at the cavity.
  For instance, a water-filled cave will have density 1 g/cm^3, an air-filled cave a density of ~0 g/cm^3, compared to the host rock density of e.g. 2.6 g/cm^3

- Nuclear magnetic resonance anomalies, caused by presence of a larger quantity of free (not surface-bound) water in a water-filled cave compared to in the surrounding aquifer matrix
- Conductivity or resistivity anomalies, caused by the fact that a water-filled cave will have a higher electrical conductivity (or lower electrical resistivity) than the surrounding aquifer matrix, due to absence of resistive rock material and presence of conductive fluid within the cave. There may thus be a significant resistivity contrast. In the case of an air-filled cave in e.g. limestone, the difference between the high resistivity of the host rock and the very high resistivity of the air may not be distinguishable, especially not with active EM methods

Seismics has a depth resolution which surpasses that of most other methods. Seismics has successfully been used to locate faulted and fractured zones in karst (e.g. Šumanovac and Weisser, 2001; Guérin et al., 2009). Combined with magnetic resonance soundings (MRS) Guérin et al. (2009) also succeeded in determining the exact location and width of karstic conduits from seismic data, with an accuracy of a few meters. They further used seismics and geoelectrics to determine that the limestone surrounding the caves was not homogeneous. However, the impact of a cave on the seismic signature may be highly variable, and efforts are undertaken to understand the effect of caves and voids on the seismic waves (e.g. Hackert and Parra, 2003). The scattering of the waves by the conduits is complex, and vugs[**] may cause a degree of attenuation that depends on the wave's frequency (Hackert and Parra, 2003). Seismics is therefore not always successful for locating karst caves. Water-filled conduits may be especially hard to detect using seismics (Guérin et al., 2009).

GPR has in many cases successfully located karst caves and been useful to determine also cave dimensions and geometry (Henson et al., 1997; Beres et al., 2001; Al-fares et al., 2002). Use of GPR requires absence of clayey layers atop the medium of interest, as the GPR signal cannot penetrate clays (Doolittle and Collins, 1998). GPR is mainly useful for detecting shallow (e.g. < 20 m below surface) air-filled caves (e.g. Beres et al., 2001; Al-fares et al., 2002) or caves filled with wet or dry sediments (e.g. Henson et al., 1997). In the Yucatan Peninsula GPR has also been carried out to detect caves. The results were ambiguous due to weak reflections which only sometimes correlated with known

[**] i.e. small cavities in the rock.

cave geometry. However, the study concluded that there was a potential for GPR to detect cave dimensions in Quintana Roo's geology (Schwaiger et al., 1997).

Microgravimetric measurements can often be used for reconnaissance of an area before applying other methods to characterize subsurface cavities (Ernstson and Kirsch, 2006). However, the method requires accurate determination of topographic elevations (accuracy < 1 cm), and therefore is not feasible on larger scales. Microgravimetry is often used in conjunction with other methods, which gives improved results. For instance, by using microgravimetric measurements, Beres et al. (2001) were able to accurately model a measured GPR signal above a cave. Mochales et al. (2008) used modelling of measured microgravimetric signals to determine the shape of a filled karstic depression, and determine its type of filling. A 3D model of a submerged cave system was constructed by McGrath et al. (2002) by modelling microgravimetric measurements, and constraining depth and position using geoelectric data and survey data from cave divers.

Magnetic resonance soundings (MRS) can be used to determine the volume of submerged caves, if the water quantity in the cave is sufficiently large to be detected, e.g. $\geq$6500 m^3 when using a 100x100 m^2 MRS loop (Legchenko et al., 2008). The cave must furthermore be relatively shallow, and EM noise in the surroundings must be low (Boucher et al., 2006). The lateral and vertical locations of water-filled conduits have successfully been located with MRS by e.g. Vouillamoz et al. (2003), Boucher et al. (2006) and Legchenko et al. (2008). The MRS signal may also be used to calculate transmissivities and permeabilities (Vouillamoz et al., 2003), and to determine the volume of the conduit with ±50% and ±75% error, depending on the size of the cave relative to the size of the MRS loop (Legchenko et al., 2008).

Geoelectrics (e.g. multielectrode resistivity tomography, DC-resistivity mapping etc.) has been used to locate both water-filled (e.g. Zhou et al., 2002; Supper et al., II) and air-filled caves (e.g. Nyquist et al., 2007). Several studies have found the dipole-dipole electrode array to be favorable for detecting caves (Zhou et al., 2002; Roth and Nyquist, 2003). The orientation of the survey line relative to the strike of the cave also influences whether the geoelectric method will detect the cave. The optimal orientation (parallel or perpendicular to strike) may depend on whether the cave or fracture is water- or air-filled (Roth et al., 2002; Roth and

Nyquist, 2003). The likelihood of detecting a cave therefore increases if multiple line orientations are used above the same target (Roth and Nyquist, 2003). The type of inversion used for data interpretation also affects the ability to resolve cave structures (Supper et al., II). Through inversion, geoelectrics may yield some information about cave depth and dimensions, but cannot with present techniques resolve these parameters in detail.

Ground-based EM methods may successfully detect the location of karst faults and caves, but have yielded little information about their depth and dimensions. With the passive EM Very Low Frequency (VLF) method, that utilizes signals from radio-transmitters worldwide, fractures have been delineated in karst (Bosch and Müller, 2005). Indirect mapping of the location of a cave has been carried out with VLF by mapping the boundary between a conductive and resistive rock unit, at which the conduit was located (Guérin and Benderitter, 1995). Coppo et al. (2006) successfully delineated an air-filled karstic cave with VLF, mainly because it was bounded by fractures.

With active ground-based FDEM methods Vogelsang (1987) successfully detected sediment- and water-filled karst faults and vertical karst pipes, believed to represent cross-sections above interconnected karst fissures. Robinson-Poteet (1989) used FDEM methods to successfully locate air-filled caves in limestone. Doolittle and Collins (1998) used FDEM methods to determine the depth to the karst bedrock, but could not detect cavities with the method in their survey environments. Shah et al. (2008) used FDEM methods in combination with geoelectrics to locate karst hydrostratigraphic contacts, faults zones and possible karst features. Supper et al. (II) used FDEM methods to detect the location of a known water-filled cave. No studies have been found in the literature of ground-based TDEM being used to locate karstic caves. This may be due to the low capabilities of the method for resolving the shallow parts of the geology (e.g. <15 m below surface). Also it may be due to the fact that the method samples a larger earth volume with time. The current in TDEM spreads outwards and downwards in time like a smoke-ring, always creating an angle of 30^{o} with horizontal (Christiansen et al., 2006). Therefore, if the current starts as an e.g. 40 m diameter ring near the surface, by the time it will be at 30 m depth, it will be a ring of ca. 100 m in diameter, thus sampling and averaging over a significantly larger earth volume. Common to the ground-based EM methods used for cave exploration are that they may indicate the location of a karst cave, but cannot

provide unambiguous data that the anomaly actually represents a cave. Furthermore, depth and dimensions of the cave cannot be resolved with ground-based EM methods.

Airborne EM methods have been gaining increasing popularity for hydrogeophysical exploration in recent years. Airborne EM methods have the advantage that a much larger area can be explored in shorter time, compared to using ground-based EM methods. Furthermore, airborne EM exploration will be unaffected by obstacles on the ground, such as dense vegetation. Using airborne EM Doll et al. (2000) detected low resistivity anomalies in known karst areas, and other anomalies which might be related to fault and fracture zones. Gamey et al. (2001) used airborne EM to interpolate spatially between anomalies detected by ground geophysics, which coincided with lineaments. Smith et al. (2003) used airborne EM to map previously unknown and known linear features likely caused by karst structures, e.g. grabens. Smith et al. (2005a) also used airborne EM to map karst structures, revealing a structural complexity of the karst subsurface which was previously unknown. Although the literature thus shows the usefulness of airborne EM for karst structural exploration, specific and confirmed detection of caves had not been carried out with airborne EM (Smith et al., 2005b). Therefore, the correspondence of airborne EM anomalies with known caves, presented by Supper et al. (II), is a novel exploitation of the capability of airborne EM mapping. The dataset not only reveals the location of the caves, but may be used to obtain information on the depth of the caves. These results are summarized and briefly discussed in Chapter 4.2.

Magnetic anomalies may only in rare cases be used to distinguish caves and karst features (e.g. Rybakov et al., 2005), because the karst host rock is usually non-magnetic, making it impossible to distinguish the non-magnetic voids. Self-potential anomalies in karst have only in few cases been used to detect flowing water in the conduits (e.g. Zhou et al., 1999).

2.3 Hydrological modelling for karst groundwater management

Hydrological modelling is the discipline concerned with describing the land-phase processes of the hydrological cycle in a quantitative manner using coupled

mathematical equations (e.g. Singh and Woolhiser, 2002) (Fig. 9). The water balance equation for the vadose zone is given by:

$$\frac{dV_{soil}}{dt} = P - ET_a - Q - R \tag{21}$$

For a 3D soil volume, V: volume of water stored in the soil zone [m^3/m^3, i.e. unitless], t: time [e.g. year], P: precipitation rate, ET_a: actual evapotranspiration rate, Q: rate of surface runoff, R: groundwater recharge rate [all e.g. 1/year]. Eq. 21 is valid under the assumption of zero lateral flows in the soil. All quantities in Eq. 21 may be a function of space and time. Models with a spatial discretization are called distributed models.

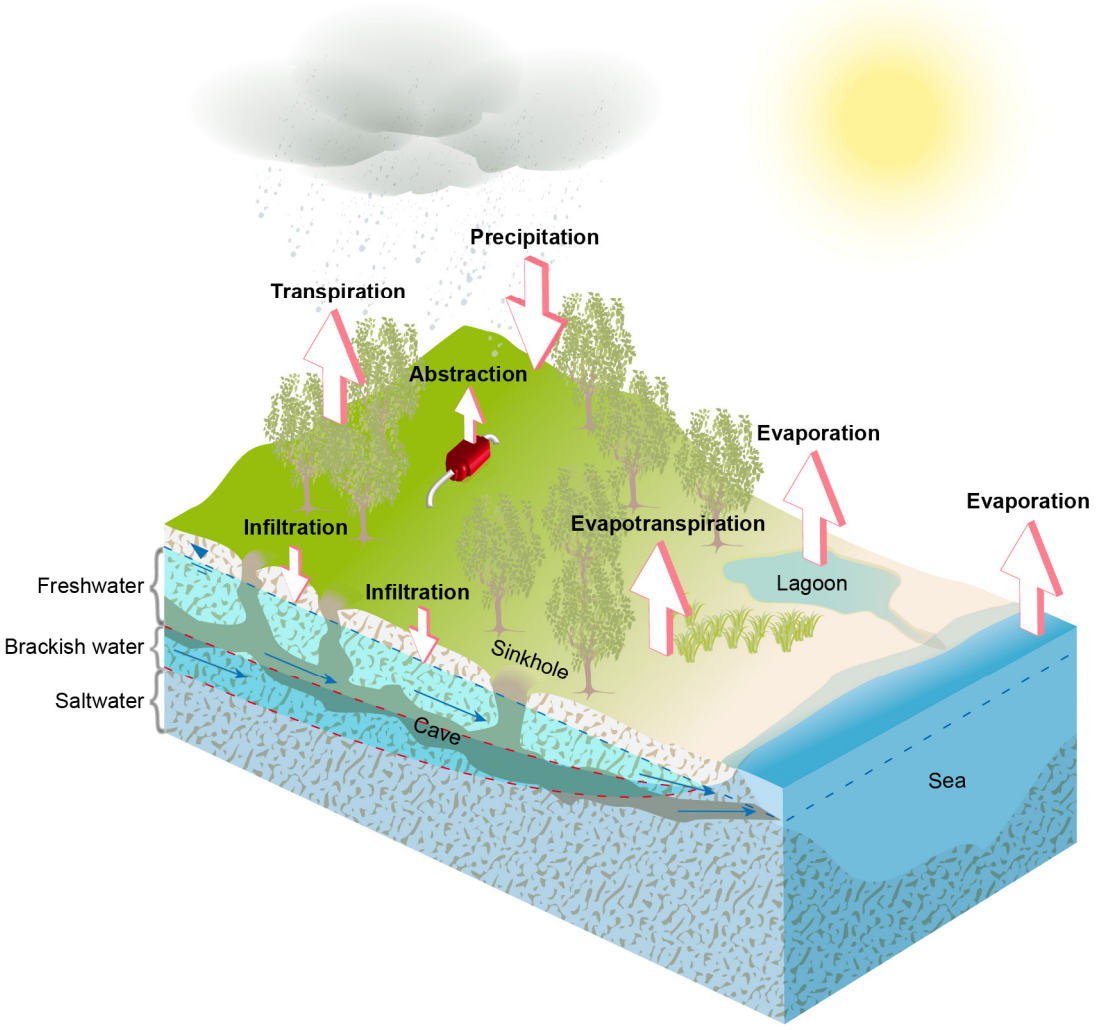

Fig. 9. Hydrological cycle.

Similarly, a water balance may be set up for the groundwater zone. This is done in the following, where also different types of distributed models for simulating karst aquifers are presented. Distributed models are now established tools used in water resources management, for instance to delineate groundwater catchments. Catchment delineation using stochastic methods will also be described in the following, along with the use of multiple conceptual models for evaluating model uncertainty.

2.3.1 Hydrological modelling of karst aquifers

Karst aquifers are triple porosity media, consisting of the rock matrix (intergranular porosity), the fractures and bedding planes and the karstic conduits (White, 1999). The majority of groundwater flow in karst takes place via the conduits, while the matrix is the major compartment for water storage (Atkinson, 1977; Worthington, 2003). For the matrix compartment, the groundwater flow can be described using Darcy's Law (e.g. Chow et al., 1988):

$$q = -K \cdot \frac{dh}{dl} \tag{22}$$

where q is the Darcy flux or specific discharge [e.g. m/s], K is the hydraulic conductivity [e.g. m/s], and dh/dl is hydraulic gradient (the change in head pr. unit length) [dimensionless]. Flow takes place in direction of negative hydraulic gradient as indicated by the negative sign.

Conservation of mass states that change in storage equals inflow minus outflow. For a 3D control volume in the groundwater matrix compartment, utilizing Eq. 22, this is for an incompressible (constant density) fluid written as:

$$S_s \frac{\partial h}{\partial t} = \frac{\partial}{\partial x}\left(K_x \frac{\partial h}{\partial x} \right) + \frac{\partial}{\partial y}\left(K_y \frac{\partial h}{\partial y} \right) + \frac{\partial}{\partial z}\left(K_z \frac{\partial h}{\partial z} \right) + W \tag{23}$$

where S_s is the specific storage [1/m], t is time [s], x, y and z are the three directions [m], and W represents sources and sinks [1/s]. S_s is only relevant for confined aquifers, since it is very small in the case of unconfined aquifers, and can then be neglected. Under steady state conditions, the term on the left hand side of Eq. 23 equals zero. Sources and sinks include groundwater recharge, which can be calculated using Eq. 21, evapotranspiration from the phreatic zone, pumping and/or injection via wells, and mass transfer to surface water bodies, if they interact with the groundwater.

Darcy's Law is applicable for laminar flow, such as that which often takes place in the rock matrix. Whether flow is laminar or turbulent can be evaluated by calculating the Reynold's number, R_e (e.g. Ford and Williams, 2007):

$$R_e = \frac{\rho_{dens} \cdot d_H \cdot v}{\mu_{vis}} \tag{24}$$

where ρ_{dens} is the density of the fluid [kg/m^3], v is the mean velocity of the fluid [m/s], μ_{vis} is the dynamic viscosity of the fluid [kg/(m·s)], and d_H is the hydraulic diameter of the conduit, equal to four times the cross-sectional area divided by the wetted perimeter. d_H equals the diameter, D, for circular pipes. If Eq. 24 is applied to granular or fractured media instead of to a conduit, v is replaced by the macroscopic velocity u, and the hydraulic diameter d_H is replaced by a length which represents the interstitial pore voids or the width of the fractures. Flow is turbulent if R_e is relatively large, and laminar if R_e is relatively small. The boundary for turbulent flow is at approximately $R_e \geq 4000$, while laminar flow occurs when $R_e \leq 2000$ (Hornberger et al., 1998; Chow et al., 1988). In between laminar and turbulent flow regimes a transition zone exists, where the flow cannot strictly be classified into one of the two categories.

If the flow is turbulent, which is often the case in karst conduits, expressions such as the Darcy-Weisbach equation may describe the flow in a conduit (e.g. Chow et al., 1988):

$$q = \sqrt{\frac{2 \cdot d_H \cdot g}{f_f} \frac{dh}{dl}} \tag{25}$$

where g is the acceleration due to gravity [≈9.82 m/s^2] and f_f is the Darcy-Weisbach friction factor [dimensionless]. The friction factor describes loss of energy due to friction with the conduit wall, increasing as the roughness increases. f_f depends on the Reynold's number. Friction factors for karst conduits are scarce, but have been reported to range from 0.12 to 340 for various cave systems (Springer, 2004 and references herein). Specifically for caves in Quintana Roo, friction factors of 1–45; 11–449 and 500–1000 have been estimated using dye tracing and various measured and estimated hydraulic gradients (Beddows, 2003; 2004).

For fully turbulent conditions, flow may also be described using Manning's equation (Chow et al., 1988):

$$q = \frac{R_H^{2/3} \cdot \sqrt{\frac{dh}{dl}}}{n} \quad (26)$$

where R_H is the hydraulic radius of the conduit [m], defined as cross-sectional area divided by wetted perimeter, and equal to $d_H/4$ for circular conduits. n is Manning's roughness coefficient [s/m$^{1/3}$] and equal to the reciprocal of Manning's M, which is sometimes given instead. Manning's n does not depend on the value of Reynold's number. n may be estimated from f_f by combining Eq. 25 and 26:

$$n = \sqrt{\frac{f_f}{8g}} R_H^{1/6} \quad (27)$$

It is seen that for laminar flow (e.g. matrix flow), flow is proportional to the hydraulic gradient, whereas for turbulent flow (e.g. conduit flow), flow is proportional to the square root of the hydraulic gradient, whether described by Darcy-Weisbach or Manning's equation (cp. Eq. 22, 25 and 26). Limited work from caves in Quintana Roo indicated high Reynold's numbers, i.e. clearly turbulent flow (Beddows, 2003; 2004). Other karst studies have shown the possibility of conduit flow being turbulent or laminar depending on season or location within the conduit system (Cheng and Chen, 2005; Barfield et al., 2004). Flow in fractures may be laminar or turbulent, but is mostly assumed laminar (Worthington, 2003).

Karst aquifers may thus be modelled by explicitly modelling each of the three compartments, and including exchange components between the three; however such triple-porosity modelling is only rarely carried out (Kaufmann, 2003; Cheng and Chen, 2005). More common is the conduit-matrix conceptualization, where conduit flow is modeled as turbulent (pipe) flow, whereas matrix flow is modeled using Darcy's Law. An exchange component (q_{ex}) is included between the two. This exchange is currently not well understood (Martin and Screaton, 2001; Bauer et al., 2003; Peterson and Wicks, 2005), but is often formulated as a linear exchange term that depends on the head difference between conduit (h_C) and matrix (h_M) (e.g. Cornaton and Perrochet, 2002; Birk et al., 2003; Arfib and de Marsily, 2004):

$$q_{ex} = \alpha_{ex} (h_M - h_C) \quad (28)$$

The exchange coefficient α_{ex} is thought to depend also on the hydraulic conductivity of the matrix component, the surface area of the conduits (area available for exchange), the geometry of the conduits, the slope of the regional

groundwater table and conduits, and the relative elevation of groundwater table and conduits (Martin and Screaton, 2001; Bauer et al., 2003). Besides conduit-matrix model codes generated by individual research institutions (e.g. used in Birk et al., 2003; Bauer et al., 2003; Liedl et al., 2003; Arfib and de Marsily, 2004), commercial and open-source software exists for creating conduit-matrix models, e.g. MIKE SHE coupled with MOUSE (DHI Software), the MODFLOW variant MODFLOW-DCM (Painter et al., 2007) and the Conduit-Flow Process module for MODFLOW (Shoemaker et al., 2008) which builds upon software developed by research institutions (Clemens, 1998; Hückinghaus, 1998; Bauer, 2002; Birk, 2002). Conduit-matrix models are physically sound but also complex and computationally expensive. Problems occur, especially on large scales, in the parameterization of the highly variable caves (e.g. cave location, course, roughness, dimensions) and in quantifying the exchange. Slight changes in some cave parameterizations can change model output notably (Peterson and Wicks, 2006). Conduit-models without the matrix-component have also been used to model karst in some cases (e.g. Halihan and Wicks, 1998; Jeannin, 2001; Springer, 2004).

A third conceptualization used in distributed karst modelling is the equivalent porous medium. This is the simplest representation of karst aquifers. The assumption that the aquifer can be represented by an equivalent porous medium is reasonable if the numerical cell size is 'large enough', i.e. equals or exceeds a "representative elementary volume" (REV). The value of *K* assigned to a cell represents the combined effect of matrix, fractures and conduits within the cell. The use of only one value of *K* throughout the model domain (single-continuum models) has only been successful in few cases (e.g. Larocque et al., 1999; 2000; Scanlon et al., 2003), and is often criticized as too simplistic to represent karst flow (e.g. Kovacs et al., 2005). A modification is the dual-continuum equivalent porous medium model, where important conduits are represented as zones of higher *K* than the matrix. Both compartments are described using Darcy's Law, but some of the heterogeneity of karst aquifers is incorporated. Water can exchange between the zones of different *K*. Sometimes, the *K* assigned to conduits varies along the course of the conduit to reflect larger conduits or an increasing number of branches in the downstream direction (e.g. Lindgren et al., 2005). Dual-continuum approaches give a higher accuracy than single-continuum models, if zonation and assignment of values are reasonably reliable (Durlofsky, 1992). Dual-continuum models have been successfully used by e.g. Teutsch and

Sauter (1991), Knochenmus and Robinson (1996), Lindgren et al. (2005) and Kiraly (2003). The approach is especially applicable for regional-scale studies and was also used in Gondwe et al. (IV).

2.3.2 Multiple Model Simulation

When using models to guide management decisions, uncertainty assessment is important. Several authors have found that uncertainty in the conceptual model usually is far greater than the impact of any model parameter uncertainty, although conceptual model uncertainty may often be neglected (Neuman and Wierenga, 2003; Højberg and Refsgaard, 2005; Refsgaard et al., 2006). Conceptual model uncertainty can be addressed using Multiple Model Simulation (MMS). In MMS a number of different plausible conceptual models are formulated and calibrated. Based on validation tests, models are accepted or rejected. All accepted models are subsequently used for prediction and uncertainty assessment. The difference between the results obtained using the different accepted models thus gives a measure of the impact of conceptual model uncertainty on the model result uncertainty (Refsgaard et al., 2006). MMS increases the robustness of model predictions and yields explicit analyses of the consequences of using alternative models. The method was used in Gondwe et al. (V). The limitations of the MMS approach are that the selection of conceptual models is necessarily subjective and often incomplete. Important plausible conceptual models may be left out, and it is not possible to quantify the probability of each alternative model (Refsgaard et al., 2006; 2007). Methods do exist for combining the results from multiple conceptual models: Pooling (linear combination of the results with equal weights assigned to each model, Block et al., 2009, and references herein); linear regression weighting (linear combination of results, weights of each model determined from regression coefficient of observed vs. modelled conditions for each model, Block et al., 2009, and references herein), and Bayesian model averaging (e.g. Neuman, 2003; Rojas et al., 2008; 2009; Li and Tsai, 2009). For transient models the 'hierarchical mixture of experts' framework (Marshall et al., 2006) and kernel density estimators (Block et al., 2009) may be used to let the weight of each model in a linear combination vary in time. Moreover, non-linear weighting of conceptual models by means of artificial neural networks has been applied (Xiong et al., 2001). Combining different conceptual models typically provides more robust results compared to using one single conceptual model (e.g. Georgakakos et al., 2004; Rojas et al., 2008; Block et al., 2009). Combinations may however be

sensitive to the assumptions used in the analysis. For instance, Rojas et al. (2009) showed that Bayesian averaging methods rely not only on the posterior probabilities of each model (i.e. the weights used) but also on the prior model probabilities, i.e. the assumed probability distributions of the model input parameters.

2.3.3 Monte Carlo catchment delineation

Catchment delineation is frequently carried out using particle tracking methods in hydrological models. However, because model parameters are often uncertain, it can be an advantage to carry out stochastic modeling of the catchments instead of relying on the result of one deterministic model (Vassolo et al., 1998). An often used group of stochastic modeling methods are the Monte Carlo methods, which use repeated random sampling of equally likely model inputs in order to generate the model results. In that way, errors in model inputs are propagated through the model, and uncertainties on model results arising from model input uncertainties can thus be quantified. Monte Carlo methods have been used to delineate the spatial probability distribution of groundwater catchments in several studies (e.g. Vassolo et al., 1998; Stauffer et al., 2002; 2005; Hendricks Franssen et al., 2004, Gondwe et al., V). In Gondwe et al. (V) multiple realizations of input parameter (*K*-value) combinations were generated using the Markov chain Monte Carlo method called the Metropolis-Hastings algorithm (Hastings, 1970), which is widely used. It requires drawing random numbers and specifying a probability density function and a proposal density function. The probability density function used in Gondwe et al. (V) was a multivariate normal distribution, and cross-correlation of the parameter values, obtained from inverse model calibration, was incorporated. In the Metropolis-Hastings algorithm the random values are then accepted or rejected using the probability density function and the proposal density function. Each new value to be tested is generated from the proposal density function as well, and depends on the previously generated value, which is where the 'Markov chain' term comes in. Further information on the Metropolis-Hastings algorithm may be found in e.g. Chib and Greenberg (1995). Following generation of the numerous realizations of the model input parameter combinations the hydrological models were run using each parameter combination, and particle tracking was carried out. Finally, the resulting spatially distributed catchment results were stacked to obtain probability maps of the catchment's spatial distribution.

3 Study area

The focus area of the PhD study is the conjectural groundwater catchment of Sian Ka'an, outlined based on topographic divides and a few known flow divides (Fig. 10). The groundwater heads available for the Peninsula are in agreement with these tentative catchment boundaries (Gondwe et al., IV), while geochemical results of Perry et al. (2002) support the water divide at Lake Chichankanab. The study area is 35000 km^2 large, and largely located within the state of Quintana Roo.

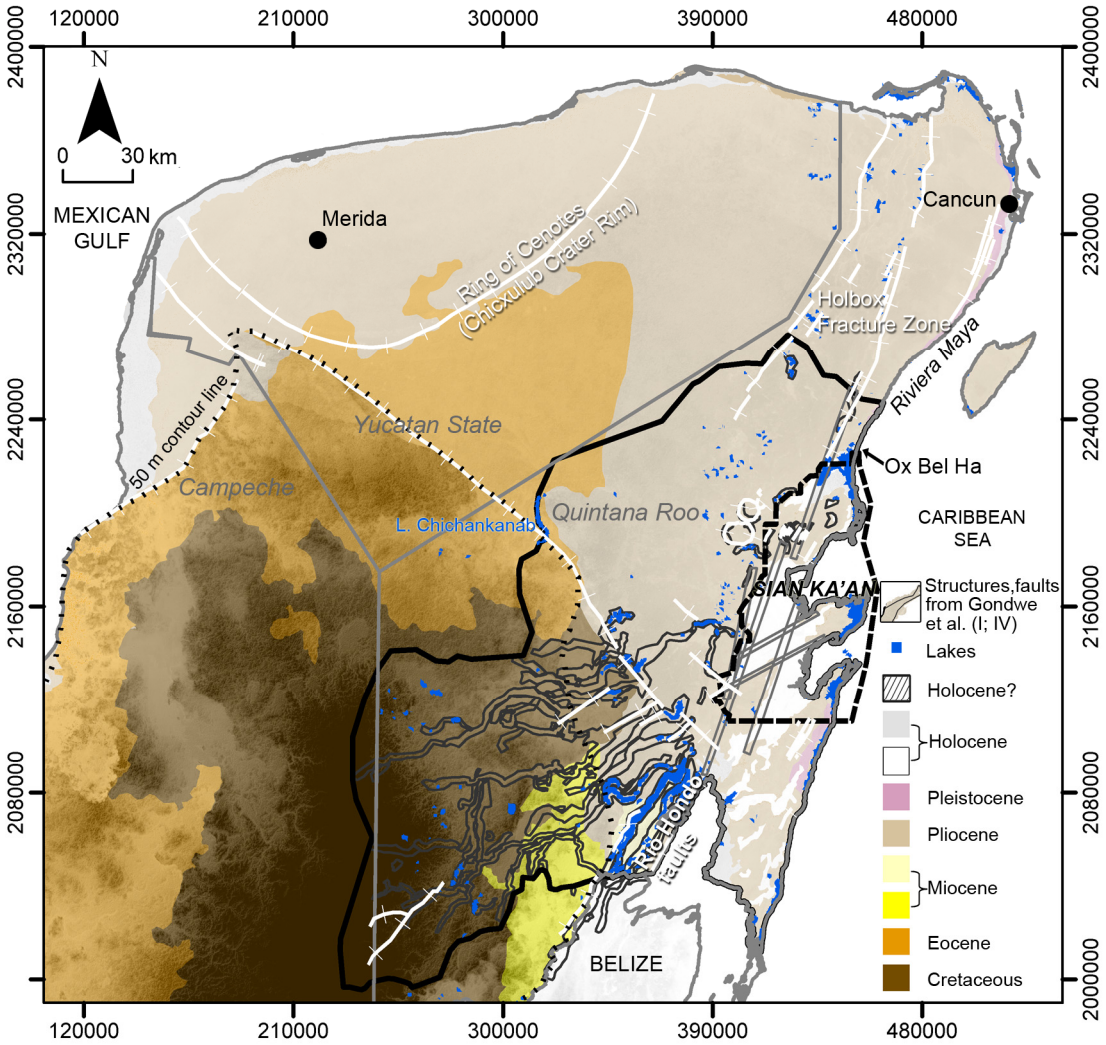

Fig. 10. Geology of the Yucatan Peninsula, modified from SGM (2007). Oldest sediments dated as Cretaceous instead of Paleocene based on Schönian (2005) and Lopez-Ramos (1975) (Ichaiche Formation). Topography from SRTM (USGS, 2006) overlain as grey-scaled transparent. Study area outlined with thick black polygon. Coordinates are UTM zone 16N, WGS84 datum and ellipsoid.

Average precipitation ranges from 840 to 1550 mm/year within the study area. Three quarters of the precipitation falls between May and October (unpubl. climate data from Comisión Nacional del Agua). Actual evapotranspiration was estimated using the 'triangle method' (e.g. Stisen et al., 2008) and MODIS data (Gondwe et al., IV). Subtracting this estimate from spatially distributed precipitation data from the Tropical Rainfall Measurement Mission yielded the average annual recharge distribution. Within the study area average recharge equals about 17% of mean annual precipitation – roughly 200 mm/year (Gondwe et al., IV). Average monthly temperatures range from 23 to 27°C. The area is subject to tropical storms.

The Yucatan Peninsula consists of limestones, dolomites and evaporites reaching thicknesses of >1500 m (Weidie, 1985). The surficial sediments span Upper Cretaceous to Holocene in age, and are generally nearly horizontally layered and off-lapping, with gradually younger carbonates deposited towards the Peninsula margins (Lopez-Ramos, 1975; SGM, 2007; Schönian et al., 2005) (Fig. 10). The Cretaceous age of the oldest surficial sediments is a recent interpretation (Schönian et al., 2005) but the possibility was already mentioned by Lesser (1976). In the southern and central Peninsula the geology is poorly constrained due to few exposures and difficulties in dating the sediments through biostratigraphy (Kenkmann and Schönian, 2006). Examples of Upper Cretaceous sediments wrongly dated to be younger were also mentioned in Pope et al., (2005). Ejecta associated with the Chicxulub meteorite impact, at the contact between Cretaceous and Paleogene sediments, has been found at the ground surface in southern Quintana Roo and neighboring Belize (Ocampo et al., 1996; Fouke et al., 2002; Pope et al., 2005; Schönian et al., 2005; Kenkmann and Schönian, 2006). The ejecta blanket's extent is not well known, but it has been proposed that it extends south and east of Lake Chichankanab (Perry et al., 2009). The ejecta is clay-rich and described to have a sealing or partially sealing effect (Ocampo et al., 1996; Grajales-Nishimura et al., 2000). Using borehole logging and airborne EM, Gondwe et al. (III; IV) found a shallow, high-conductive geological layer in the inland central and southern parts of the study area (thickness: 3–8 m, apparent conductivity 200–800 mS/m). The layer was also associated with high natural gamma radiation (about 80 counts pr. second) (Fig. 11). It was proposed that this layer might be the ejecta layer. Its location in the geological sequence appeared to correspond with being at the Cretaceous/Paleogene boundary, and the spatial occurrences of the layer partly

corresponded with other findings of surface-near ejecta (Gondwe et al., III; Schönian et al., 2004; 2005). Geochemical results showing high Sr-concentrations in the region of the anomalous layer also supported the possibility of the layer being ejecta (Gondwe et al., III; Perry et al., 2002; 2009).

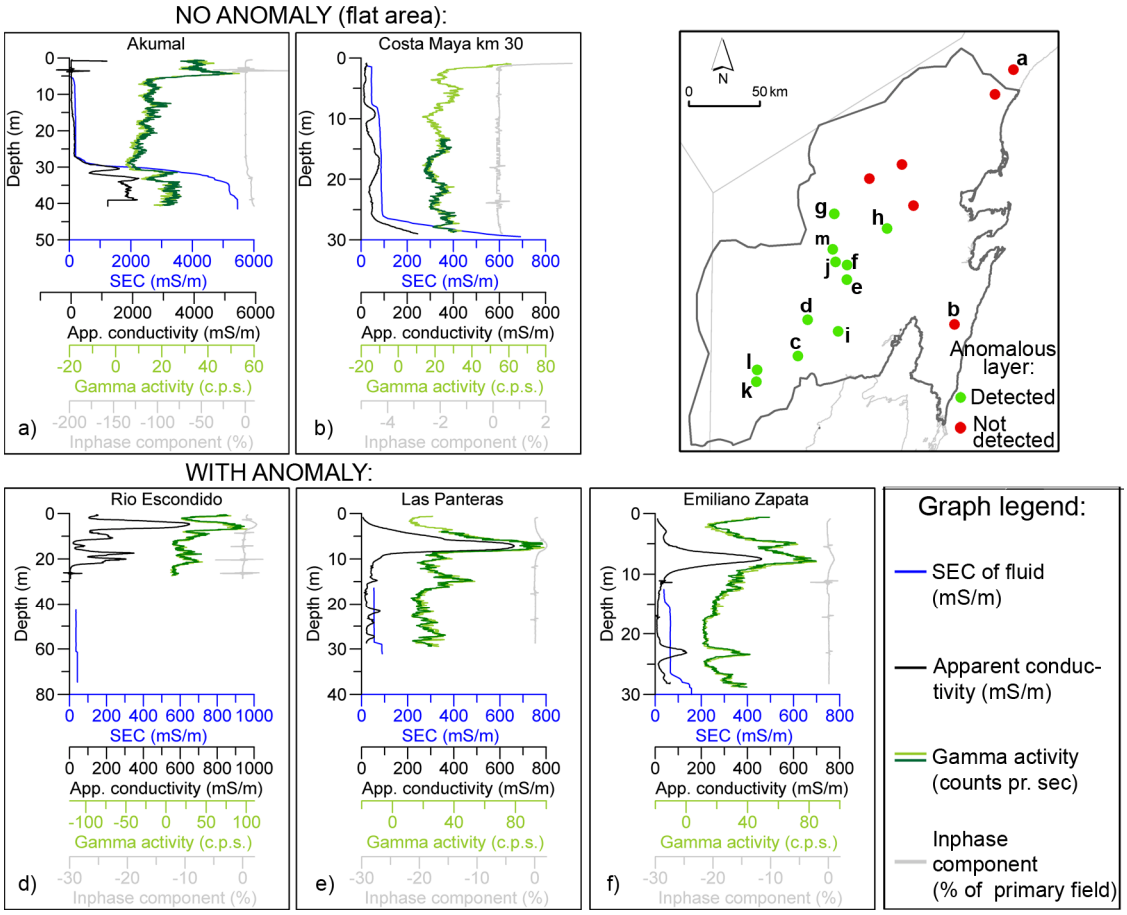

Fig. 11. Example results from the borehole logging. a) and b) show typical results from the flat area (no anomalous layer detected). d) through f) show logs with the anomalous layer detected. Lettering follows that used in Gondwe et al. (IV). SEC: specific electrical conductivity of the well fluid – its top indicates location of water table. Location map at top right. Modified from Gondwe et al. (IV).

Topographically the study area contains a notable contrast. Large parts of the Pliocene geology is rather flat, with elevations ranging 0–20 meters above mean sea level (mamsl). In the area of the oldest, Cretaceous, geology, cone karst hilly landforms dominate, and elevations range between 50 and 340 mamsl. In between a transition zone with moderately undulating relief exists (20–50 mamsl) (Fig. 10).

The Yucatan carbonates and evaporites are heavily karstified. Some of the world's longest underwater cave systems have been mapped along the Riviera Maya by cave divers (www.caves.org/project/qrss/qrlong.htm; www.caverbob.com/uwcave.htm). Mapped caves may be >30 m wide and up to 10 meters high. Maximum mapped cave depths are 22.3 ± 8.7 m for inland caves, and 11.8 ± 6.2 m for coastal caves. In the Riviera Maya the overall passage density is 1.8 km/km^2, but may locally be up to 4.3 km/km^2 (Beddows, 2004; Smart et al., 2006). Most parts of the study area have not been explored by cave divers and the location and properties of caves here are therefore unknown. Regional-scale zones of potential higher permeability were mapped and explored by Gondwe et al. (III); some of which were found to be associated with the two regional fault systems present in the study area – the Río Hondo faults and the Holbox fracture zone (Fig. 10). Additional faults located within the Sian Ka'an Biosphere Reserve and possibly connecting the Río Hondo and Holbox systems were proposed by Gondwe et al. (I), based on surface water flow patterns and the shape of wetland boundaries (Fig. 10). Further investigation of these zones and faults is elaborated upon in Chapter 4.2 and 4.3.

Groundwater in the Yucatan Peninsula is a 0–100 m thick freshwater lens floating on top of saline water (Gondwe et al., IV; Perry et al., 1989; Steinich and Marin, 1996; Marin et al., 2004). In the Pliocene geology the depth to the saltwater-freshwater interface was found to be described well, on a regional scale, by the Dupuit-Ghyben-Herzberg relationship, where depth to interface equals 40 times the height of the freshwater table (all with respect to mean sea level) (Gondwe et al., IV).

A notable contrast was found in the measured groundwater heads across the study area. Like the topographical contrast, the boundary between the contrasting areas appears coincident with geological boundaries. Within the Pliocene geology measured heads range from 0 to 3 mamsl, yielding low hydraulic gradients of 3–7 cm/km, and water level variations are relatively small (5–40 cm within a year) (Gondwe et al., IV) (Fig. 12). This indicates high transmissivity. Hydraulic gradients in the same range have been found in the Pliocene geology in the northwestern and northeastern parts of the Peninsula (Back and Hanshaw, 1970; Marin, 1990; Moore et al., 1992; Beddows, 2004). In the hilly area, mainly covered by the Cretaceous geology, measured water levels range from 4 to 92 mamsl, yielding hydraulic gradients of 10 to 190 cm/km (Gondwe et al., IV).

Geochemical results show that only in the hilly area, waters are close to saturation with gypsum and anhydrite (Gondwe et al., IV; Perry et al., 2002). Gypsum and anhydrite are known to have low primary porosity, with water flow mainly taking place through developed karst features, if any are present (Klimchouk, 1997; Mayr et al., 2008). Consequently, measured groundwater heads and water chemistry indicate a lower transmissivity of the geology in the hilly area, compared to that of the flat, Pliocene area. In addition, water level measurements in the study area revealed the presence of perched aquifers in the hilly area and transition zone (Fig. 12). These perched aquifers may be formed due to the shallow, likely clayey, layer detected in the borehole logs and airborne EM (Gondwe et al., III; IV).

From the measured groundwater heads in the study area, overall groundwater flow directions appear to be from SW to NE within the hilly area, and from W to E within the Pliocene geology (Gondwe et al., IV) (Fig. 12).

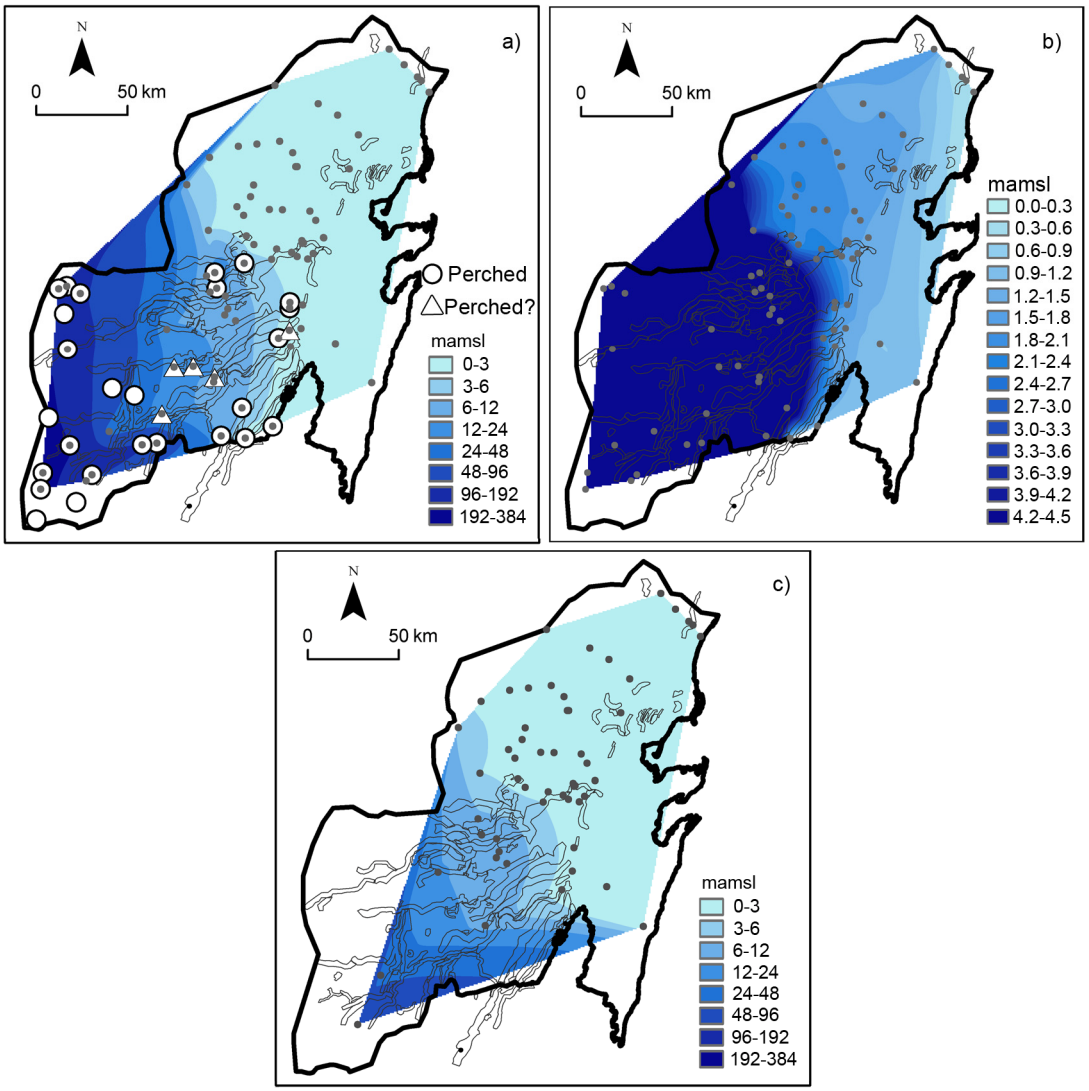

Fig. 12. Examples of water levels measured in the dry season, interpolated using Natural Neighbor algorithm. a+b) are including, c) is excluding points believed to be perched water. The "Perched?" label in a) indicates localities with possibly perched aquifers. a + b) show the same data, but with different legends to show the overall regional water level differences. Water levels refer to meters above mean sea level. Modified from Gondwe et al. (IV).

4 Results from radar remote sensing, EM exploration of geological structures and groundwater modelling

4.1 Wetland hydrodynamics derived from radar data

4.1.1 Mapping flooding extent from SAR backscatter data

For Sian Ka'an, the temporal dynamics of flooding extent in the period August 2006 to February 2008 was investigated using SAR backscatter data (Gondwe et al., I). The wetland extent varied between 1067 km^2 and 2588 km^2. The flooding extent was found to be correlated with a 3-month backward moving average of precipitation (Fig. 13), indicating the likely effect of a larger groundwater catchment on the wetland hydroperiod. The largest wetland extent during normal years was found to occur in December, two months after the end of the rainy season. However, when an extreme rainfall from a hurricane took place in September 2007, this month yielded the largest flooding extent that year. Lowest flooding extent occurred in May, at the end of the dry season. The flooding maps further indicated areas providing main water inflow to the wetlands. These were seen as the areas which were still flooded at the driest time of the year, and may be caused by water-carrying faults providing water to the wetlands (Gondwe et al., I).

The accuracy of the flooding map was evaluated by comparing with a flooding extent classification created using nearly cloud-free Landsat imagery. Landsat and other optical imagery is generally evaluated as optimal for flood extent mapping, but is limited by the cloud cover often present in the images, as well as the inability to penetrate through vegetation. Landsat imagery for flood extent mapping has been carried out by e.g. Pietroniro et al., (1999), Hudson and Colditz (2003), Wright and Gallant (2007) and Islam et al. (2008). Using SAR data the classification accuracies obtained in the Sian Ka'an study ranged between 63% and 75%, depending on class. These accuracies were in agreement with that of other studies (e.g. User's accuracies: 65–95% in Hess et al., 2003; 56–80% in Bourgeau-Chavez et al., 2005).

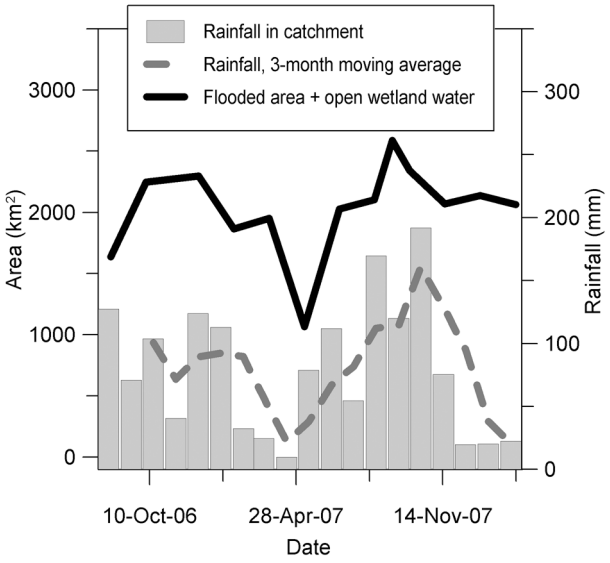

Fig. 13. Flooding extent variations with time, mapped by classification of SAR backscatter data. Precipitation data (histogram) from the Tropical Rainfall Measuring Mission (TRMM, NASDA/NASA, 2008), along with a 3-month backward moving average of this precipitation (thick dashed line). These data are a spatial average for the study area (conjectural catchment of Sian Ka'an). From Gondwe et al. (I).

4.1.2 Surface water flow directions and water level changes from InSAR

For the Sian Ka'an wetlands, interferogram fringe directions along with the shape of tree islands, which indicate up- and downstream directions of dominant water flows, were used to deduce the overall surface water flow directions within Sian Ka'an (Fig. 14) (Gondwe et al., I). The interferograms analyzed spanned the time period from July 2006 to March 2008. Fringe directions also revealed local-scale water divides. These may not necessarily be impenetrable to water, but the flooding regime differs on either side of the divide (Fig. 14). This information on the surface water flows and flooding regimes has not previously been known for Sian Ka'an. It is often difficult or impossible to obtain such data for vast wetlands, but these results illustrate how InSAR offers new possibilities for learning about the hydrodynamics of large and often inaccessible wetlands. The surface water flow directions and local-scale water divides of Sian Ka'an can be used to guide water quality monitoring programs with the aim of identifying pollution transport pathways. These results are also important for further studies on the interaction between ecology and hydrology in the wetlands.

The interferograms generated over Sian Ka'an showed that relative water level changes are generally small. The areas with the largest relative water level

changes were the sloughs and four main coastal outlets of Sian Ka'an (Fig. 14, interferogram example in Fig. 6). Due to the lack of radar altimetry and gauge data, the results of water level change over Sian Ka'an focus on the relative changes rather than absolute changes. Detected relative water level changes were up to 28 cm within 24 or 48 days (Gondwe et al., I). The interferograms produced over Sian Ka'an were smooth at times with large water amounts in the wetlands (November and December). These were the same times when the flooding extent was largest, also indicating large water amounts. However, mostly Sian Ka'an interferograms showed irregular fringe patterns, with some areas of steep relative water level changes (the local-scale water divides, with several fringes over short distances). Irregular fringe patterns appear to characterize natural wetlands, because this was also found by Alsdorf et al. (2007b) and Wdowinski et al. (2008). The most irregular fringe patterns were in Sian Ka'an observed at the beginning and middle of the wet season, where surface water level changes were more localized (July–September). The fringe patterns may be compared with the results of hydrological models, to verify and/or constrain the models. This was partly done in Gondwe et al. (V).

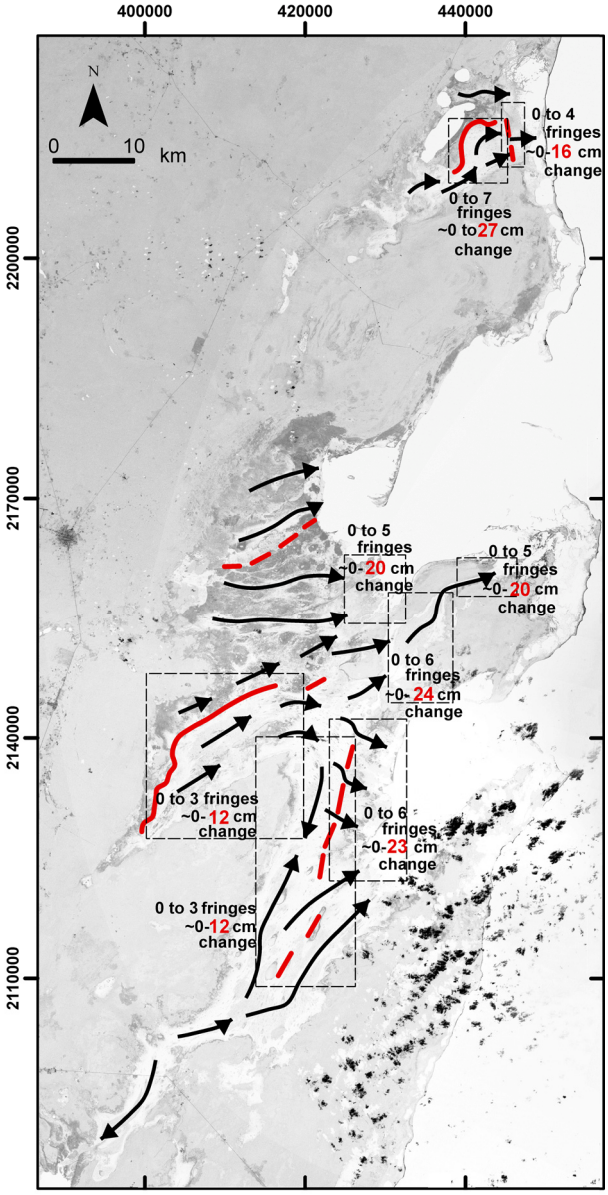

Fig. 14. Black arrows: Surface water flow directions, deduced from interferograms and visual inspection of Landsat imagery. Red lines: Semi- or impermeable water divides, deduced from abrupt phase changes and fringe lines. Dashed boxes: Areas with largest relative water level changes (most fringes). Background image: Grey-scaled Landsat TM Tri-Decadal mosaic, band 7. From Gondwe et al. (I).

4.2 Investigation of karst features using EM

4.2.1 Local-scale exploration of karst caves

Airborne EM measurements were carried out over the well-mapped Ox Bel Ha cave system, located just north of Sian Ka'an. The purpose was to determine the usefulness of airborne EM in detecting submerged caves in the geology of Quintana Roo. Finding out the location and properties of caves and highly permeable geological zones is crucial in order to determine the groundwater flow patterns in karst. The equipment used in the exploration was a modified Geotech Hummingbird of the Geological Survey of Austria, applying four frequencies (340 Hz, 3200 Hz, 7190 Hz and 28850 Hz) (Motschka, 2001). The cave system clearly appeared in the data set as anomalies of higher signal strength (Fig. 15). Most anomalies were correlated with the location of caves known from cave maps constructed by scuba divers. Others had not previously been mapped by divers, but some of them were verified at dive expeditions following the airborne EM campaign (Supper et al., II). The inphase components of the 3200 Hz and 7190 Hz frequencies responded most strongly to the presence of caves in this survey. That is likely because the main depths of the explored caves corresponded well with the exploration depth of these two frequencies in this geological configuration.

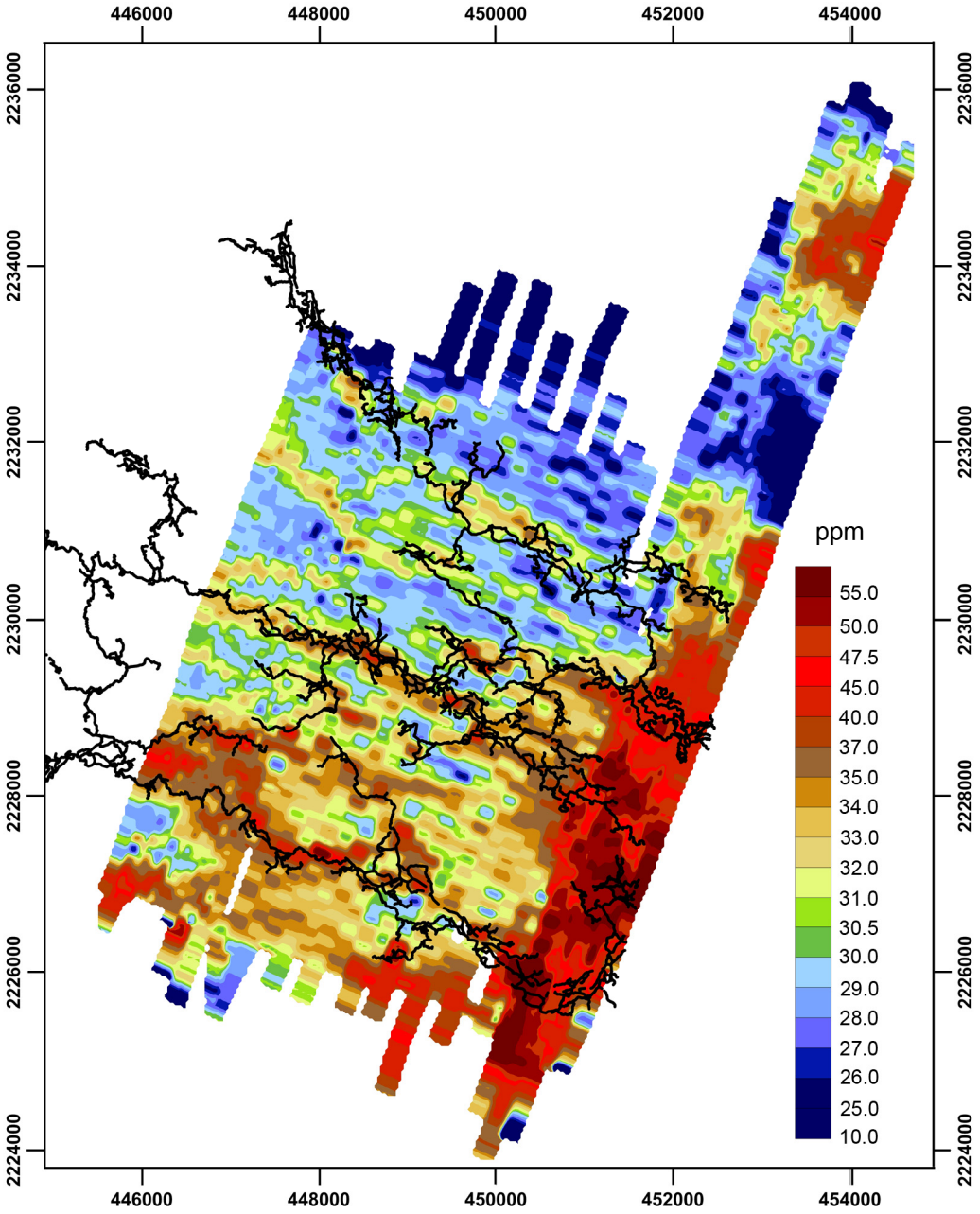

Fig. 15. Inphase component of the 7190 Hz frequency, measured over the Ox Bel Ha cave system, after rough empirical altitude correction and profile leveling. Known caves (black lines) are overlain. Ox Bel Ha cave line map kindly provided by Grupo de Exploracion Ox Bel Ha and Quintana Roo Speleological Survey 2006. Principal explorers of the Ox Bel Ha system: B. Birnbach, S. Bogaerts, F. Devos, C. Le Maillot, S. Meacham, B. Philips, S. Richards, D. Riordan, S. Schnittger, G. Walten and K. Walten. From Supper et al. (II).

Layered inversions of the Ox Bel Ha airborne EM dataset have shown that the EM data can not only be used to determine the lateral location of caves, but can also be used to obtain information on the depth of the caves. In fact the caves represent a 3D exploration problem, but interpretations using 1D multilayered inversions have shown to work well (Y. Ley-Cooper, Royal Melbourne Institute of Technology University, unpublished results) (Fig. 16). However, determining exact cave dimensions from the EM data does not appear possible with the present knowledge. One reason appears to be that the bulk rock matrix immediately surrounding the caves has a strong impact on the measured signal.

3D forward modelling of the Ox Bel Ha signal, using cave dimensions known from dive surveys, indicates that the modelled signal anomalies are smaller than the actual measured signal anomalies over the caves (Ottowitz, 2009). One explanation for this may be that the matrix surrounding the caves has an increased porosity, yielding a lower bulk matrix resistivity in the vicinity of caves, and increasing the signal magnitude (see Fig. 15 and Fig. 16). This topic has received little attention in the literature. A 'halo' effect is known to occur around man-made caves, resulting in a zone of increased fracturing surrounding the cavity. This makes the effective geophysical size of the cavity larger than the cavity itself. In natural caves, secondary effects on the surrounding rock may also be present (Daniels, 1988). The limestone medium surrounding karst conduits was in one case described as inhomogeneous, based on geophysical measurements (Guérin et al., 2009). A higher porosity surrounding karst caves may also correspond to the proposed "annex-to-drain" conceptualization, where storage in the karst aquifer is believed to take place in large karstic voids with a high head loss connected to conduits (Mangin, 1974; Bakalowitz, 2005). However, the nature of the medium surrounding caves in Quintana Roo remains to be determined, and therefore it is difficult to state exactly when airborne EM will be able to detect caves in this medium. However, besides the matrix surrounding the caves, the airborne EM signal is sensitive to the following factors: the proportion of saltwater in the cave (for instance, Ox Bel Ha caves are filled partly with fresh, partly with saline water); the size of the cave; the presence of several caves in the vicinity of each other; the shape and depth of the cave; the resistivity contrast in the geology, and the sensor height (Gondwe, unpubl. results of forward modelling experiments).

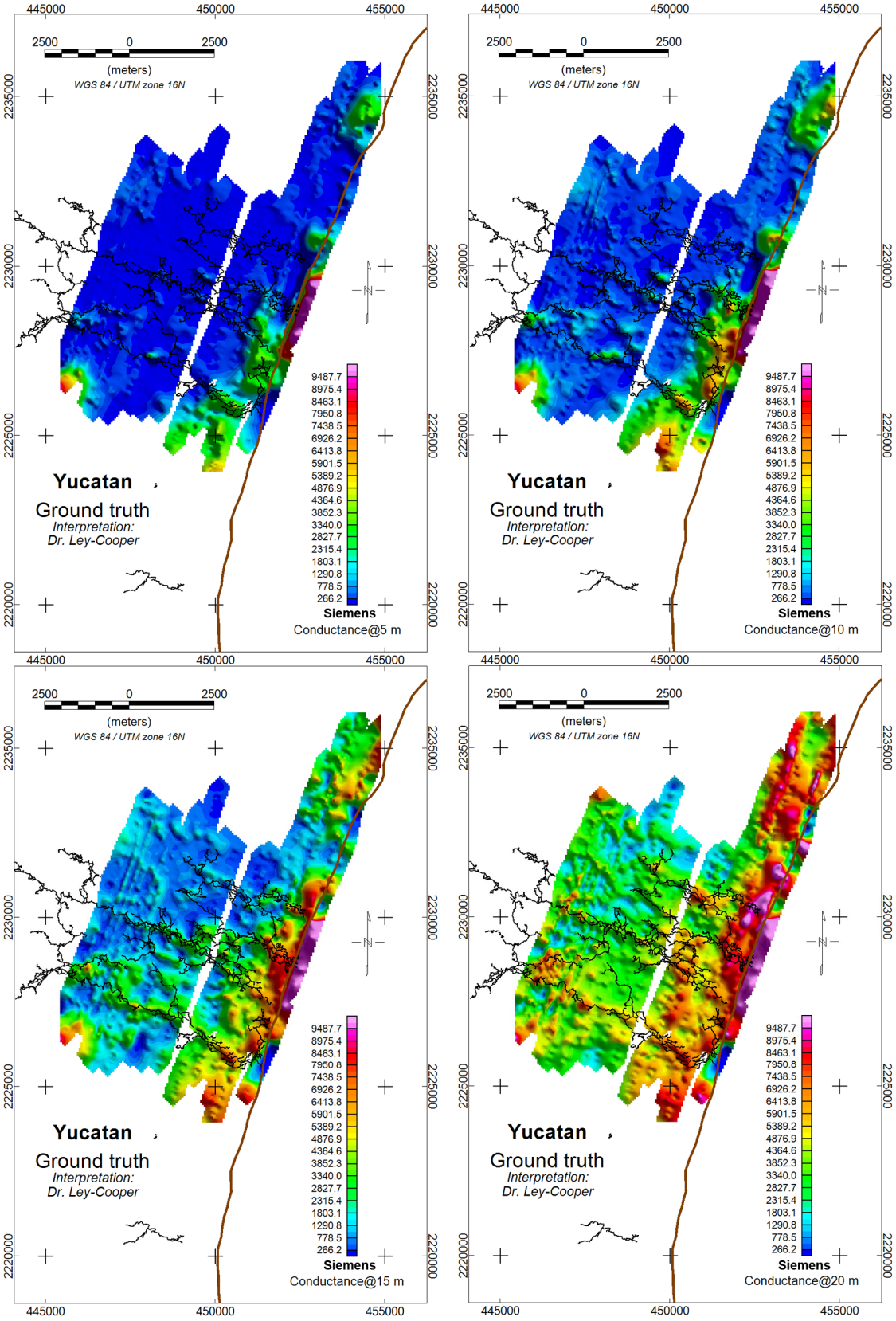

Fig. 16. Layered inversion results of the Ox Bel Ha survey. Inversion made by Dr. Yusen Ley-Cooper, RMIT Australia. Unit: Conductance (conductivity times thickness) in Siemens. Ox Bel Ha cave line map credits: Please see figure text below Fig. 15.

4.2.2 Regional-scale structure investigation

After showing that airborne EM *is* able to locate subsurface caves in Quintana Roo, the next step was to investigate parts of the study area, where the location and extent of caves and high permeable zones were unknown. The airborne EM measurements were focused on areas in which the likelihood of encountering high permeable zones was expected to be comparatively higher, by using the structures delineated from visual inspection of satellite imagery as a guide (Gondwe et al., III) (Fig. 10). Airborne EM results obtained over a structure which is part of the Holbox fracture zone showed higher signal strength over this zone, compared to over the bulk rock surrounding the zone. Layered inversions showed that the bulk resistivity in the freshwater part of the Holbox fracture zone was about 50 Ωm, whereas outside the zone it was >130 Ωm (Fig. 17). If applying Archie's Law (Eq. 6) and assuming freshwater resistivities (ρ_w) between 4 and 10 Ωm (i.e. 2.5 to 1 mS/cm, Beddows, 2004), and typical values for the constants in Archie's Law (a=1.5, m=n=2), then this resistivity difference across the Holbox zone corresponded to a higher porosity within the zone. With ρ_w = 4 Ωm, Holbox zone porosity would be ~0.35 while bulk matrix porosity would be <0.25. With ρ_w = 10 Ωm, Holbox zone porosity would be ~0.55 while bulk matrix porosity would be <0.4. By inference, this structure in the Holbox zone is therefore also likely to be a zone of higher permeability to water flow.

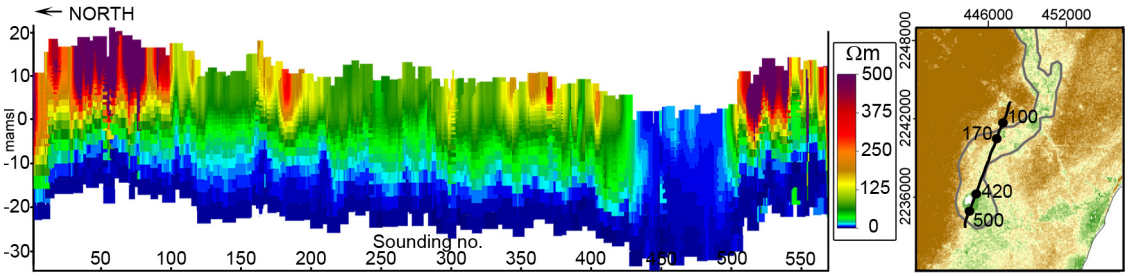

Fig. 17. Inversion results from profiles over the Holbox fracture zone. Soundings 170 to ~500 are within the delineated Holbox zone and appear as more conductive than surroundings. Sounding 420–500 is an open water body (Laguna La Union). Sounding 100–170 likely represents an irrigated field. Location map at right side. Modified from Gondwe et al. (III).

Airborne EM data on transects across structures in the inland areas also showed a higher signal strength above structures compared to the inter-structure areas (Fig. 18). However, forward modelling showed that these anomalous signals could not be explained by caves of realistic dimensions (Gondwe et al., III). Instead, the anomalous shallow conductive layer encountered in the inland borehole logs (Gondwe et al., IV) was useful to obtain a reasonable explanation of the signals measured across inland structures. The airborne EM signals across the inland structures could be modelled well if the high-conductive, shallow layer was simulated to be present along the full length of all transects. The reason for a stronger EM signal over the structures was then simply that in these areas, which also corresponded to topographic depressions, the layer was exposed relatively closer to the surface. Likely erosion by surface water runoff within the structures, would have removed relatively larger portions of the strata above the anomalous layer over structures, compared to the inter-structure areas.

Due to the presence of the high-conductive, shallow layer, little information could be obtained about the subsurface beneath it, using the airborne EM. Higher-strength anomalies over structures in the 340 Hz part of the signal could be matched well when a low-resistivity zone of ~5 Ωm was included at depth. This could suggest higher bulk porosity beneath the anomalous layer at the structure locations. However, this possibility is highly uncertain because of equivalences and the low sensitivity to the geology beneath the conductive, shallow anomalous layer. The 340 Hz signal was furthermore more affected by data noise and drift than the more reliable 3200 Hz and 7190 Hz parts of the signal. Forward calculations showed that signal perturbations due to high-permeable freshwater zones beneath the conductive, shallow anomalous layer would only be observable in the most reliable 3200 Hz and 7190 Hz signal components if the sensor height was relatively low ($\leq$ 30 m) – a sensor height difficult to obtain in the study area due to tall vegetation. In addition, such signal perturbations would not be distinguishable from changes caused by slight variation in the resistivity and/or thickness of the low-resistive layer. Such changes do characterize the anomalous layer encountered in the borehole logs, and therefore, the airborne EM system used would not be capable of detecting high-permeable zones in the inland areas throughout which the shallow, conductive layer appears to be present.

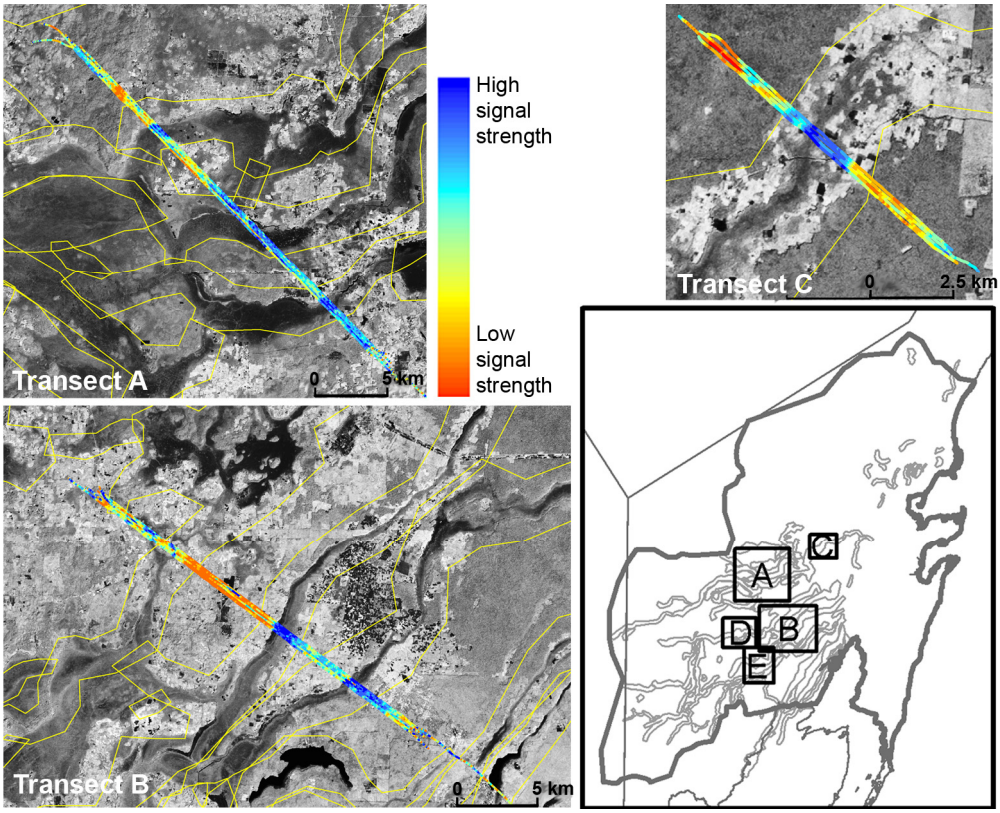

Fig. 18. Examples of HEM signals measured over inland structures, transformed with Eq. 1 in Gondwe et al. (III). Thin yellow lines outline structures. Background: Landsat Tri-Decadal TM band 4. Location map also shows the structures delineated, and the location of Transects D and E (not shown). Modified from Gondwe et al. (III).

4.3 Hydrological modelling of the Sian Ka'an catchment

4.3.1 Multiple Model Simulation of the Sian Ka'an catchment

Distributed hydrological modelling of the Sian Ka'an catchment was carried out to investigate central management questions such as the extent of the groundwater catchment for Sian Ka'an's wetlands, and the extent of travel time zones of groundwater flow from the catchment to the Reserve. However, the hydrogeological role of the structures outlined with satellite imagery could not be determined from the field data sets. Therefore, inverse hydrological modelling and Multiple Model Simulation was chosen as methods to investigate the possible role of the structures for the groundwater flow patterns in the catchment.

Seven different conceptual models were set up for the conjectural catchment of Sian Ka'an's wetlands (Gondwe et al., V) (Fig. 19). The equivalent porous

medium modelling approach was used. Only the flat area was discretized; the hilly region was modelled as a lumped inflow boundary, due to lack of sufficient data to represent this area with a discretized model. The conceptual models differed with respect to whether the structures were assigned a different hydraulic conductivity ($K_{structures}$) than the rest of the domain (K_{matrix}) (single- or dual-continuum equivalent porous medium models), and with respect to the magnitude of the lumped inflow from the hilly area. Finally, the coastal resistance to flow was differentiated at the coast north of Sian Ka'an in one conceptual model (Model 7), to accommodate the theoretical possibility of caves not being distributed evenly in the Tertiary sediments but only being present in the Pleistocene sediments along Riviera Maya (Gondwe et al., V, and references herein).

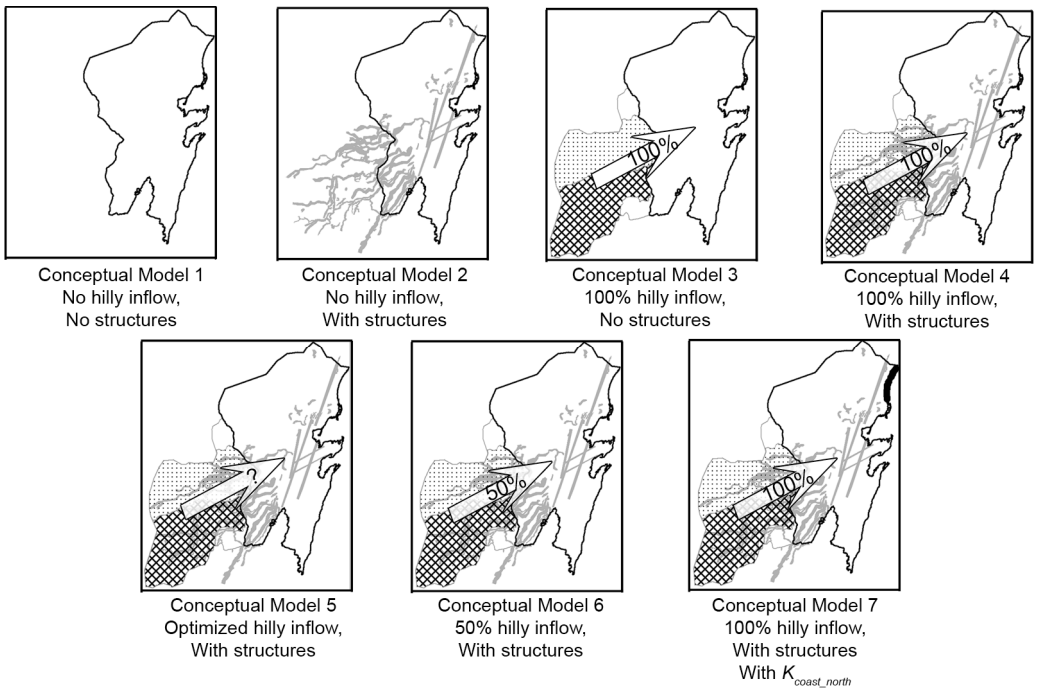

Fig. 19. The different conceptual models used in the Multiple Model Simulation.

In the cases where coastal resistance to outflow was assumed homogeneous along the whole coastal boundary, the six conceptual models showed an improvement in model fit to measured groundwater heads when structures were assigned a different hydraulic conductivity than the rest of the domain (dual-continuum approach). Model fit also improved when inflow from the hilly area was included. In these six cases $K_{structures}$ was always calibrated to be 1–2 orders

of magnitude larger than K_{matrix}, indicating that the structures would be zones of higher permeability. However the seventh conceptual model, which differentiated the coastal resistance across the domain, gave an equally good fit to data. In this model, coastal resistance north of Sian Ka'an was calibrated to be lower than the coastal resistance of the remaining coastline. In this model, there was little difference between K_{matrix} and $K_{structures}$. By comparing output from all models with data published in the literature on e.g. coastal discharge and maximum flows in high permeable zones, both Model 7 and three of the conceptual models which had a constant coastal resistance, were found to be plausible. Only two conceptual models could be rejected based on comparison with system data from the literature. Model 5 was largely similar to Model 4, because the automatically optimized hilly inflow in Model 5 became close to the magnitude of the hilly inflow in Model 4. Model 5 was therefore not included in the further analysis (Gondwe et al., V).

Stochastic modelling of the steady state catchment was carried out with the four accepted models. The results illustrated the effect of model structure uncertainty on the management decisions. It was seen that if structures in reality do have a different hydraulic conductivity than the rest of the domain, then areas in the south-central part of the study area would also contribute with water to Sian Ka'an (Gondwe et al., V) (Fig. 20). Finding out whether these areas are part of the catchment is critical because these are the areas where agricultural activities are expanding, possibly leading to increased use of pesticides and fertilizers.

Travel time zones delineated with transient versions of two of the hydrological models illustrate the significant influence that the choice of conceptual model and effective porosity has on management decisions (Fig. 21). Again the influence of the structures on the areas that need to be protected is clear. The effective porosity controls the travel times, and is an uncertain parameter. In Gondwe et al. (V), scenarios were modelled by calibrating effective porosities so that modelled groundwater velocities would match values reported in the literature.

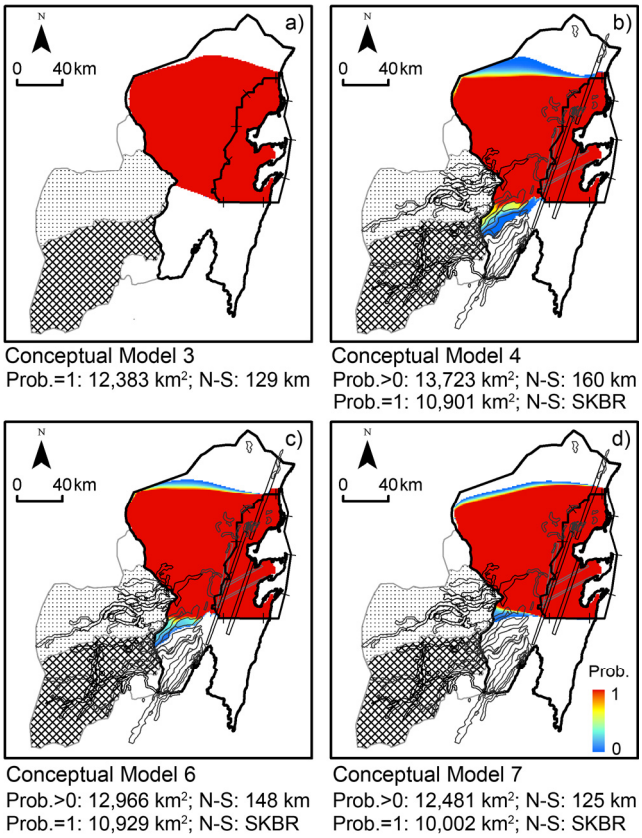

Fig. 20. Probability (Prob.) of a cell belonging to Sian Ka'an's steady state catchment, for Conceptual Models 3, 4, 6 and 7.

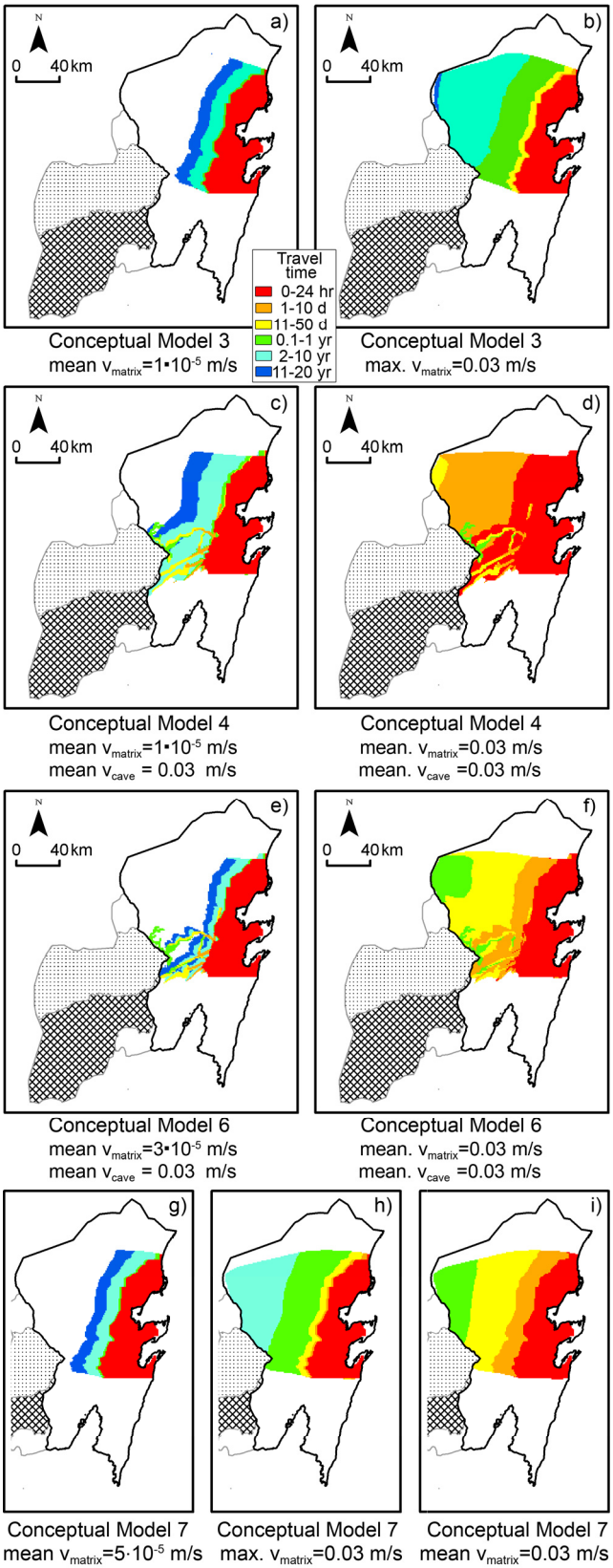

Fig. 21. Modelled travel time zones for different conceptual models and different values of effective porosity, adjusted to give the indicated modelled water travel times (v).

4.3.2 Robust modelling results independent of conceptual model choice

All the plausible hydrological models show that Sian Ka'an's wetlands only exist due to recharge from the catchment. Recharge over Sian Ka'an itself only constitutes on average about 41 mio. m^3/year. In comparison, the total outflow from Sian Ka'an according to the models is ~2700–2900 mio. m^3/year, of which ~280–540 mio. m^3/year exits via the wetlands (overland flow) (Gondwe et al., V).

Recharge to the aquifer in the model domain constitutes 17% ± 3% of the mean annual precipitation (4400 mio. m^3/year ± 700 mio. m^3/year). Results from the automatic calibration indicate that boundary inflows from the hilly area to the model domain may be of similar magnitude. Water exits the domain through overland flow (4–12%) and groundwater flow (88–96%). The latter is distributed between coastal outflow to the sea, and groundwater outflow towards the north via the Holbox fracture zone. Outflow from the domain via the Holbox zone towards the north is in agreement with dye tracing results of Beddows and Hendrickson (2008). However, the magnitude of this Holbox outflow can not be determined with the present range of plausible hydrological models (Gondwe et al., V).

Groundwater outflow through Sian Ka'an's coastal boundary is 68–90 m^3/s. The groundwater that passes through Sian Ka'an is therefore a significant contribution to the marine environment. Hence, if the groundwater that flows into Sian Ka'an is protected, a high water quality for the marine environment, which hosts one of the most productive coral reef systems in the world, can also be ensured (Gondwe et al., V).

The modelled flooding dynamics of Sian Ka'an's wetlands generally corresponds well with the flooding dynamics observed using SAR data. Both show that the timing of Sian Ka'an's flooding peak is different from the timing of the yearly rainfall maximum (Gondwe et al., I; V). This is a further indication that Sian Ka'an's wetland dynamics is controlled by the catchment. The months April to August are the times with least water in the wetlands, and therefore are likely the most vulnerable times of the wetlands, since any water-borne pollutants may be less diluted at these times, and low water amounts may create increased vulnerability to reduction in water quantity. The remaining months of high and medium flows are however also important to maintain the natural cycle of the wetlands (Gondwe et al., V).

5 Conclusions and perspectives

The previous two chapters have summarized the results that answer to the objectives stated with bullet points in Chapter 1. Those results will not be repeated here. Instead this chapter focuses on the general advantages of the presented multi-disciplinary approach applied to study groundwater-dependent ecosystems in karst, as well as on how the results of the research can be applied.

5.1 Advantages of the multi-disciplinary multi-scale approach

When studying data-scarce regional-scale areas as the one investigated in this thesis, it is inconvenient to rely solely on ground-based field data, because they are limited in number and have a limited spatial support scale. Combining ground-based field data with data from remote sensors (aircrafts and satellites) allows the coverage of a greater area, and the investigation of the study area with a wide variety of data types. The methods complement each other, both in information types and in scale. To tackle problems such as the management of Sian Ka'an, a multi-disciplinary and multi-scale approach is needed.

The remotely sensed SAR data used in this study provided information on wetland hydrodynamics. Such data is otherwise difficult to obtain, because wetlands are often vast and largely inaccessible. The remotely sensed data used for recharge estimation enabled spatial estimates of this parameter to be generated. Actual evapotranspiration is generally difficult to estimate, and obtaining estimates for a regional scale requires remote sensing data (e.g. Stisen et al., 2008). The use of remotely sensed precipitation estimates ensures data coverage even over areas not monitored by gauges. A spatial estimate of recharge is more suitable for distributed modelling than point-based estimates, especially when ground-based point density is limited as it often is in real cases (e.g. Brunner et al., 2007). Remotely sensed estimates can sometimes circumvent scaling issues, because the estimates may be provided on the same scale as the regional-scale hydrological model is formulated on (e.g. Grayson et al., 2002).

Ground-based methods are needed to obtain calibration data for groundwater flow models. Groundwater level data can presently only be collected in situ. Likewise, water chemistry data can only be collected as point samples from ground-based field work, but provides useful information about the geology of the subsurface. In the Sian Ka'an case such indirect data were valuable because borehole lithological logs are extremely scarce.

The airborne geophysical measurements gave important information on geological structures and caves on a local to regional scale. The advantage of airborne geophysical measurements is the dense sampling, the ability to access vast areas during short times, and the ability to measure in areas which may otherwise be difficult to access. The approach used in the present study of letting the airborne EM measurements be guided by satellite-derived maps of potential high-permeable zones improved data-collection efficiency, because areas likely to be highly permeable could be targeted. In the case of airborne geophysical measurements used for investigating regional-scale catchments this is important, because the high cost of airborne EM and the large size of the study area means that it will be practically impossible to cover the whole study area completely by airborne EM measurements.

The map of remotely sensed structures also provided an opportunity to upscale airborne EM measurements from transects to the catchment scale. However, in the present case the EM data interpretation was more complex, because the shallow, high-conductive geological layer obstructed the airborne EM sensors from obtaining geological information at depth in the inland areas.

The ground-based geophysical measurements enabled a better interpretation of the airborne EM data. Data from the geoelectric, time-domain EM and borehole logging induction measurements could be used to constrain the inversions. The borehole logging method was able to look beyond the shallow, high-conductive layer in the inland regions. Other ground-based EM methods would not have been able to do so, because the induced current would have been confined to the shallow, high-conductive layer without penetrating further down into the subsurface. Geoelectrics could also have been used to look beyond the shallow anomalous layer in the inland regions, but the method is tedious to apply in the study area, due to difficulties in inserting the electrodes into the hard carbonates that often outcrop beneath a thin or inexistent soil layer. This geology also makes

it difficult to maintain electrical contact between the electrodes and the geology. Applying borehole logging in private wells belonging to ranches gave a relatively good spatial distribution of data, which enabled the distinction of regional geological differences across the study area. Likewise, a relatively good spatial distribution across the study area could be obtained with the ground-based time-domain EM method, so that the regional shape of the freshwater lens could be delineated. As an additional advantage, carrying out ground-based field measurements gave an insight into the functioning of the study area which cannot always be obtained from desktop studies, because ground-based field work enables direct observation as well as discussions with local inhabitants.

Applying hydrological modelling as a method enables the estimation of a water balance. By comparing modelled water fluxes with values estimated in the literature, hydrological modelling of the Sian Ka'an catchment enabled the distinction between plausible and unlikely conceptualizations of the aquifer. Hydrological models are useful tools for delineating catchment areas and travel time zones. Such results are valuable within groundwater management. The use of the results for management is further discussed in the following Chapter 5.2. Moreover, the data collection and the hydrological modelling work have pointed to areas which should be given highest priority in future research efforts. These are discussed in Chapter 5.3.

5.2 Perspectives for management

5.2.1 Management setup for water resources

In Mexico, water is national property according to the Constitution, and is managed by the federal agency Comisión Nacional del Agua (aka. CONAGUA – the National Water Commission), as stipulated in the National Water Act ("Ley de Aguas Nacionales") from 1992, and its revision from 2004. CONAGUA is a relatively new institution. It was formed in 1989, and only in 2004 regional and state offices of CONAGUA were created (Sánchez Meza, 2006). In addition, three different types of decentralized management bodies exist, whose roles are to support CONAGUA: Water Basin Councils, Water Basin Commissions and Technical Committees. Not all types exist in all regions (Escolero et al., 2002). The Yucatan Peninsula, which is one hydrological-administrative region within CONAGUA, has a Water Basin Council. It is comprised of the CONAGUA

director, representatives of different users (irrigation users, water abstraction companies etc.), representatives of federal, state and municipal agencies and societal organizations. The aim of the Water Basin Councils is to develop and implement programs and activities to improve water management and preserve the water resources in the basin (Sánchez Meza, 2006). Although CONAGUA bases some decisions on recommendations from the Basin Council in the Yucatan Peninsula (Merediz Alonso, 2007) the Basin Council itself has no executing power, and agreements made within the Council are not binding (Sánchez Meza, 2006; Vaux, 2007a). Water management is therefore solely the responsibility of CONAGUA at present, although several authors argue for the transfer of power from CONAGUA to decentralized bodies with multiple stakeholder participation, such as the Basin Councils (Sánchez Meza, 2006; Asad and Garduño, 2005; Vaux, 2007a). The responsibility to in practice carry out water abstraction and provide wastewater infrastructure, is authorized to state and sub-state institutions. In the study area this organization is Comisión de Agua Potable y Alcantarillado (CAPA). However, CONAGUA maintains the regulatory power and the overall responsibility for aquifer protection (Sánchez Meza, 2006).

As indicated by the relatively recent institutional development, groundwater management and use of hydrological sciences on a catchment scale is a relatively new field within Mexico. For example a register of the nationwide concessions to extract water was completed as recently as 2002 (Asad and Garduño, 2005) and the first water balance of a river basin in Mexico was made in 2003 (Arreguín-Cortés and López-Pérez, 2007). In Quintana Roo, only about 35 groundwater monitoring stations exist, and are solely located in the part of the state stretching from Tulum northward to Cancun (unpublished data from CONAGUA). The institutional capacity of CONAGUA is presently described as weak with respect to enforcement of the laws (Asad and Garduño, 2005). The water management setup is thus in a developing state. However, although there may be a difference between the aims and objectives of the water management institution, and what is in practice being carried out by it, it is clear that stakeholders and CONAGUA agree on that there is a need for groundwater monitoring (quality and quantity), maintaining a database on water-related datasets and sustainably developing the groundwater resources in the Yucatan Peninsula (Arreguín-Cortés and López-Pérez, 2007; Vaux, 2007a).

5.2.2 Use of the thesis results within water management on short time-scale

An important result of mapping the aquifer thickness, the estimation of recharge and the hydrological modelling of the study area (Gondwe et al. IV; V) is that the available water resources have been assessed for the first time in the region. From this it is clear that groundwater quantity does not appear to be a problem in relation to abstraction rates, except possibly in coastal areas where the freshwater lens is thin and hotel and urban demands may be high. The hydrological modelling results show that in the study area, focus in water management should first and foremost be on protecting groundwater quality. Water, and any associated pollutions, may travel far in a short time – e.g. 6.5 km/day, possibly even tens of kilometers pr. day (Beddows, 2003; Gondwe et al., V). The probability maps of the steady state groundwater catchment of Sian Ka'an and the travel time zones delineated in Gondwe et al. (V) are directly useful for protecting the groundwater quality. In a short-term perspective, these results could be taken into use immediately to guide management initiatives. Within a short time-scale, better information is unlikely to be attained, so although the results show a wide range of uncertainty depending on conceptual model and effective porosity used, authorities should act on these presently available working estimates. In spite of the uncertainty, they represent science-based knowledge on groundwater flow patterns previously unavailable for the area.

Typical tools for managing groundwater in karst are (Kacaroglu, 1999; Escolero et al., 2002; Merediz Alonso, 2007): land use zonation; pollution risk assessment and management; groundwater monitoring; increased public awareness of the value and vulnerability of the aquifer; and a Code of Practice reviewed in detail by Drew and Höltz (1999) and including e.g. highways design, solid wastes and toxic substances management, disposal of municipal sewage, control of seawater intrusion, spring protection and codes dealing with agricultural practices. A first step of implementing groundwater management in karst is the delineation of catchment areas of wells and wetlands. Such results outline the areas on which groundwater protection efforts should in general be focused, and therefore, the catchment probability maps in Gondwe et al. (V) are useful. In Europe, delineating catchments is required by the Water Framework Directive and is also done for karst wetlands, although it is often difficult (Kilroy et al., 2005). The difficulty of obtaining a precise catchment for a karst aquifer is illustrated in the case of Mammoth Cave in USA, where it took hundreds of dye tracing

experiments and >20 years of investigations to ascertain the drainage network (Watson et al., 1997). Uncertainty in catchment delineation is therefore expected within karst, and should not be a justification for lack of action. Rather, being open with regard to the uncertainties of the model results may increase confidence in hydrological models, rather than keeping uncertainties secret, which may raise suspicion and skepticism. Model uncertainty does complicate decision- and policy making, but models without uncertainties are unrealistic. Instead, scenario testing is advocated (Ivanović and Freer, 2009). The results from using different conceptual models are a form of extended scenario testing. When uncertain estimates are involved, using the precautionary principle (e.g. Ivanović and Freer, 2009) or adaptive management (Vaux, 2007b) may be advocated.

Currently there is no legislation on groundwater protection zones in Mexico, neither for ecosystem nor for well protection. Milanović (2004) has suggested criteria which could be used (Table 1), primarily based on travel time zones. Thus, the travel time results could be used to guide land use zonation. With regard to travel times it is also worth noting that bacteria have a 50 day survival rate, while viruses may survive for 1 year (Kacaroglu, 1999).

In addition to Table 1, a new official standard in Mexico (Norma Oficial Mexicana NOM-014-CONAGUA-2003, available on http://dof.gob.mx/nota_detalle.php?codigo=5105753&fecha=18/08/2009), adopted in September 2009, regulates artificial infiltration of wastewater in Mexico. For the first time in Mexico, the travel time zone concept is used. The standard states that travel time from the recharge point of the wastewater to the extraction point should be at least 1 year for the type of infiltration allowed in karst. Although technically this applies only to groundwater abstraction points, it may provide a useful perspective for ecosystem protection in Mexico as well, supporting the use of travel times for protection of resources. The standard could provide the legal framework for the beginning of land use zonation. From modelled depths to groundwater, and actual evapotranspiration rates compared to potential evapotranspiration rates, Gondwe et al., (V) generated maps that showed ecosystems likely to be groundwater-dependent. These maps should also be used in the land use zonation.

Within the zones of importance, active and potential pollution activities should be mapped and possibly relocated, as suggested in Escolero et al. (2000; 2002). Compared to other catchments, the study area is not extensively developed yet. Therefore, if land use regulation is implemented now, it will be easier to enforce strict protection. An example of an activity which should be highly considered within the perspectives outlined in Table 1 is the location of a proposed airport near Tulum. Proposals have included sites atop the Holbox fracture zone. However, airports are known to yield high risks of pollution by leakage of fuels. Gondwe et al. (III) showed that the Holbox zone is likely to be a zone of high permeability. Therefore, locating the airport on this zone would be highly disadvantageous.

Table 1. Criteria for groundwater protection zonation in karst, proposed by Milanović (2004). The importance of regular groundwater monitoring in combination with implementation of the zones was emphasized in Milanović (2004).

		Delineation	**Restrictions**
Zone I	Protection area of spring/well	Min. 50 m from well/spring	Only water supply activities. Protect all karst openings. Prohibited: - public traffic, traffic infrastructure on conduits leading to Zone I - agriculture
Zone II	Very severe protection and restriction	24 hr travel time zone + any sinkholes connected with the well/spring + any sinkholes (and 20–30 m zone around them) located in Zone III but which communicate with the well/spring within 24 hrs	Strict control of all caves, sinkholes, shafts. No use of them for dumping of waste. All houses must have safe and water-tight septic tank. Prohibited: - transport and storage of dangerous materials, esp. low-degradable chemicals and oil tanks - industry - use of pesticides - waste disposal - settlements - roads - railroads - farms - quarries
Zone III	Protection area	E.g. 1–50 days travel time zone + all sinkholes outside Zone II in direct contact with the well/spring + all conduits in contact with the well/spring	All roads and settlements need effective drainage systems. Pesticide use should be strictly controlled. Prohibited: - use of sinkholes for waste dumping - chemical industry - oil tanks
Zone IV	External protection area	Rest of the catchment, with travel times > 50 days Areas with groundwater velocities <1 cm/s	Prohibited: - storage of radioactive material - storage of chemical wastes

5.2.3 Use of the thesis results within water management on long time-scale

On a longer time-scale, vulnerability mapping should be carried out. The use of travel-times for land use zonation is known to give very large areas of maximum protection in karst compared to in other types of aquifers. Protecting such large areas may not be practically possible. Instead, vulnerability mapping is a way to prioritize areas for protection in a science-based way, balancing groundwater protection and socioeconomic considerations (Kacaroglu, 1999; Milanović, 2004; Goldscheider, 2005).

A number of methods for vulnerability mapping of aquifers exist. For porous and fractured media they include DRASTIC (Aller et al., 1987); GOD (Foster, 1987); AVI (Van Stempoort et al., 1993); and the GLA method (aka. the "The German concept") (Hölting et al., 1995). Specifically for karst and carbonate aquifers, the methods include: EPIK (Doerfliger, 1996); SINTACS (Civita and De Maio, 1997); the Irish groundwater protection scheme (Daly and Drew, 1999); REKS (Malik and Svasta, 1999); the PI method (Goldscheider et al., 2000); VULK (Jeannin et al., 2001); the Time-Input-Method (Kralik, 2001); COP (Vías et al., 2004); COP+K (Andreo et al., 2009); LEA (Dunne, 2003); VURAAS (Laimer, 2005); and the Transit Time Method (Brosig et al., 2008). Numerous studies compare the different methods (e.g. Vías et al., 2005; Morales López, 2007). The overall principles of vulnerability mapping are to assess the resource vulnerability spatially by obtaining spatially distributed indexes for the degree of protection by overlying geologic and soil layers, the degree of concentrated inflow and the degree of precipitation intensity and quantity. These indexes may in karst be combined with a spatial assessment of the horizontal flow paths' effect on vulnerability. In the case of the study area, it would be most reasonable to use one of the vulnerability mapping techniques developed for karst. Which one to use should be decided upon by the decision-makers, since they should trust in the method in order to be able to have confidence in and use the results. The modelling results of the present study, which are directly applicable within vulnerability mapping, are depth to groundwater table and the geological structure maps. Vulnerability mapping was carried out in a sub-set of the study area around Tulum in a study by Morales López (2007). The study contains an exhaustive review of the approach step by step. This example could be imitated for the rest of the catchment area delineated by the hydrological modelling results. In the Tulum area, the aquifer was found to be 'extremely vulnerable' in

a belt 0–10 km from the coast and 'highly vulnerable' further inland (Morales López, 2007).

Vulnerability mapping should be integrated into a groundwater protection scheme, and may be validated e.g. by tracer tests (Goldscheider, 2001; Goldscheider, 2005). Vulnerability maps can be coupled with hazard maps (detailed mapping of possible polluting activities) to generate risk maps. An elaborate example of how this may be done is found in e.g. Mimi and Assi (2009). Land use zonation could then be based on the risk map. Another form of risk assessment in karst has been carried out using quantitative groundwater tracing, as detailed in Field and Nash (1997).

A long term groundwater management solution, which is not directly related to the modelling results, is implementation of cleaner technology. For instance, artificial wetlands and composting toilets have been advocated for in order to deal with Quintana Roo's wastewater (Beddows, 2002; Morales López, 2007; Krekeler, 2007). City-wide sewage and wastewater treatment have elsewhere in the Peninsula been stated to be unlikely due to high economic costs (Marin et al., 2000). Cleaner technology could also be implemented with respect to e.g. design of highways (Drew and Höltz, 1999) and landfills (Morales López, 2007 and references herein). Technological advances may also be applied to solve the groundwater *quantity* problems which may exist or develop along the coasts, through the implementation of water-saving initiatives and technologies. Improved water distribution infrastructure may also be required. In an example from Yucatan State, the distribution system was pointed out to be reason for loss of as much as 50% of the water abstracted from the aquifer (Marin et al., 2000).

Finally, compensation schemes have been suggested on a long-term, as part of a land use zonation program, in order to protect critical recharge areas in the catchments (Gondwe et al., 2010). The idea is to create a fund with money from water fees collected from the large tourist resorts. This money should then be used to compensate landowners in the critical recharge areas, in order to provide incentive to preserve the land in a pristine state and prevent polluting activities.

The above-mentioned actions deal with threats to the groundwater which are created by local human activity. Another threat, which has not been dealt with in the research of the thesis, is the threat from global climate changes. Central

America is a climate change hotspot. A regional climate model has predicted a 40% reduction in rainy season precipitation (May–Oct) using the Intergovernmental Panel for Climate Change's A2 scenario for the year 2100, that represents a heterogeneous world with substantial population growth (Karmalkar et al., 2009). Other climate change scenarios used in other climate models also predict a reduction in precipitation over the study area (e.g. Neelin et al., 2006; Christensen et al., 2007). A reduction in precipitation will likely mean a reduction of recharge to the aquifer. In a long-term perspective this would mean a decrease in the volumes of freshwater in the aquifer and a thinner freshwater lens. The latter could give a higher susceptibility to up-coning of saltwater during water abstraction, mainly near the coasts. Less rainfall could also give higher concentrations of groundwater pollutants, due to reduced dilution. For Sian Ka'an's wetlands, reduction in the precipitation amounts could change the length of the hydroperiod, which could have consequences for the ecosystems. Likewise a change in the precipitation patterns could affect the hydroperiod distribution patterns, which are also important for wetland ecosystem functioning. Potential sea level changes, caused by climate changes, would also affect Sian Ka'an's ecosystems, as they are low-lying and coastal. The impact depends on the magnitude of sea level change, and can best be predicted if better micro-topographic maps of Sian Ka'an become available. Possible sea level rises of 19 cm to 1 m by year 2100 have been mentioned (Meehl et al., 2007; Painter, 2009). A higher sea level would likely flood parts of Sian Ka'an's wetlands with saltwater, which could give changes in the ecosystem distribution.

5.3 Future research directions

Future research directions within the catchment of Sian Ka'an should mainly focus on obtaining more data on the catchment, and feeding it into the existing models. It is still required to mainly work on a large scale. The Multiple Model Simulation and scenarios to investigate the impact of input parameter uncertainty (Gondwe et al., V) showed that the present hydrological models developed are not yet robust. However, their results indicate the way forward. With more data improved models can be built or extracted from the conceptual models presented. The modelling results indicated where it would be worthwhile to focus future efforts for characterization and management of Sian Ka'an's catchment. The main points are: characterizing the nature of the structures; determining better the

travel times and effective porosities within the catchment; investigating the flow within the Holbox fracture zone; determining coastal leakage; and further investigating the role of the hilly area for Sian Ka'an's catchment.

The differences between the conceptual models showed that it is important to further investigate the properties of the structures – specifically whether or not they conduct water flow more easily than the surrounding matrix. The properties of the structures could be investigated through geophysical measurements, direct drillings into the structures and flow measurements within and outside structures.

Dye tracing and/or testing with other tracers could be carried out in the zones likely to be part of the short groundwater travel-time zones, in order to better determine the value of the effective porosity, and the extent of the travel time zones. Dye tracing can yield useful results, such as mean residence time, mean flow velocities, dispersivity data and conduit geometric parameters useful for further detailed groundwater transport modelling (Field and Nash, 1997).

Quantification and characterization (e.g. temporally) of the flow through the Holbox fracture zone would be useful in order to determine whether the high flows simulated in Conceptual Model 3, 4 and 6 are realistic, or the outflows from Model 7 appear more reasonable (see Gondwe et al., V). Besides determining which conceptual model is more plausible, such a quantification might also be able to narrow down the uncertainty on the recharge estimate, as it was seen that the Holbox outflow was sensitive to variations in the recharge estimate (and, to a smaller degree, sensitive to the variations in the Holbox fixed head boundary level). Investigations of the Holbox flow could for instance be carried out using flow-meters inserted into some of the many sinkholes atop the Holbox zone, and possibly through dye tracing.

If it would be possible to measure or estimate total groundwater outflow along the coast of Sian Ka'an the uncertainty on the recharge input could be minimized, since this outflow is of the same magnitude in spite of which conceptual model is used. Identification of submarine springs along Sian Ka'an's coast and measurements of their outflow could be a first-order approach to this, although it is expected to be a tedious and costly affair, as the submarine springs are likely to be numerous. Furthermore, the results would be highly uncertain, since a large part of the outflow is expected to also take place through the aquifer matrix. If it

could be determined whether leakage appears larger at the northern part of the coast around Tulum than in the remaining coastline of the domain, such investigation could – together with the structure properties analysis – enable determination of whether Conceptual Model 4 or 7 is more likely.

The present plausible hydrological models indicate that inflow from the Cretaceous area to the Pliocene geology may be important. However the extent of the catchment in the hilly, Cretaceous region has not been explored. The similarity between Conceptual Model 4 and 5 indicates that the surface water catchments delineated in the hilly area may indeed be related to groundwater catchments in this area (Gondwe et al., V). These surface water catchments may be an acceptable first order approach to determine where the water in the hilly area comes from. However, further studies of the hilly area's hydrogeology are warranted. A better conceptualization could enable the inclusion of this area into a distributed hydrological model which could give an improved spatial understanding and zonation of the catchment. In addition, the extent of the model domain, especially along the western boundary, should be checked, to ensure that areas further west do not influence the hydrology of Sian Ka'an.

Finally, although not a research direction per se, an important measure to implement in the future is a dense monitoring network of groundwater heads, flows and quality. Monitoring data with a representative spatial and temporal resolution are absolutely essential both for the understanding and modelling of the water resources of the area, and for the management of these resources. CONAGUA, as the responsible agency, should ensure that an effective monitoring system is implemented in the region as soon as possible.

6 References

Acreman, M., Dunbar, M.J., 2004. Defining environmental river flow requirements – a review. Hydrol. and Earth Syst. Sci. 8 (5), 861–876.

Al-fares, W., Bakalowicz, M., Guérin, R., Dukhan, M., 2002. Analysis of the karst aquifer structure of the Lamalou area (Hérault, France) with ground penetrating radar. J. Applied Geophysics 51, 97–106.

Aller, L., Bennet, T., Lehr, J.H., Petty, R.J., 1987. DRASTIC: a standardized system for evaluating ground water pollution potential using hydrogeological settings. U.S. Environmental Protection Agency Report EPA-600/2-87-035. 622 pp.

Alsdorf , D.E., Melack, J.M., Dunne, T., Mertes, L.A.K., Hess, L.L., Smith, L.C., 2000. Interferometric radar measurements of water level changes on the Amazon floodplain. Nature 404, 174–177.

Alsdorf, D.E., Smith, L.C., Melack, J.M., 2001. Amazon floodplain water level changes measured with interferometric SIR-C radar. IEEE Transactions on Geoscience and Remote Sensing 39, 423–431.

Alsdorf, D.E., Rodríguez, E., Lettenmaier, D.P., 2007a. Measuring surface water from space. Reviews of Geophysics 45, RG2002. 24 pp.

Alsdorf, D., Bates, P., Melack, J., Wilson, M., Dunne, T., 2007b. Spatial and temporal complexity of the Amazon flood measured from space. Geophysical Research Letters 34, L08402. doi:10.1029/2007GL029447.

Andreo, B., Ravbar, N., Vías, J.M., 2009. Source vulnerability mapping in carbonate (karst) aquifers by extension of the COP method: application to pilot sites. Hydrogeol. J. 17, 749–758. doi: 10.1007/s10040-008-0391-1.

Amelung, F., Galloway, D.L., Bell, J.W., Zebker, H.A., Laczniak, R.J., 1999. Sensing the ups and downs of Las Vegas: InSAR reveals structural control of land subsidence and aquifer-system deformation. Geology 27, 483–486.

Archie, G.E., 1942. The electrical resistivity log as an aid in determining some reservoir characteristics. T. Am. Inst. Mineral. Metall. Petrol. Eng. 146, 54–62.

Arfib, B., de Marsily, G., 2004. Modeling the salinity of an inland coastal brackish karstic spring with a conduit-matrix model. Water Resour. Res. 40 (11), W115061–W1150610.

Arreguín-Cortés, F., López-Pérez, M., 2007. An overview of Mexico's water regime and the role of groundwater. p. 13–26 in: Holliday, L., Marin, L., Vaux, H. (Eds.). Sustainable management of groundwater in Mexico: Proceedings of a Workshop (Series: Strengthening science-based decision making in developing countries). National Research Council. The National Academies Press, Washington D.C., USA. ISBN: 0-309-10583-8.

Asad, M., Garduño, H., Water resources management in Mexico: The role of the Water Rights Adjustment Program (WRAP). Sustainable Development Working Paper No. 24. 34636. The World Bank, Latin America and the Caribbean Region, Environmentally and Socially Sustainable Development Department. 73 pp.

ASK, 2003. Tratamiento de Aguas Residuales. Report prepared by Amigos de Sian Ka'an A. C. (ASK). Available on the cd-rom of the workshop: Construyendo las Bases Para la Conservación del Agua y su Biodiversidad Asociada en la Península de Yucatan". 10 y 11 de noviembre 2003, Cancún Quintana Roo,

Organizado por Amigos de Sian Ka'an, The Nature Conservancy y la Comisión de Áreas Naturales Protegidas.

Atkinson, T.C., 1977. Diffuse flow and conduit flow in limestone terrain in the Mendip Hills, Somerset (Great Britain). J. Hydrol. 35, 93–110.

Auken, E., Guerin, R., de Marsily, G., Sailhac, P., 2009. Hydrophysics foreword. Comptes Rendus Geoscience 341 (10–11), 795–799. doi: 10.1016/j.crte.2009.09.003.

Avdeev, D.B., 2005. Three-dimensional electromagnetic modelling and inversion from theory to application. Surveys in Geophysics 26, 767–799.

Back, W., Hanshaw, B.B., 1970. Comparison of chemical hydrogeology of the carbonate peninsulas of Florida and Yucatan. J. Hydrol. 10, 330–368.

Back, W., Lesser, J.M., 1981. Chemical constraints of groundwater management in the Yucatan Peninsula, Mexico. J. Hydrol. 51, 119–130.

Back, W., Hanshaw, B., Herman, J.S., Van Driel, J.N., 1986. Differential dissolution of a Pleistocene reef in the ground-water mixing zone of coastal Yucatan, Mexico. Geol. 14, 137–140.

Bakalowicz, M., 2005. Karst groundwater: a challenge for new resources. Hydrogeol. J. 13, 148–160. doi: 10.1007/s10040-004-0402-9.

Barfield, B.J., Felton, G.K., Stevens, E.W., McCann, M., 2004. A simple model of karst spring flow using modified NRCS procedures. J. Hydrol. 287, 34–48.

Batu, V., 1998. Aquifer hydraulics: a comprehensive guide to hydrogeologic data analysis. Wiley-IEEE. 727 pp. ISBN: 0-471-18502-7.

Bauer, S., 2002. Simulation of the genesis of karst aquifers in carbonate rocks. Tübinger Geowissenshaftliche Arbeiten, Vol. 62. Reihe C. Institut und Museum für Geologie und Paäontologie der Universität Tübingen. Tübingen, Germany. 143 pp.

Bauer, S., Liedl, R., Sauter, M., 2003. Modeling of karst aquifer genesis: influence of exchange flow. Water Resour. Res. 39 (10), SBH61–SBH612.

Bauer-Gottwein, P., Gondwe, B.N., Christiansen, L., Herckenrath, D., Kgotlhang, L., Zimmermann, S., 2010. Hydrogeophysical exploration of three-dimensional salinity anomalies with the time-domain electromagnetic method (TDEM). J. Hydrol. 380 (3–4), 318–329. doi: 10.1016/j.jhydrol.2009.11.007.

Bautista, F., Quintana, P., Aguilar Duarte, Y., Pacheco, J., Cabañas, D., 2009. Programa General. Seminario: Análisis de la vulnerabilidad y riesgo de contaminación de las aguas subterráneas en la Península de Yucatán. Mérida, Yucatán, 10–11 December 2009.

Beddows, P.A., 2002. Where does the sewage go? The karst groundwater system of Municipalidad Solidaridad, Quintana Roo. Assoc. for Mex. Cave Stud. Activities Newsl. 25, 47–52.

Beddows, P.A., 2003. Cave hydrology of the Caribbean Yucatan coast. Assoc. for Mex. Cave Stud.. Bull. 11. Austin, TX, USA.

Beddows, P.A., 2004. Groundwater hydrology of a coastal conduit carbonate aquifer: Caribbean coast of the Yucatán Peninsula, México. PhD thesis. Sch. of Geogr. Sci.. Univ. of Bristol, UK.

Beddows, P.A., Smart, P.L., Whitaker, F.F., Smith, S.L., 2007. Decoupled fresh-saline groundwater circulation of a coastal carbonate aquifer: Spatial patterns of temperature and specific electrical conductivity. J. Hydrol. 346, 18–32.

Beddows, P.A., Hendrickson, M.R., 2008. When the survey is not enough: temperature, salinity and dye tracing reveal flow paths. p. 198–203 in: Elliott, W.R. (Ed.). Proceedings of the 18th National Cave and Karst Management Symposium, St. Louis, USA.

Beres, M., Luetscher, M., Olivier, R., 2001. Integration of ground-penetrating radar and microgravimetric methods to map shallow caves. J. Applied Geophysics 46, 249–262.

Berg, R.R., 1970. Method for determining permeability form reservoir rock properties. T. Gulf Coast Assoc. Geol. Soc. 20, 303–317.

Berry, P.A.M., Garlick, J.D., Freeman, J.A., Mathers, E.L., 2005. Global inland water monitoring from multi-mission altimetry. Geophysical Research Letters 32, L16401. doi: 10.1029/2005GL022814.

Birk, S., 2002. Characterization of karst systems by simulating aquifer genesis and spring responses: model development and application to gypsum karst. Tübinger Geowissenshaftliche Arbeiten, Vol. 60. Reihe C. Institut und Museum für Geologie und Paäontologie der Universität Tübingen. Tübingen, Germany. 122 pp. ISSN: 1610-4706. Accessed at http://tobias-lib.uni-tuebingen.de/volltexte/2002/558/pdf/tga_c60.pdf in Jan 2010.

Birk, S., Liedl, R., Sauter, M., Teutsch, G., 2003. Hydraulic boundary conditions as a controlling factor in karst genesis: a numerical modeling study on artesian conduit development in gypsum. Water Resour. Res. 39 (1), SBH21–SBH214.

Block, P., Souza Filho, F.A., Sun, L., Kwon, H.-H., 2009. A streamflow forecasting framework using multiple climate and hydrological models. J. Am. Water Res. Assoc. 45 (4), 828–843. doi: 10.111/j.1752-1688.2009.00327.x.

Bosch, F., Müller, I., 2005. Improved karst exploration by VLF-EM gradient surveys: comparison with other geophysical methods. Near Surf. Geophys. 3, 299–310.

Boucher, M., Girard, J.-F., Legchenko, A., Baltassat, J.-M., Dörfliger, N., Chalikakis, K., 2006. Using 2D inversion of magnetic resonance soundings to locate a water-filled karst conduit. J. Hydrol. 330, 413–421.doi: 10.1016/j.jhydrol.2006.03.034.

Bourgeau-Chavez, L.L., Smith, K.B., Brunzell, S.M., Kasischke, E.S., Romanowicz, E.A., Richardson, C.J., 2005. Remote monitoring of regional inundation patterns and hydroperiod in the Greater Everglades using synthetic aperture radar. Wetlands 25, 176–191.

Brosig, K., Geyer, T., Subah, A., Sauter, M., 2008. Travel time based approach for the assessment of vulnerability of karst groundwater: the Transit Time Method. Environ. Geol. 54, 905–911. doi: 10.1007/s00254-007-0898-0.

Brunner, P., Hendricks Franssen, H.-J., Kgotlhang, L., Bauer-Gottwein, P., Kinzelbach, W., 2007. How can remote sensing contribute in groundwater modeling? Hydrogeol. J. 15, 5–18. doi: 10.1007/s10040-006-0127-z.

Bürgmann, R., Rosen, P.A., Fielding, E.J., 2000. Synthetic aperture radar interferometry to measure Earth's surface topography and its deformation. Annu. Rev. Earth Planet. Sci. 28, 169–209.

Chen, C.W., Zebker, H.A., 2001. Two-dimensional phase unwrapping with use of statistical models for coast functions in nonlinear optimization. J. Opt. Soc. Amer. A 18, 338–351.

Cheng, J.M, Chen, C.X., 2005. An integrated linear/non-linear flow model fort he conduit-fissure-pore media in the karst triple void aquifer system. Environ. Geol., 47, 163–174. doi: 10.1007/s00254-004-1128-7.

Chib, S., Greenberg, E., 1995. Understanding the Metropolis-Hastings algorithm. The American Statistician 49 (4), 327–335.

Chow, V.T. Maidment, D.R., Mays, L.W., 1988. Applied hydrology. McGraw-Hill Series in Water Resources and Environmental Engineering. Singapore. 1988. ISBN 0-07-100174-3. 572 pp.

Christensen, J.H., Hewitson, B., Busuioc, A., Chen, A., Gao, X., Held, I., Jones, R., Kolli, R.K., Kwon, W.-T., Laprise, R., Magaña Rueda, V., Mearns, L., Menéndez, C.G., Räisänen, J., Rinke, A., Sarr, A., Whetton, P., 2007. Regional climate projections. In: Solomon, S., Qin, D., Manning, M., Chen, Z., Marquis, M., Averyt, K.B., Tignor, M., Miller, H.L. (Eds.). Climate Change 2007: The Physical Science Basis. Contribution of Working Group I to the Fourth Assessment Report of the Intergovernmental Panel on Climate Change. Cambridge University Press, Cambridge, United Kingdom and New York, NY, USA.

Christiansen, A.V., Auken, E., Sørensen, K., 2006. The transient electromagnetic method. Chapter 6 in: Kirsch, R. (Ed.), Groundwater geophysics – A tool for hydrogeology. Springer. ISBN: 3-540-29383-3.

Civita, M., De Maio, M., 1997. SINTACS – Un sistema parametric per la valtazione e la cartografia della vulnerabilitá degli acquiferi all' inquinamento. Metodologia & automatizzazione (SINTACS – a parametrical system for assessment and vulnerability mapping of aquifer pollution). Collana "Quaderni di Techniche di Protezione Ambientale" 60, 208 pp.

Clemens, T., 1998. Simulation der Entwicklung von Karstaquiferen. PhD dissertation submitted to Eberhard-Karls Universtät Tübingen, Germany.

Coppo, N., Schnegg, P.-A., Défago, M., GSCB, 2006. Mapping a shallow large cave using a high-resolution Very Low Frequency electromagnetic method. p. 71–74 in Goldscheider, N., Mudry, J., Savoy, L., Zwahlen, F. (Eds.). Proceeding of the 8th conference on limestone hydrogeology, 2006, Neuchätel, Switzerland. ISBN 2-87867-143-2.

Cornaton, F., Perrochet, P., 2002. Analytical 1D Dual-Porosity Equivalent Solutions to 3D Discrete Single-Continuum Models. Application to Karstic Spring Hydrgraph Modelling. J. Hydrol. 262, 165–176.

Dalton, F.N., Herkelrath, W.N., Rawlins, D.S., Rhoades, J.D., 1984. Time-domain reflectometry – simultaneous measurement of soil-water content and electrical-conductivity with a single probe. Science 224, 989–990.

Daly, D., Drew, D., 1999. Irish methodologies for karst aquifer protection. p. 267–272 in: Beck, B.F., Pettit, A.J. and Herring, J.G. (Eds.). Hydrogeology and Engineering geology of sinkholes in karst. Balkema, Rotterdam, The Netherlands. ISBN: 9-0580-9046-9.

Daniels, J., 1988. Locating caves, tunnels and mines. Geophysics: The Leading Edge of Exploration. 32–52.

Doerfliger, N., 1996. Advances in karst groundwater protection strategy using artificial tracer tests analysis and multiattribute vulnerability mapping (EPIK Method). PhD thesis. University Neuchâtel. 308 pp.

Doll, W.E., Nyquist, J.E., Beard, L.P., Gamey, T.J., 2000. Airborne geophysical surveying for hazardous wast site characterization on the Oak Ridge Reservation, Tennessee. Geophys. 65 (5), 1372–1387.

Doolittle, J., Collins, M., 1998. A comparison of EM and GPR methods in areas of karst. Geoderma 85, 83–102.

Drew, D.P., Höltz, H., 1999. The management of karst environments. pp. 259–273 in : Drew, D.P., Höltz, H. (Eds.). Karst hydrogeology and human activities. Impacts, consequences and implications. IAH International Contributions to Hydrogeology 20. A.A. Balkema, Rotterdam, The Netherlands. ISBN: 9-0541-0464-3.

Dunne, S., 2003. Vulnerability mapping for the protection of UK karst aquifers. PhD thesis. Geography Department, Trinity College Dublin, Ireland.

Durlofsky, L.J., 1992. Representation of grid block permeability in course scale models of randomly heterogeneous porous media. Water Resour. Res. 28 (7), 1791–1800.

Eamus, D., Froend, R., 2006. Groundwater-dependent ecosystems: the where, what and why of GDEs. Aust. J. of Bot. 54, 91–96.

Ernstson, K., Kirsch, R., 2006. Aquifer structures: fracture zones and caves. Chapter 13 in in: Kirsch, R. (Ed.), Groundwater geophysics – A tool for hydrogeology. Springer. ISBN: 3-540-29383-3.

Escolero, O.A., Marin, L.E., Steinich, B., Pacheco, J., 2000. Delimitation of a hydrogeological reserve for a city within a karstic aquifer: the Merida, Yucatan example. Landsc. and Urban Plan. 51, 53–62.

Escolero, O.A., Marin, L.E., Steinich, B., Pacheco, J., 2002. Development of a protection strategy of karst limestone aquifers: The Merida Yucatan, Mexico case study. Water Resour. Manage. 16, 351–367.

Ferré, T., Bentley, L., Binley, A., Linde, N., Kemna, A., Singha, K., Holliger, K., Huisman, J.A., Minsley, B., 2009. Critical steps for the continuing advancement of hydrogeophysics. EOS Trans. AGU 90 (23). doi: 10.1029/2009EO230004.

Fideicomiso para la Promoción Turística de la Rivera Maya, 2006. Resumen de la actividad turistica 2005. Power Point presentation obtained from the Fideicomiso.

Field, M.S., Nash, S.G., 1997. Risk assessment methodology for karst aquifers: (1) Estimating karst conduit flow parameters. Environ. Monitoring and Assessment 47, 1–21.

Ford, D.C., Williams, P., 2007. Karst hydrogeology and geomorphology. Chichester, Wiley. ISBN: 978-0-470-84997-2. 576 pp.

Foster, S., 1987. Fundamental concepts in aquifer vulnerability, pollution risk and protection strategy. In: Van Duijvenbooden, W., Van Waegeningh, H.G. (Eds.). Vulnerability of soil and groundwater to pollutants. Proc. Inf. TNO Comm. Hydrol. Res., The Hague, The Netherlands 68, 69–86.

Foster, J., Brooks, B., Cherubini, T., Chacat, C., Businger, S., Werner, C.L., 2006. Mitigating atmospheric noise for InSAR using a high resolution weather model. Geophysical Research Letters 33, L16304. doi: 10.1029/2006GL026781.

Fouke, B.W., Zerkle, A.L., Alvarez, W., Pope, K.O., Ocampo, A.C., Wachtman, R.J., Grajales Nishimura, J.M., Claeys, P., Fischer, A.G.., 2002. Cathodoluminescence petrography and isotope geochemistry of KT impact ejecta deposited 360 km from the Chicxulub crater, at Albion Island, Belize. Sedimentol. 49, 117–138.

Gamey, T. J., Thompson, M., Mandell, W., Frano, G., 2001. Karst pathway delineation using combined spatial and geophysical analysis at Camp Crowder, Missouri. In Abstracts with Programs, Geol. Soc. Am. 33 (6), 132.

Georgakakos, K., Seo, D.-J., Gupta, H., Shaake, J., Butts, M.B., 2004. Towards the characterization of streamflow simulation uncertainty through multimodel ensembles. J. Hydrol. 298, 222–241. doi: 10.1016/j.jhydrol.204.03.037.

Ghiglia, D.C., Pritt, M.D., 1998. Two-dimensional phase unwrapping: theory, algorithms and software. Wiley Interscience. 493 pp.

Goldman, M., Gilad, D., Ronen, A., Melloul, A., 1991. Mapping of seawater intrusion into the coastal aquifer of Israel by the time domain electromagnetic method. Geoexplor. 28 (2), 153–174. doi: 10.1016/0016-7142(91)90046-F.

Goldscheider, N., Klute, M., Sturm, S., Hötzl, H., 2000. The PI method: a GIS-based approach to mapping groundwater vulnerability with special consideration of karst aquifers. Z. Angew. Geol. 463, 157–166.

Goldscheider, N., Hötzl, H., Fries, W., Jordan, P., 2001. Validation of a vulnerability map (EPIK) with tracer tests. 7th Conference on Limestone Hydrology and Fissured Media. Besancon, France, 20–22 Sept. 2001. Sci. Tech. Environ. Mém. 13, 167–170.

Goldscheider, N., 2005. Karst groundwater vulnerability mapping: application of a new method in the Swabian Alb, Germany. Hydrogeol. J. 13 (4), 555–564.

Goldstein, R.M., Zebker, H.A., Werner, C.L., 1988. Satellite radar interferometry - two-dimensional phase unwrapping. Radio Science 23, 713–720.

Goldstein, R.M., Engelhardt, H., Kamb, B., Frolich, R.M., 1993. Satellite radar interferometry for monitoring ice-sheet motion - Application to an Antarctic ice stream. Science 262, 1525−1530.

Gondwe, B.N., Bauer-Gottwein, P., Merediz-Alonso, G., Fregoso, A., Supper, R., 2010. Groundwater resources management in Quintana Roo, Mexico: Problems, scientific tools and policy. In: Friedman, M.J. (Ed.): Global water issues. U.S. Department of State, Bureau of International Information Programs. In press.

González-Herrera, R, Sánchez-y-Pinto, I., Gamboa-Vargas, J., 2002. Groundwater-flow modeling in the Yucatan karstic aquifer, Mexico. Hydrogeol. J. 10, 539–552.

Grajales-Nishimura, J.M., Cedillo-Pardo, E., Rosales-Domínguez, C., Morán-Zenteno, D.J., Alvarez, W., Claeys, P., Ruíz-Morales, J., García-Hernández, J., Padilla-Avila, P., Sánchez-Ríos, A., 2000. Chicxulub impact: the origin of reservoir and seal facies in the southeastern Mexico oil fields. Geol. 28 (4), 307–310.

Grayson, R.B., Blöschl, G., Western, A.W., McMahon, T.A., 2002. Advances in the use of observed spatial patterns of catchment hydrological response. Advances in Water Resources 25, 1313–1334.

Grecu, M., Olson, W.S., 2006. Bayesian estimation of precipitation from satellite passive microwave observations using combined radar-radiometer retrievals. J. of Applied Meteorology and Climatology 45, 416–433.

Groom, R., Alvarez, C., 2002. 3D EM modelling application of the localized non-linear approximator to near surface applications. Abstract, SAGEEP 2002. Accessed from URL: www.petroseikon.com in December 2007.

Guérin, R., Benderitter, Y., 1995. Shallow karst exploration using MT-VLF and DC resistivity methods. Geophys. Prospect. 43, 635–653.

Guérin, R., Baltassat, J.-M., Boucher, M., Chalikakis, K., Galibert, P.-Y., Girard, J.-F., Plagnes, V., Valois, R., 2009. Geophysical characterization of karstic networks - Application to the Ouysse system (Poumeyssen, France). Comptes Rendous Géoscience. doi: 10.1016/j.crte.2009.08.005.

Hackert, C.L., Parra, J.O., 2003. Estimating scattering attenuation from vugs or karsts. Geophysics 68 (4), 1182–1188.

Halihan, T., Wicks, C. M., 1998. Modeling of Storm Responses in Conduit Flow Aquifers with Reservoirs. J. Hydrol. 208, 82–91.

Hanshaw, B.B., Back, W.,1980. Chemical mass-wasting of the northern Yucatan Peninsula by groundwater dissolution. Geol., 8, 222–224.

Hanssen, R. F., 2001. Radar interferometry – data interpretation and error analysis. Remote Sensing and Digital Image Processing Series. Kluwer Academic Publishers, Dordrecht, The Netherlands. ISBN: 0-7923-6945-9.

Hastings, W.K., 1970. Monte Carlo sampling methods using Markov chains and their applications. Biometrika 57 (1), 97–109.

Henderson, F.M., Lewis, A.J., 2008. Radar detection of wetland ecosystems: a review. International Journal of Remote Sensing 29 (20), 5809–5835. doi: 10.1080/01431160801958405.

Hendricks Franssen. H.-J., Stauffer, F., Kinzelbach, W., 2004. Joint estimation of transmissivities adn recharges – application: stochastic characterization of well capture zones. J. Hydrol. 294, 87–102. doi: 10.1016/j.jhydrol.2003.10.021.

Henson, H., Sexton, J., Henson, M., Jones, P., 1997. Georadar investigation of karst in a limestone quarry near Anna. 67th Ann. Internat. Meet. SEG, 763–767.

Hess, L.L., Melack, J.M., Simonette, D.S., 1990. Radar detection of flooding beneath the forest canopy: a review. Int. J. Remote Sens. 5, 1313–1325.

Hess, L.L., Melack, J.M., Filoso, S., Wang, Y., 1995. Delineation of inundated area and vegetation along the Amazon floodplain with the SIR-C synthetic aperture radar. IEEE Transactions on Geoscience and Remote Sensing 33 (4), 896–904.

Hess, L.L., Melack, J.M., Novo, E.M.L.M., Barbosa, C.C.F., Gastil, M., 2003. Dual-season mapping of wetland inundation and vegetation for the central Amazon basin. Remote Sensing of Environment 87, 404–428. doi:10.1016/j.rse.2003.04.001.

Hinsby, K., Condesso de Melo, M.T., Dahl, M., 2008. European case studies supporting the derivation of natural background levels and groundwater threshold values for the protection of dependent ecosystems and human health. Sci. Total Environ. 401, 1–20. doi: 10.1016/j.scitotenv.2008.03.018.

Holliday, L., Marin, L., Vaux, H. (Eds.), 2007. Sustainable management of groundwater in Mexioc: Proceedings of a Workshop (Series: Strengthening science-based decision making in developing countries). National Research Council. The National Academies Press, Washington D.C., USA. 126 pp. ISBN: 0-309-10583-8.

Hölting, B., Haertle, T., Hohberger, K.H., Nachtigall, K.H., Villinger, E., Weinzierl, W., Wrobel, J.P., 1995. Konzept zur Ermittlung der Schutzfunktion der Grundwasserüberdeckung (Concept of protection assessment of the groundwater ocver). Geologisches Jahrbuch C63, Hannover, Germany. 5–24.

Hornberger, G.M., Raffensperger, J.P., Wiberg, P.L., Eshleman, K.N., 1998. Elements of physical hydrology. The Johns Hopkins University Press. Baltimore and London. ISBN: 0-8018-5856-9. 302 pp.

Hückinghaus, D., 1998. Simulation der Aquifergenese und des Wärmetransports in Karstaquiferen. Tübinger Geowissenshaftliche Arbeiten, Vol. 42. Reihe C. Institut und Museum für Geologie und Paäontologie der Universität Tübingen. Tübingen, Germany. 124 pp. ISSN: 1610-4706. Accessed at http://tobias-lib.uni-tuebingen.de/volltexte/2005/2030/pdf/42.pdf in Jan 2010.

Hudson, P.F., Colditz, R.R., 2003. Flood delineation in a large and complex alluvial valley, lower Pánuco basin, Mexico. J. Hydrol. 280, 229–245. doi: 10.1016/S0022-1694(03)00227-0.

Højberg, A.L., Refsgaard, J.C., 2005. Model uncertainty – parameter uncertainty versus conceptual models. Water Sci. and Technol. 52 (6), 177–186.

Islam, M.A., Thenkabail, P.S., Kulawardhana, R.W., Alankara, R., Gunasinghe, S., Edussriya, C., Gunawardana, A., 2008. Semi-automated methods for mapping wetlands using Landsat ETM+ and SRTM data. Int. J. Remote Sens. 29 (24), 7077–7106. doi: 10.1080/01431160802235878.

Ivanović, R.F., Freer, J.E., 2009. Science versus politics: truth and uncertainty in predictive modelling. Hydrological Processes 23, 2549–2554. doi: 10.1002/hyp.7406.

Jeannin, P.-Y., 2001. Modeling Flow in Phreatic and Epiphreatic Karst Conduits in the Hölloch Cave (Muotatal,Switzerland). Water Resour. Res. 37 (2), 191–200.

Jeannin, P.Y., Cornaton, F., Zwahlen, F., Perrochet, P., 2001. VULK: a tool for intrinsic vulnerability assessment and validation. 7th Conference on Limestone Hydrology and Fissured Media. Besancon, France, 20–22 Sept. 2001. Sci. Tech. Environ. Mém. 13, 185–190.

Kacaroglu, F., 1999. Review of groundwater pollution and protection in karst areas. Water, Air and Soil Pollution 113, 337–356.

Kafri, U., Goldman, M., 2005. The use of the time domain electromagnetic method to delineate saline groundwater in granular and carbonate aquifers and to evaluate their porosity. J. Applied Geophys. 57, 167–178. doi: 10.1016/j.jappgeo.2004.09.001.

Karmalkar, A.V., Bradley, R.S., Diaz, H.F., 2009. Regional hydrological response to climate change in Mexico and Central America. AGU Fall Meeting 2009, San Francisco, USA, 14–18 Dec. 2009. Abstract A33A-0219.

Kasischke, E.S., Melack, J.M., Dobson, M.C., 1997. The use of imaging radars of ecological applications – a review. Remote Sens. Environ. 59, 141–156.

Kaufmann, G., 2003. A model comparison of karst aquifer evolution for different matrix-flow formulations. J. Hydrol. 283 (1–4), 281–289. doi: 10.1016/S0022-1694(03)00270-1.

Kenkmann, T., Schönian, F., 2006. Ries and Chicxulub: Impact craters on Earth provide insights for Martian ejecta blankets. Meteorics and Planet. Sci. 41 (10), 1587–1603.

Kilroy, G., Coxon, C., Ryan, J., O'Connor, Á, Daly, D., 2005. Groundwater and wetland management in the Shannon river basin (Ireland). Environ. Sci. and Policy 8, 219–225. doi: 10.1016/j.envsci.2005.03.001.

Kim, S.-W., Wdowinski, S., Amelung, F., Dixon, T.H., 2005. C-band interferometric SAR measurements of water level change in the wetlands: examples from Florida and Louisiana. Geoscience and Remote Sensing Symposium. IGARSS '05. IEEE International 4, 2708−2710.

Kim, J.-W., Lu, Z., Lee, H., Shum, C.K., Swarzenski, C.M., Doyle, T.W., Baek, S.-H., 2009. Integrated analysis of PALSAR/Radarsat-1 InSAR and ENVISAT altimeter data for mapping of absolute water level changes in Louisiana wetlands. Remote Sensing of Environment 113, 2356–2365. doi: 10.1016/j.rse.2009.06.014.

Kiraly, L., 2003. Karstification and groundwater flow. Speleogenesis and Evolut. of Karst Aquifers 1 (3). 26 pp.

Kirsch, R., 2006. Electromagnetic methods – frequency domain. Ground based techniques. Chapter 5.2 in: Kirsch, R. (Ed.), Groundwater geophysics – A tool for hydrogeology. Springer. ISBN: 3-540-29383-3.

Klein, J., Lajoie, J., 1980. Electromagnetic prospecting for minerals. Practical Geophysics for the Exploration Geologist. Northwest Mining Association, Spokane, WA, USA, pp. 239–290.

Klimchouk, A.B., 1997. The role of karst in the genesis of sulfur deposits, Pre-Carpathian region, Ukraine. Environ. Geol. 31 (1–2), 1–20.

Knochenmus, L.A., Robinson, J.L., 1996. Descriptions of anisotropy and heterogeneity and their effect on ground-water flow and areas of contribution to public supply wells in a karst carbonate aquifer system. U.S. Geol. Surv. Water-Supply Pap. 2475. 46 pp. ISBN 0-607-86216-5.

Kovacs, A., Perrochet, P., Király, L., Jeannin, P.-Y., 2005. A quantitative method for the characterisation of karst aquifers base don spring hydrograph analysis. J. Hydrol. 303, 152–164. doi: 10.1016/j.jhydrol.2004.08.023.

Kralik, M., 2001. Spring dynamics as a tool to evaluate groundwater vulnerability. 7th Conference on Limestone Hydrology and Fissured Media. Besancon, France, 20–22 Sept. 2001. Sci. Tech. Environ. Mém. 13, 215–218.

Krause, S., Heathwaite, A.L., Miller, F., Hulme, P., Crowe, A., 2007. Groundwater-dependent wetlands in the UK and Ireland: controls, functioning and assessing the likelihood of damage from human activities. Water Resour. Manage. 21, 2015–2025. doi: 10.1007/s11269-007-9192-x.

Krekeler, M.P.S., Probst, P., Samsonov, M., Tselepis, C.M., Bates, W., Kearns, L.E., Barry Maynard, J., 2007. Investigations of subsurface flow constructed wetlands and associated geomaterial resources in the Akumal and Reforma regions, Quintana Roo, Mexico. Environ. Geol. 53, 709–726. doi: 10.1007/s00254-007-0684-z.

Laimer, H.J., 2005. Die Erfassung der Karstgrundwasser-Vulnerabilität mit der Metode "VURAAS" (Karst groundwater vulnerability assessment with the "VURAAS" method). Springer, Grundwasser, 167–176.

Lang, M.W., Kasischke, E.S., 2008. Using C-band synthetic aperture radar data to monitor forested wetland hydrology in Maryland's coastal plain, USA. IEEE Transactions on Geoscience and Remote Sensing 46, 535–546. doi: 10.1109/TGRS.2007.909950.

Lang, M.W., Kasischke, E.S., Prince, S.D., Pittman, K.W., 2008. Assessment of C-band synthetic aperture radar data for mapping and monitoring Coastal Plain forested wetlands in the Mid-Atlantic Region, USA. Remote Sensing of Environment 112, 4120–4130. doi: 10.1016/j.rse.2007.08.026.

Larocque, M., Banton, O., Ackerer, P., Razack, M., 1999. Determining karst transmissivities with inverse modeling and an equivalent porous media. Ground Water 37 (6), 897–903.

Larocque, M., Banton, O., Razack, M., 2000. Transient-state history matching of a karst aquifer ground water flow model. Ground Water 38 (6), 939–946.

Legchenko, A., Ezersky, M., Camerlynck, C., Al-Zoubi, A., Chalikakis, K., Girard, J.-F., 2008. Locating water-filled karst caverns and estimating their volume using magnetic resonance soundings. Geophysics 73 (5), G51–G61. doi: 10.1190/1.2958007.

Lesser, J. M., 1976. Estudio hidrogeologico e hidrogeoquimico de la Peninsual de Yucatan. Proyecto Conacyt-NSF 704, Secretaria de Recursos Hidraulicos, Direccion de Geohidrologia y Zonas Aridas, Mexico. 64 p.

Li, X., Tsai, F. T.-C., 2009. Bayesian model averaging for groundwater head prediction and uncertainty analysis using multimodel and multimethod. Water Resour. Res. 45, W09403. doi: 10.1029/2008WR007488.

Liedl, R., Sauter, M., Hückinghaus, D., Clemens, T., Teutsch, G., 2003. Simulation of the development of karst aquifers using a coupled continuum pipe flow model. Water Resour. Res. 39 (3), SBH61-SBH611.

Lindgren, R.J., Dutton, A.R., Hovorka, S.D., Worthington, S.R.H., Painter, S., 2005. Conceptualization and simulation of the Edwards Aquifer, San Antonio Region, Texas. In: Kuniansky, E. (Ed.). Sci. Investig. Rep. 2005-5160, 48–57.

Lopez-Ornat A., Ramo C., 1992. Colonial waterbird populations in the Sian Ka'an Biosphere Reserve (Quintana Roo, Mexico). Wilson Bull. 104, 501–515.

Lopez-Ramos, E., 1975. Geological summary of the Yucatan Peninsula. Chap. 7. In: Nairn, A.E.M., Stehli, F.G. (Eds.) The ocean basins and margins. Vol. 3 The Gulf of Mexico and the Caribbean. Plenum Press, NY, USA.

Lu, Z., Crane, M., Kwoun, O., Wells, C., Swarzenski, C., Rykhus, R., 2005. C-band radar observes water level change in swamp forests. EOS Transactions, AGU 86, 141–144.

Lu, Z., Kwoun, O., 2008. Radarsat-1 and ERS InSAR analysis over southeastern coastal Louisiana: Implications for mapping water-level changes beneath swamp forests. IEEE Transactions on Geoscience and Remote Sensing 46, 2167–2184. doi: 10.1109/TGRS.2008.917271.

Lu, Z., Kim, J.-W., Lee, H., Shum, C.,K., Duan, J., Ibaraki, M., Akyilmaz, O., Read, C.-H., 2009. Helmand river hydrologic studies using ALOS PALSAR InSAR and ENVISAT altimetry. Marine Geodesy 32 (3), 320–333. doi: 10.1080/01490410903094833.

Malik, P., Svasta, J., 1999. REKS – an alternative method of karst groundwater vulnerability estimation. Hydrogeology and Land Use Management, Proceedings of the XXIX Congress of the International Association of Hydrogeologists, Bratislava, September 1999, 79–85.

Mangin, A., 1974. Contribution à l'étude hydrodynamique des aquifers karstiques (Contribution the hydrodynamics of karst aquifers). Ann. de Spéléol. 29 (3), 283–332; 29 (4), 495–601; 30 (1), 21–124.

Marin, L.E., 1990. Field investigations and numerical simulation of ground-water flow in the karstic aquifer of northwestern Yucatan, Mexico. PhD thesis. Dept. of Geol., North. Ill. Univ., USA.

Marin, L.E., Steinich, B., Pacheco, J. Escolero, O.A., 2000. Hydrogeology of a contaminated sole-source karst aquifer, Mérida, Yucatán, Mexico. Geofís. Int. 49 (4), 359–365.

Marin, L.E., Perry, E.C., Essaid, H.I., Steinich, B., 2004. Hydrogeological investigations and numerical simulation of groundwater flow in the karstic aquifer of northwestern Yucatan, Mexico. p. 257–278. In: Cheng, A., H.-D., Ouazar, D., 2004. Coastal aquifer management: monitoring, modeling and case studies. CRC Press LLC. ISBN 1-56670-605-X.

Marshall, L., Sharma, A., Nott, D., 2006. Modeling the catchment via mixtures: Issues of model specification and validation. Water Resour. Res. 42, W11409. doi: 10.1029/2005WR004613.

Martin, J.B., Screaton, E.J., 2001. Exchange of matrix and conduit water with examples from the Floridan aquifer. In : Kuniansky, E. (Ed.). Water-Resources Investigations Report 01-4011, U.S. Geological Survey. 38–44

Martinez, J.-M., Le Toan, T., 2007. Mapping of flood dynamics and spatial distribution of vegetation in the Amazon floodplain using multitemporal SAR data. Remote Sensing of Environment 108, 209–223.

Massonnet, D., Rossi, M., Carmona, C., Adragna, F., Peltzer, G., Feigl, K., Rabaute, T., 1993. The displacement field of the Landers earthquake mapped by radar interferometry. Nature 364, 138–142.

Massonnet, D., Feigl, K.L., 1998. Radar interferometry and its application to changes in the Earth's surface. Reviews of Geophysics 36, 441–500.

Mayr, S.I., Burkhardt, H., Popov, Y., Wittmann, A., 2008. Estimation of hydraulic permeability considering the micro morphology of rocks of the borehole YAXCOPOIL-1 (Impact crater Chicxulub, Mexico). Int. J. Earth Sci. (Geol. Rundsch.) 97, 385–399.

Mazzotti, F.J., Fling, H.E., Merediz, G., Lazcano, M., Lasch, C., Barnes, T., 2005. Conceptual ecological model of the Sian Ka'an Biosphere Reserve, Quintana Roo, Mexico. Wetl. 25 (4), 980–997.

McGrath, R.J., Styles, P., Thomas, E., Neale, S., 2002. Integrated high-resolution geophysical investigations as potential tools for water resource investigations in karst terrain. Environ. Geol. 42: 552–557. doi: 10.1007/s00254-001-0519-2.

Meehl, G.A., Stocker, T.F., Collins, W.D., Friedlingstein, P., Gaye, A.T., Gregory, J.M., Kitoh, A., Knutti, R., Murphy, J.M., Noda, A., Raper, S.C.B., Watterson, I.G., Weaver, A.J., Zhao, Z.-C., 2007. Global Climate Projections. In: Solomon, S., Qin, D., Manning, M., Chen, Z., Marquis, M., Averyt, K.B., Tignor, M., Miller, H.L. (Eds.)Climate Change 2007: The Physical Science Basis. Contribution of Working Group I to the Fourth Assessment Report of the Intergovernmental Panel on Climate Change. Cambridge University Press, Cambridge, United Kingdom and New York, NY, USA.

Merediz Alonso, G., 2007. Science and NGO's: Collaboration for the conservation of groundwater resources in the Yucatan Peninsula. p. 97–103 in: Holliday, L., Marin, L., Vaux, H. (Eds.), 2007. Sustainable management of groundwater in Mexioc: Proceedings of a Workshop (Series: Strengthening science-based decision making in developing countries). National Research Council. The National Academies Press, Washington D.C., USA. ISBN: 0-309-10583-8.

Milanović, P.T., 2004, Water resources engineering in karst. CRC Press, Florida, USA. 312 pp. ISBN 1-56670-671-8.

Mimi, Z.A., Assi, A., 2009. Intrinsic vulnerability, hazard and risk mapping for karst aquifers: a case study. J. Hydrol. 364, 298–310. doi: 10.1016/j.jhydrol.2008.11.008.

Mochales, T., Casas A.M., Pueyo, E.L., Pueyo, O., Román, M.T., Pocoví, A., Soriano, M.A., Ansón, D., 2008. Detection of underground cavities by combining gravity, magnetic and ground penetrating radar surveys: a case study from the Zaragoza area, NE Spain. Environ. Geol. 53, 1067–1077. doi: 10.1007/s00254-007-0733-7.

Moore, Y.H., Stoessell, R.K., Easley, D.H., 1992. Fresh-water/sea-water relationship within a ground-water flow system, northeastern coast of the Yucatan Peninsula. Ground Water 30 (3), 343–350.

Morales López, J.A., 2007. Estrategia de manejo y conservación de recursos hídricos para la zona de influencia norte de Sian Ka'an. M.Sc. thesis. Universidad Autónoma de Querétaro. Querétaro, Mexico.

Motschka, K., 2001. Aerogeophysics in Austria. Bull. of Geol. Surv. of Jpn. 52 (2–3), 83–88.

Münch, Z., Conrad, J., 2007. Remote sensing and GIS based determination of groundwater dependent ecosystems in the Western Cape, South Africa. Hydrogeol. J. 15, 19–28. doi: 10.1007/s10040-006-0125-1.

Murray, I.R., Alvarez, C., Groom, R.W., 1999. Modelling of complex electromagnetic targets using advanced non-linear approximator techniques. Extended Abstracts, 69th SEG Conference, Houston, Texas.

NASDA/NASA, 2008. Tropical Rainfall Measuring Mission (TRMM), data product 3B43. TRMM algorithms were developed by the TRMM Science Team. TRMM data were processed by the TRMM Science Data and Information System (TSDIS) and the TRMM Office; archived and distributed by the Goddard Distributed Active Archive Center. TRMM is an international project jointly sponsored by the Japan National Space Development Agency (NASDA) and the U.S. National Aeronautics and Space Administration (NASA) Office of Earth Sciences.

Neelin, J.D., Münnich, M., Su, H., Meyerson, J.E., Holloway, C.E., 2006. Tropical drying trends in global warming models and observations. PNAS 103 (16), 6110–6115. doi: 10.1073/pnas.0601798103.

Neuman, S.P., 2003. Maximum likelihood Bayesian averaging of uncertain model predictions. Stoch. Environ. Res. and Risk Assess. 17, 291–305. doi:10.1007/s00477-003-0151-7.

Neuman, S.P., Wierenga, P.J., 2003. A comprehensive strategy of hydrogeologic modeling and uncertainty analysis for nuclear facilities and sites. Univ. of Ariz., Rep. NUREG/CR-6805.

Newman, G.A., Commer, M., 2005. New advances in three dimensional transient electromagnetic inversion. Geophysical Journal Internaitonal 160 (1), 5–32.

Nielsen, L., Jørgensen, N.O., Gelting, P., 2007. Mapping of the freshwater lens in a coastal aquifer on the Keta Barrier (Ghana) by transient electromagnetic soundings. J. Applied Geophys. 62, 1–15. doi: 10.1016/j.jappgeo.2006.07.002.

Nyquist, J.E., Peake, J.S., Roth, M.J.S., 2007. Comparison of an optimized resistivity array with dipole-dipole soundings in karst terrain. Geophys. 72, F139.

Oberstadler, R., Hönsch, H., Huth, D., 1997. Assessment of the mapping capabilities of ERS-1 SAR data for flood mapping: a case study in Germany. Hydrological Processes 11, 1415–1425.

Ocampo, A.C., Pope, K.O., Fischer, A.G., 1996. Ejecta blanket deposits of the Chicxulub crater from Albion Island, Belize. p. 75–88. In: Ryder, G., Fastovsky, D., Gartner, S. (Eds.) The Creataceous-Tertiary event and other catastrophes in Earth history. Geol. Soc. Am. Spec. Pap. 307.

Ottowitz, D., 2009. 3-D Modellrechnung der Karststrukturen des Ox Bel Ha Höhlensystems zur Methodenevaluierung - Aeroelektromagnetic. M.Sc. Thesis, Univ. of Vienna, Austria.

Pacheco, J., Marín, L., Cabrera, A., Steinich, B., Escolero, O., 2001. Nitrate temporal and spatial Patterns in 12 water-supply wells, Yucatan, Mexico. Environ. Geology 40 (6), 708–715.

Pankratov, O.V., Kuvshinov, A.V., Avdeev, D.B., 1997. High performance three-dimensional three-dimensional electromagnetic modelling using modified Neumann series. Anisotropic Earth. J. Geomag. Geoelectr. 49, 1541–1547.

Painter, S.L., Sun, A., Green, R.T., 2007. Enhanced characterization and representation of flow through karst aquifers. Am. Water Works Assoc. ISBN 1-8532-1489-5. 83 pp.

Painter, J., 2009. Americas on alert for sea level rise. BBC news article, accessed on URL: http://news.bbc.co.uk/2/hi/americas/7977263.stm in January 2010.

Pellerin, L., Holliger, K., Slater, L., Yaramanci, U., 2009. Special issue on Hydrogeophysics – Methods and processes foreword. Near Surface Geophysics 7 (5–6), 303–305.

Perry, E., Swift, J., Gamboa, J., Reeve, A., Sanborn, R., Marín, L, Villasuso, M., 1989. Geologic and environmental aspects of surface cementation, north coast, Yucatan, Mexico. Geol. 17, 818–821.

Perry, E.C., Marín, L.E., McClain, J., Velazquez, G., 1995. The Ring of Cenotes (sinkholes) northwest Yucatan, Mexico: Its hydrogeologic characteristics and association with the Chicxulub Impact Crater. Geol. 23, 17–20.

Perry, E., Velazquez-Oliman, G., Marin, L., 2002. The hydrogeochemistry of the karst aquifer system of the northern Yucatan Peninsula, Mexico. Int. Geol. Rev. 44, 191–221.

Perry, E., Paytan, A., Pedersen, B., Velazquez-Oliman, G., 2009. Groundwater geochemistry of the Yucatan Peninsula, Mexico: constraints on stratigraphy and hydrogeology. J. Hydrol. 367 (1–2), 27–40. doi: 10.1016/j.jhydrol.2008.12.026.

Peterson, E.W., Wicks, C.M., 2005. Fluid and solute transport from a conduit to the matrix in a carbonate aquifer system. Mathematical Geology 37 (8), 851–867. doi: 10.1007/s11004-005-9211-5.

Peterson, E.W., Wicks, C.M., 2006. Asessing the importance of conduit geometry and physical parameters in karst systems using the storm water management model (SWMM). J. Hydrol. 329, 294–305. doi: 10.1016/j.jhydrol.2006.02.017.

PetRos EiKon, 2003. EMIGMA Version 7.5. Software. Copyright © PetRos EiKon. Ontario, Canada.

Pietroniro, A., Prowse, T., Peters, D.L., 1999. Hydrologic assessment of an inland freshwater delta using multi-temporal satellite remote sensing. Hydrol. Process. 13, 2483–2498.

Pope, K.O., Rejmankova, E., Paris, J.F., 2001. Spaceborne imaging radar-C (SIR-C) observations of groundwater discharge and wetlands associated with the Chicxulub impact crater, northwestern Yucatan Peninsula, Mexico. Geol. Soc. America Bull. 113 (3), 403–416.

Pope, K.O., Ocampo, A.C., Fischer, A.G., Vega, F.J., Ames, D.E., King Jr., D.T., Fouke, B.W., Wachtman, R.J., Kletetschka, G., 2005. Chicxulub impact ejecta deposits in southern Quintana Roo, México, and central Belize. p. 171–190. In: Kenkmann, T., Hörz, F., Deutsch, A. (Eds.) Large meteorite impacts III. Geol. Soc. Am. Spec. Pap. 384.

Powell, S.J., Letcher, R.A., Croke, B.F.W., 2008. Modelling floodplain inundation for environmental flows: Gwydir wetlands, Australia. Ecol. Modelling 211, 350–362.

Pozo de la Tijera, C., Escobedo Cabrera, J.E., 1999. Mamíferos terrestres de la Reserva de la Biosfera de Sian Ka'an, Quintana Roo, México. Revista de Biología Tropical 47, 251–262.

Refsgaard, J.C., van der Sluijs, J.P., Brown, J., van der Keur, P., 2006. A framework for dealing with uncertainty due to model structure error. Adv. in Water Resour. 29, 1586–1597.

Refsgaard, J. C., van der Sluijs, J.P., Højberg, A.L., Vanrolleghem, P.A., 2007. Environ. Modelling & Softw. 22, 1543–1556. doi: 10.1016/j.envsoft.22007.02.004.

Revil, A., Cathles, L.M.I., 1999. Permeability of shaly sands. Water Resour. Res. 35 (3), 651–662.

Robinson-Poteet, D., 1989. Using terrain conductivity to detect subsurface voids and caves in a limestone formation. pp. 271–280 in: Beck, B.F., (Ed.). Engineering and environmental impacts of sinkholes and karst: proceedings of the third Multidisciplinary Conference on Sinkholes and the Engineering and Environmental Impacts of Karst, St. Petersburg Beach, FL, USA. ISBN: 90-6191-987-8.

Rodríguez-Rodríguez, M., Moral, F., Benavente, J., 2008. Hydrogeological characteristics of a groundwater-dependent ecosystem (La Lantejuela, Spain)., Water and Environ. J. 22, 137–147. doi: 10.1111/j.1747-6593.2007.00092.x.

Rojas, R., Feyen, L., Dassargues, A., 2008. Conceptual model uncertainty in groundwater modeling: Combining generalized likelihood uncertainty estimation and Bayesian model averaging. Water Resour. Res. 44, W12418. doi: 10.1029/2008WR006908.

Rojas, R., Feyen, L., Dassargues, A., 2009. Sensitivity analysis of prior model probabilities and the value of prior knowledge in the assessment of conceptual model uncertainty in groundwater modelling. Hydrol. Process. 23, 1131–1146. doi: 10.1002/hyp.7231.

Rosen, P.A., Hensley, S., Joughin, I.R., Li, F.K., Madsen, S.N., Rodríguez, E., Goldstein, R.M., 2000. Synthetic aperture radar interferometry. Proceedings of the IEEE 88 (3), 333–381.

Roth, M.J.S., Mackey, J.R., Mackey, C., Nyquist, J.E., 2002. A case study of the reliability of multielectrode earth resistivity testing for geotechnical investigations in karst terrains. Eng. Geol. 65 (2–3), 225–232.

Roth, M.J.S., Nyquist, J.E., 2003. Evaluation of multi-electrode earth resistivity testing in karst. Geotechnical Testing J. 26 (2), 1–12.

Rubin, Y., Hubbard, S.S., 2005. Introduction to hydrogeophysics. Chapter 1 in: Rubin, Y., Hubbard, S.S. (Eds.). Hydrogephysics. Springer, Dordrecht, The Netherlands, 3–21.

Rybakov, M., Rotstein, Y., Shirman, Al-Zoubi, A., 2005. Cave detection near the Dead Sea – a micromagnetic feasibility study. The Leading Edge 585–590.

Sánchez Meza, J.J., 2006. Se ha descentralizado la gestión del agua en México? Reporte de investigación. Comisión Estatal del Agua, Gobierno del Estado de Sonora. Centro del Tercer Mundo para Manejo de Agua A.C. www.thirdworldcentre.org. 24 pp.

Sasaki, Y., 2001. Full 3-D inversion of electromagnetic data on PC. J. Applied Geophys 46 (1), 45–54.

Sass,G.Z., Creed, I.F., 2008. Characterizing hydrodynamics on boreal landscapes using archived synthetic aperture radar imagery. Hydrological Processes 22, 1687–1699. doi: 10.1002/hyp.6736.

Scanlon, B.R., Mace, R.E., Barrett, M.E., Smith, B., 2003. Can we simulate regional groundwater flow in a karst system using equivalent porous media models? Case study, Barton Springs Edwards Aquifer, USA. J. Hydrol. 276, 137–158. doi: 10.1016/S0022-1694(03)00064-7.

Schumann, G., Di Baldassarre, G., Bates, P.D., 2009. The utility of spaceborne radar to render flood inundation maps based on multialgorithm ensembles. IEEE Transactions on Geoscience and Remote Sensing 47 (8), 2801–2807.

Schönian, F., Stöffler, D., Kenkmann, T., Wittmann, A., 2004. The fluidized Chicxulub ejecta blanket, Mexico: Implications for Mars. Poster, 35th Annu. Lunar and Planet. Sci. Conf., Leag. City, TX, USA.

Schönian, F., Tagle, R., Stöffler, D., Kenkmann, T., 2005. Geology of southern Quintana Roo (Mexico) and the Chicxulub ejecta blanket. Abstract #2389. 36th Annu. Lunar and Planet. Sci. Conf., Leag. City, TX, USA.

Schwaiger, H.F., Murray, C., Brown, L., 1997. Effectiveness of ground penetrating radar in detecting caves in karst limestone of the Yucatan Peninsula, Mexico. Proceedings of the Symposium on the Application of Geophysics to Engineering and Environmental Problems, Reno, NV, USA. 588–586.

SEDUMA, 2003. Programa subregional de desarrollo urbano de la Región Caribe Norte. Secretaria de Desarrollo Urbano y Medio Ambiente, Quintana Roo. Accessed on URL: http://seduma.qroo.gob.mx/PDUs/2.-%20PDU%20SUBREGIONAL%20CARIBE%20NORTE%20(30%20MAYO%202003)/PDU%20SUBREGIONAL.pdf

SGM, 2007. Carta geológica de México. Escala 1:2,000,000. 6ª edición. Servicio Geológico Mexicano (SGM).

Shah, S.D., Smith, B.D., Clark, A.K., Kress, W.H., 2008. A multi-tool geophysical and hydrogeological investigation of a karst aquifer system, Cibolo Canyon Deveopment Area, Bexar County, Texas. In: Kuniansky, E. (Ed.). U. S. Geol. Surv. Karst Interest Group Proc., Bowling Green, Kentucky, USA. p. 107–116.

Shen, G., Guo, H., Liao, J., 2008. Object oriented method for detection of inundation extent using multi-polarized synthetic aperture radar image. J. Applied Remote Sens. 2, 023512. doi: 10.1117/1.2911669.

Shoemaker, W.B., Kuniansky, E.L., Birk, S., Bauer, S., Swain, E.D., 2008. Documentation of a Conduit Flow Process (CFP) for MODFLOW-2005. U. S. Geol. Surv. Techniques and Methods, Book 6, Chapter A24, 50 pp.

Siemon, B., 2006. Electromagnetic methods – frequency domain. Airborne techniques. Chapter 5.1 in: Kirsch, R. (Ed.), Groundwater geophysics – A tool for hydrogeology. Springer. ISBN: 3-540-29383-3.

Singh, V.P., Woolhiser, D.A., 2002. Mathematical modelling of watershed hydrology. J. Hydrol. Engineering 7 (4), 270–292.

Slater, L., 2007. Near surface electrical characterization of hydraulic conductivity: from petrophysical properties to aquifer geometries – a review. Surv. Geophys. 28, 169–197. doi: 10.1007/s10712-007-9022-y.

Smart, P.L., Beddows, P.A., Coke, J., Doerr, S., Smith, S., Whitaker, F.F., 2006. Cave development on the Caribbean coast of the Yucatan Peninsula, Quintana Roo, Mexico. In: Harmon, R.S., Wicks, C. (Eds.) Perspectives on karst geomorphology, hydrology and geochemistry – A tribute volume to Derek C. Ford and William B. White. Geol. Soc. Am.. Spec. Pap. 404, 105–128.

Smith, B.D., Smith, D.V., Hill, P.L., Labson, V.F., 2003. Helicopter electromagnetic and magnetic survey data and maps, Seco Creek Area, Medina and Uvalde Counties, Texas. U. S. Geol. Surv. Open-File report 03-226. 60 pp.

Smith, B.D., Cain. M.J., Clark, A.K., Moore, D.W., Faith, J.R., Hill, P.L., 2005a. Helicopter electromagnetic and magnetic survey data and maps, Northern Bexar County, Texas. U. S. Geol. Surv. Open-File report 05-1158. 122 pp.

Smith, B.D., Gamey, J.T., Hodges, G., 2005b. Review of airborne electromagnetic geophysical surveys over karst terrains. In: Kuniansky, E. (Ed.). U. S. Geol. Surv. Karst Interest Group Proc., Rapid City, South Dakota, USA. p. 17–19.

Solbø, S., Malnes, E., Guneriussen, T., Solheim, I., Eltoft, T., 2003. Mapping surface-water with Radarsat at arbitrary incidence angles. Geoscience and Remote Sensing Symposium, 2003, IGARSS '03. Proceedings IEEE International. 4, 2517–2519. doi: 10.1109/IGARSS.203.1294494.

Springer, G.S., 2004. A Pipe-Based, First Approach to Modeling Closed Conduit Flow in Caves. J. Hydrol. 289, 178–189.

Stauffer, F., Attinger, S., Zimmermann, S., Kinzelbach, W., 2002. Uncertainty estimation of well catchments in heterogeneous aquifers. Water Resour. Res. 38 (11), 1238. doi: 10.1029/2001WR000819.

Stauffer, F., Guadagnini, A., Butler, A., Hendricks Franssen, H.-J., Van de Wiel, N., Bakr, M., Riva, M., Guadagnini, L., 2005. Delineation of source protection zones using statistical methods. Water Resour. Manage. 19, 163–185. doi: 10.1007/s11269-005-3482-7.

Steinich, B., Marin, L.E., 1996. Hydrogeological investigations in northwestern Yucatan, Mexico, using resistivity surveys. Ground Water 34 (4), 640–646.

Steinich, B., Marin, L.E., 1997. Determination of flow characteristics in the aquifer of the Northwestern Peninsula of Yucatan, Mexico. J. Hydrol. 191, 315–331.

Stisen, S., Sandholt, I., Nørgaard, A., Fensholt, R., Høegh Jensen, K., 2008. Combining the triangle method with thermal intertia to estimate regional evapotranspiration – Applied to MSG-SEVIRI data in the Senegal River basin. Remote Sens. Environ. 112, 1242–1255.

Stoessell, R.K., Ward, W.C., Ford, B.H., Schuffert, J.D., 1989. Water chemistry and $CaCO_3$ dissolution in the saline part of an open-flow mixing zone, coastal Yucatan Peninsula, Mexico. Geol. Soc. of America Bull. 101 (2), 159–169.

Stoessell, R.K., Moore, Y.H., Coke, J.G., 1993. The occurrence and effect of sulfate reduction and sulfide oxidation on coastal limestone dissolution in Yucatan cenotes. Ground Water 31 (4), 566–575.

Stoessell, R.K., 1995. Dampening of tranverse dispersion in the halocline in karst limestone in the Northeastern Yucatan Peninsula. Ground Water 33 (3), 366–371.

Stoessell, R.K., Coke, J.G., Easley, D.H., 2002. Localized thermal anomalies in haloclines of coastal Yucatan sinkholes. Ground Water 40 (4), 416–424.

Šumanovac, F., Weisser, M., 2001. Evaluation of resistivity and seismic methods for hydrogeological mapping in karst terrains. J. Applied Geophysics 47, 13–28.

Tang, Q., Gao, H., Lu, H., Lettenmaier, D.P., 2009. Remote sensing: hydrology. Progress in Physical Geography 33 (4), 490–509. doi: 10.1177/0309133309346650.

Telford., W. M., Geldart, L. P., Sheriff, R. E., 1990. Applied Geophysics. Second Edition, Cambridge University Press, 770 pp. ISBN 0-521—33938-3.

Teutsch, G., Sauter, M., 1991. Groundwater modeling in karst terranes: Scale effects, data acquisition and field validation. Proc. 3rd conf. on hydrogeology, ecology, monitoring and management of groundwater in karst terranes. Nashv., Tenn., USA. Natl. Ground Water Assoc., Dublin, Ohio, USA, 17–34.

Thomas, C., 1999. Aspects hydrogéologiques du Yucatan (Mexique). Karstologia 34 (2), 9–22.

Topp, G.C., Davis, J.L., Annan, A.P., 1980. Electromagnetic determination of soil water content: measurements in coaxial transmission lines. Water Resources Res. 16 (3), 574–582.

Ulaby, F.T., Moore, R. K., Fung, A.K., 1982. Microwave Remote Sensing: Active and Passive, Vol. II – Radar Remote Sensing and Surface Scattering and Emission Theory. Addison-Wesley, Advanced Book Program, Reading, Massachusetts, USA. 609 pp.

USGS, 2006. Shuttle Radar Topography Mission, 3 Arc Second, Finished 2.0. Global Land Cover Facility, University of Maryland, College Park, MD, USA. Accessed 15 June 2006.

Van Stempoort, D., Ewert, L., Wassenaar, L., 1993. Aquifer Vulnerability Index (AVI): a GIS compatible method for groundwater vulnerability mapping. Can. Water Res. J. 18, 25–37.

Vassolo, S., Kinzelbach, W., Schäfer, W., 1998. Determination of a well head protection zone by stochastic inverse modelling. J. Hydrol. 206, 268–280.

Vaux Jr., H., 2007a. Chairman's summary. p. 1–5 in: Holliday, L., Marin, L., Vaux, H. (Eds.). Sustainable management of groundwater in Mexico: Proceedings of a Workshop (Series: Strengthening science-based decision making in developing countries). National Research Council. The National Academies Press, Washington D.C., USA. ISBN: 0-309-10583-8.

Vaux Jr., H., 2007b. The elements of scientific advice. p. 36–43 in: Holliday, L., Marin, L., Vaux, H. (Eds.). Sustainable management of groundwater in Mexico: Proceedings of a Workshop (Series: Strengthening science-based decision making in developing countries). National Research Council. The National Academies Press, Washington D.C., USA. ISBN: 0-309-10583-8.

Vías, J.M., Andreo, B., Perles, M.J, Carrasco, F., Vadillo, I., Jiménez, P., 2004. The COP method. pp. 163–171 in: Zwahlen, F. (Ed.). Vulnerability and risk mapping for the protection of carbonate (karst) aquifers. Final report of COST Action 620, European Commission, Directorate-General XII Science, Research and Development, Brussels, Belgium.

Vías, J.M., Andreo, B., Perles, M.J., Carrasco, F., 2005. A comparative study of four schemes for groundwater vulnerability mapping in a diffuse flow carbonate aquifer under Meditarranean climatic conditions. Environ. Geol. 47, 586–595. doi: 10.1007/s00254-004-1185-y.

Vogelsang, D., 1987. Examples of electromagnetic prospecting for karst and fault systems. Geophys. Prospect. 35, 604–617.

Vouillamoz, J.M., Legchenko, A., Albouy, Y., Bakalowicz, M., Baltassat, J.M., Al-Fares, W., 2003. Location of saturated karst aquifer with magnetic resonance sounding and resistivity imagery. Ground Water 41 (5), 578–586.

Ward, S. H., Hohmann, G.W., 1988. Electromagnetic theory for geophysical applications. Chapter 4 (p. 131-312) in: Nabaighian, M.N. (Ed.), Electromagnetic methods in applied geophysics – Volume 1, Theory. Tulsa. Society of Exploration Geophysicists.

Watson, J., Hamilton-Smith, E., Gillieson, D., Kiernan, K. (Eds.), 1997. Guidelines for cave and karst protection. IUCN, Gland, Switzerland and Cambridge, UK. 63 pp.

Wdowinski, S., Amelung, F., Miralles-Wilhelm, F., Dixon, T.H., Carande, R., 2004. Space-based measurements of sheet-flow characteristics in the Everglades wetland, Florida. Geophysical Research Letters 31, L15503. doi: 10.1029/2004GL020383.

Wdowinski, S., Kim, S.-W., Amelung, F., Dixon, T., Miralles-Wilhelm, F., Sonenshein, R., 2008. Space-based detection of wetlands' surface water level changes from L-band SAR interferometry. Remote Sensing of Environment 112, 681–696. doi: 10.1016/j.rse.2007.06.008.

Weidie, A.E., 1985. Geology of Yucatan Platform. p. 1–12 in: Ward, W.C., Weidie, A.E., Back, W. (Eds.). Geology and hydrogeology of the Yucatan and Quaternary geology of northeastern Yucatan Peninsula. New Orleans Geol. Soc. Publ., New Orleans, LA, USA.

West, G. F., Macnae, J.C., 1991. Physics of the electromagnetic induction exploration method. p. 5–45 in Nabighian, M.N. (Ed.). Electromagnetic methods in applied geophysics - Volume 2 - Applications, part A and part B. Tulsa. Society of Exploration Geophysicists.

White, W.B., 1999. Conceptual models for karstic aquifers. p. 11–16 in: Palmer, A.N., Palmer, M.V., Sasowsky, I.D. (Eds.). Karst modeling. Spec. Publ. 5, The Karst Waters Institute, Charles Town, West Virginia, USA.

Worthington, S.R.H., Ford, D.C., Beddows, P.A., 2000. Porosity and permeability enhancement in unconfined carbonate aquifers as a result of solution. p. 463–471 in: Klimchouk, A., Ford, D., Palmer, A., Dreybrodt, W. (Eds.). Speleogenesis: Evolution of karst aquifers. Cave Books, St. Louis, USA. ISBN: 978-1-57958-399-6.

Worthington, S.R.H., 2003. A comprehensive strategy for understanding flow in carbonate aquifer. Speleogenesis and Evol. of Karst Aquifers 1 (1), 1–8.

Wright, C., Gallant, A., 2007. Improved wetland remote sensing in Yellowstone National Park using classification trees to combine TM imagery and ancillary environmental data. Remote Sens. Environment 107, 582–605.

Xiong, L., Shamseldin, A.Y., O'Connor, K.M., 2001. A non-linear combination of the forecasts of rainfall-runoff models by the first-order Takagi-Sugeno fuzzy system. J. Hydrol. 245, 196–217.

Young, W.J., Lam, D.C.L., Ressel., V., Wong, I.W., 2000. Development of an environmental flows decision support system. Environ. Modelling & Softw. 15, 257–265.

Zhou, W., Beck, B.F., Stephenson, J.B., 1999. Investigation of groundwater flow in karst areas using component separation of natural potential measurements. Environmental Geol. 37 (1–2), 19–25.

Zhou, W., Beck, B.F., Adams, A.L., 2002. Effective electrode array in mapping karst hazards in electrical resistivity tomography. Environmental Geol. 42, 922–928. doi: 10.1007/s00254-002-0594-z.

Zribi, M., Pardé, M., De Rosnay, P., Baup, F., Boulain, N., Descroix, L., Pellarin, T., Mougin, E., Ottlé, C., Decharme, B., 2009. ERS scatterometer surface soil moisture analysis of two sites in the south and north of the Sahel region of West Africa. J. of Hydrol. 375, 253–261. doi: 10.1016/j-jhydrol.2008.11.046.

7 Appendices

I Gondwe, B.R.N., Hong, S.-H., Wdowinski, S., Bauer-Gottwein, P. (2010). Hydrologic dynamics of the ground-water-dependent Sian Ka'an wetlands, Mexico, derived from InSAR and SAR data. Wetlands 30 (1), 1–13. doi: 10.1007/s13157-009-0016-z.

II Supper, R., Motschka, K., Ahl, A., Bauer-Gottwein, P., Gondwe, B., Alonso, G.M., Romer, A., Ottowitz, D., Kinzelbach, W. (2009). Spatial mapping of submerged cave systems by means of airborne electromagnetics: an emerging technology to support protection of endangered karst aquifers. Near Surface Geophysics 7 (5–6), 613–327.

III Gondwe, B.R.N., Ottowitz, D., Supper, R., Motschka, K., Merediz-Alonso, G., Bauer-Gottwein, P. (submitted). Exploring regional-scale preferential flow paths in the karst aquifer of Southern Quintana Roo, Mexico. Manuscript submitted.

IV Gondwe, B.R.N., Lerer, S., Stisen, S., Marín, L., Rebolledo-Vieyra, M., Merediz-Alonso, G., Bauer-Gottwein, P. (in review). Hydrogeology of the south-eastern Yucatan Peninsula: New insights from water level measurements, geochemistry, geophysics and remote sensing. Manuscript submitted.

V Gondwe, B.R.N., Merediz-Alonso, G., Bauer-Gottwein, P. (submitted). The influence of conceptual model uncertainty on management decisions for a groundwater-dependent ecosystem in karst. Manuscript submitted.

VI Technical Note. Maps and coordinates of field data points.

Please note that the papers (Appendix I through V) are not included in this web-version but may be obtained from the library at Department of Environmental Engineering, DTU, Miljoevej, Building 113, DK-2800 Kgs. Lyngby, Denmark, library@env.dtu.dk.

VI

Technical Note

Maps and coordinates of field data points.

Appendix VI – Technical Note

This appendix contains maps and coordinates of the field measurements that have been carried out during the PhD research. All coordinates are UTM, zone 16, WGS84 datum and ellipsoid. The actual data may be obtained from Amigos de Sian Ka'an (afregoso@amigosdesiankaan.org; gmerediz@amigosdesiankaan.org) or Peter Bauer-Gottwein (pbg@env.dtu.dk) in electronic format. Inventory of the data available electronically is given in Section A6.7.

A6.1 Groundwater head measurement points

Places where groundwater heads and surface water levels have been measured.
Points believed to represent perched aquifers are marked with "P".
Points outside the study area, and surface water levels are separated in the table.
Water level recorded by automatic data loggers indicated with time span covered.

Elevations of reference points at wells, usually marked with painted crosses, are given in meters above mean sea level in the table. The water level data may be found in the electronic data material in the folder WaterLevels. In the sub-folders WaterLevels\Bibi and WaterLevels\Chiara Word-documents with photos and detailed descriptions/maps of each water level measurement site may be found.

Water level measurements in July 2007 were carried out by Chiara Fratini, whereas those in Nov-Dec 2008 were carried out by Amigos de Sian Ka'an. Those in April 2009, north of the study area, were carried out by Guillaume Charvet. Reading of surface water levels within Sian Ka'an ("SKBR") were carried out by CONANP and the author. Data loggers were installed at 4 sites, indicated in the table with time span covered. Automatic water level and temperature recording was carried out every 30 minutes within these time intervals.

Location	Northing	Easting		Collect dates 2007	Collect dates 2008 (or 2009 if noted	Elevation of reference point at well (mamsl)
Macario Gomez	2250445	439830		25-Feb, 15-Apr, 29-Jul	03-Feb, 18-Dec	16.60
Chankah Veracruz 1	2155872	395708		27-Feb, 01-Jul, 24-Jul	18-Feb, 03-Nov	7.30
Chankah Veracruz 2	2155958	395627		27-Feb, 01-Jul, 24-Jul	18-Feb, 03-Nov	7.33
Uhmay 1	2147337	389903		27-Feb, 10-Apr, 01-Jul	18-Feb, 03-Nov	6.57
Uhmay 2	2147279	389963		27-Feb, 01-Jul,	18-Feb,	6.77
Xpichil	2178418	355574		28-Feb, 30-Jun	19-Feb, 20-Dec	25.25
Chunhuas	2171192	373083		01-Mar, 10-Apr, 30-Jun, 24-Jul	19-Feb, 20-Dec	15.86
San Andres	2145706	381136		01-Mar, 14-Apr, 01-Jul	18-Feb, 19-Dec	7.93
Muyil	2220482	435844		02-Mar, 12-Apr, 29-Jun	04-Nov	7.77
Polyuc	2169003	336095		05-Mar, 22-Mar, 16-Apr, 30-Jun, 24-Jul	20-Dec	16.33
Nuevo Israel	2128279	336941	P	06-Mar, 16-Mar, 16-Apr, 02-Jul	20-Feb, 03-Nov	24.33
Las Panteras	2116966	343026		06-Mar, 16-Mar, 16-Apr, 02-Jul	20-Feb, 03-Nov	23.49
Los Divorciados	2110462	347284		06-Mar, 16-Mar, 16-Apr, 02-Jul	20-Feb, 03-Nov	31.93
Nuevo San Antonio	2170399	388132		07-Mar, 17-Mar, 30-Jun	17-Feb, 21-Dec	7.62
Señor	2194844	381145		07-Mar, 17-Mar, 30-Jun	17-Feb, 21-Dec	20.20
Tuzik	2202466	378648		07-Mar, 17-Mar,	17-Feb, 21-Dec	19.59

				30-Jun		
San Jose Segundo	2208588	371582		07-Mar, 17-Mar, 30-Jun	17-Feb, 21-Dec	22.63
Andres Quinta Roo	2119220	384115		08-Mar, 14-Apr, 01-Jul, 25-Jul	04-Feb, 03-Nov	12.72
Noh-Bec	2117429	377037	P	08-Mar, 14-Apr, 01-Jul	21-Feb, 03-Nov	7.74
Polinkin	2120586	377220	P	08-Mar, 14-Apr, 01-Jul	21-Feb, 03-Nov	10.80
Petcacab (Data logger: 14 Apr 2007 – 24 Jul 2007)	2133152	371317		08-Mar, 14-Apr, 01-Jul, 24-Jul		22.09
X-hacil 1	2144330	387057		09-Mar, 17-Mar, 14-Apr, 01-Jul	18-Feb, 19-Dec	7.67
X-hacil 2	2144310	386970		09-Mar, 17-Mar, 14-Apr, 01-Jul	18-Feb, 19-Dec	9.22
Noh-Cah 1	2147914	378136		09-Mar, 14-Apr, 01-Jul	18-Feb, 19-Dec	8.91
Noh-Cah2	2147818	378219		09-Mar, 14-Apr, 01-Jul	18-Feb, 19-Dec	7.13
Mixtequilla	2144148	367151		09-Mar, 19-Apr, 01-Jul, 24-Jul	18-Feb, 19-Dec	16.70
Santa Maria Poniente	2142013	352118	P	09-Mar, 01-Jul	18-Feb, 03-Nov	12.45
Limones	2106297	383198		10-Mar, 16-Mar, 16-Apr, 01-Jul, 25-Jul	20-Feb, 03-Nov	7.70
Chacchoben	2105314	376815	P	10-Mar, 16-Mar, 16-Apr, 01-Jul, 25-Jul	20-Feb, 03-Nov	14.11
Rancho La Herradurra	2100867	370950	P	10-Mar, 16-Mar, 16-Apr, 01-Jul	20-Feb, 03-Nov	7.86
Rancho La Herradurra	2100978	371005	P	10-Mar, 16-Mar, 16-Apr, 01-Jul	20-Feb, 03-Nov	8.36
Pedro A. Santos	2096201	377441		10-Mar,	20-Feb,	9.21

				02-Jul	03-Nov	
Tepich	2239246	368971		19-Mar, 29-Jun	17-Feb, 21-Dec	24.47
Francisco I. Madero	2229157	392735		19-Mar, 29-Jun	17-Feb, 21-Dec	16.35
Chumpon	2212198	414787		20-Mar, 29-Jun	17-Feb, 22-Dec	8.88
Chunya	2222926	403359		20-Mar, 29-Jun,	17-Feb,	15.05
San Luis	2172925	348144		22-Mar, 16-Apr, 30-Jun, 24-Jul	19-Feb, 20-Dec	25.50
Presidente Juarez (Data logger: 16 Apr 2007 – 25 Aug 2008)	2136769	335923	P	22-Mar, 16-Apr, 01-Jul, 24-Jul	20-Feb, 03-Nov	26.66
Betania	2171336	365858		22-Mar, 16-Apr, 30-Jun,	19-Feb, 20-Dec	15.57
Tres Reyes	2193589	409785		28-Mar, 14-Apr,	28-Feb, 22-Dec	7.26
Felipe Carrillo Puerto	2165409	391327		29-Mar, 14-Apr, 01-Jul	18-Feb, 21-Dec	9.71
San Francisco Ake	2207122	359071		30-Mar, 30-Jun	19-Feb, 20-Dec	23.62
Dzoyola	2205977	348808		30-Mar, 30-Jun	19-Feb,	17.66
Javier Rojo Gomez	2199865	333110		30-Mar, 30-Jun	19-Feb, 20-Dec	26.04
Santa Isabel	2153153	384697		31-Mar, 19-Apr, 01-Jul	18-Feb, 19-Dec	10.17
Laguna Ocom	2152742	384075		31-Mar, 19-Apr, 01-Jul	18-Feb, 03-Nov	3.22
Chunkakah	2154329	383716		31-Mar,	18-Feb, 03-Nov	10.87
Reforma	2079163	335824	P	03-Apr,	23-Feb, 02-Nov	29.65
Altos de Sevilla	2085154	324046	P	03-Apr, 02-Jul	22-Feb, 02-Nov	72.28
Morocoy (Data logger: 25 Feb 2008 – 28 Apr 2008)	2059112	306809	P	04-Apr	12-Feb, 31-Oct	69.01
Rio Escondido	2084621	313615	P	05-Apr 02-Jul	11-Feb, 30-Oct	59.68
Otillo Montaño	2105810	309561		05-Apr, 02-Jul	22-Feb, 02-Nov	50.11
Dzulá (Data logger: 24 Jul 2007 – 06 Feb 2008)	2168142	351695		07-Apr, 30-Jun, 24-Jul	05-Feb, 19-Dec	20.61
Laguna Kaná	2156930	353304		07-Apr, 01-Jul,	18-Feb, 19-Dec	23.53

				24-Jul		
Yoactun	2152193	357352		07-Apr, 01-Jul, 24-Jul	18-Feb, 19-Dec	23.49
Tulum federal plot	2235499	453592		08-Apr, 16-Apr, 29-Jun	03-Feb, 04-Nov	3.24
Holbox depression	2241759	449387		13-Apr, 16-Apr, 29-Jun	03-Feb, 01-Nov	1.00
Manuel Antonio May	2259019	431705		17-Apr,	03-Feb, 18-Dec	20.16
Centro Nocturno	2243783	447206		18-Apr, 29-Jun	03-Feb, 18-Dec	6.47
Cenote Azul	2062180	350879	P	03-Jul	23-Feb, 02-Nov	16.80
Santa Elena	2045599	352682	P	05-Jul	23-Feb	2.23
Calderitas	2052206	367799	P	05-Jul	23-Feb	9.11
Ucum Qroo	2046815	339502	P	05-Jul	23-Feb, 31-Oct	23.97
El Cedral	2069074	291758	P	07-Jul	01-Nov	88.14
Francisco Villa	2042999	304163	P	07-Jul	23-Feb, 02-Nov	85.80
Nicholas Bravo	2042066	296126	P	07-Jul	24-Feb, 31-Oct	102.89
Felipe Anjeles	2010502	259888	P	10-Jul	01-Nov	209.45
La Lucha	2025628	268554	P	10-Jul	24-Feb, 01-Nov	181.39
Veinte de Noviembre	2041729	256347	P	11-Jul	26-Feb, 02-Nov	202.90
Richardo Payro	2026620	241515	P	11-Jul	26-Feb, 01-Nov	262.39
El Once	2000876	237966	P	12-Jul	01-Nov	265.75
Narciso Mendoza pozo	2017596	240428	P	12-Jul	26-Feb, 01-Nov	245.64
Bel Ha	2094686	255190	P	13-Jul	27-Feb, 01-Nov	137.59
José Maria Morelos	2184891	320643		22-Jul	19-Feb	20.76
Nuevo Becar chico	2073045	279704	P	09-Jul	02-Nov	95.42
Xkan-Ha	2114278	253374	P	13-Jul	01-Nov	126.59
Ucum Campeche	2129315	254671	P	15-Jul	27-Feb, 01-Nov	106.00
Chanchen	2125415	262064	P	15-Jul	27-Feb, 01-Nov	150.31
Xmejia	2128053	250212	P	15-Jul	27-Feb, 01-Nov	4.98
Chunhuhub	2156398	332620		23-Jul		26.28
X-pichil_deep (logging site)	2184785	357307			06-Feb	26.38
Las Panteras_deep (logging site)	2113715	341417			07-Feb	21.90
Nuevo Israel_deep (logging site)	2126121	333379			08-Feb	26.36
Presidente Juarez_deep (logging site)	2134993	331399			08-Feb	27.83

Reforma_deep (logging site)	2076459	335318			11-Feb, 02-Nov	20.82
Chankah_Derrepente_deep (logging site)	2149759	369928			14-Feb	17.43
Señor_deep (logging site)	2194778	380402			14-Feb	19.65
Chunhuhub_deep (logging site)	2159949	332456			15-Feb	28.72
Emiliano_Zapata_deep (logging site)	2124021	341666			15-Feb	21.16
Nuevo_Becar_deep (logging site)	2049273	278016			16-Feb	125.22
La_Lucha_deep (logging site)	2022253	265349			26-Feb	194.43
Surface water bodies						
Laguna La Union	2235654	444141		18-Apr		0.96
Muyil lagoon	2219946	436454		26-Feb, 21-Mar, 18-Apr, 30-Jun, 17-Jul		1.91
SKBR Ruina X-lapak	2219026	441366		21-Mar, 06-Apr, 19-Apr, 30-Jun, 17-Jul		1.84
SKBR Boater stop	2219366	442750		21-Mar, 10-Apr		2.22
SKBR Place C	2217047	446296		21-Mar, 30-Jun, 17-Jul		0.85
SKBR Termite	2218158	445132		21-Mar, 30-Jun, 17-Jul		1.07
Laguna Nopalita	2223456	439192		13-Apr, 18-Apr, 01-Jul		1.38
Laguna Kaan Luum	2229886	442298		12-Apr, 18-Apr, 01-Jul		1.03
Laguna Chichankanab	2198918	314612	P	22-Jul		4.98
Zoh Laguna	2056997	244807	P	11-Jul		257.73
Uaymil_Vertice_7	2097806	402104			21-Feb	0.86
Uaymil_Vertice_9	2076134	422143			21-Feb	2.40
Points outside the study area						
La Union	1981106	300777	P	06-Jul		12.63
Tòmas Garrido	1996078	281219	P	08-Jul		48.04
Tres Garantias	2012759	290296	P	08-Jul		146.37
OjoDeAgua	1986995	263863	P	09-Jul		76.06

Conhuas	2052115	191369	P	09-Jul		152.35
Costitucion	2062674	168168	P	10-Jul		82.35
Hopelchen_Petch_Base	2185555	201617	P	14-Jul		93.58
Pakchèn	2161784	206915	P	14-Jul		147.48
Dzibalchèn_Base	2153764	213062	P	16-Jul		161.82
Chencoh	2150063	205250	P	16-Jul		170.69
Kancabchèn	2136764	223131	P	17-Jul		156.66
Chiunchintok	2142793	228841	P	17-Jul		132.46
Ich-Ek_Base	2184542	189028	P	17-Jul		77.77
RamonCorona_Rancho_Base	2155271	237352	P	17-Jul		137.01
Iturbide	2167100	227166	P	18-Jul		119.51
Campeo Aleman	2192356	143845	P	18-Jul		13.57
Bolonchel Cahuich	2152922	163275	P	18-Jul		29.66
Uayamòn	2176953	141188	P	19-Jul		27.01
Tikinmul_Base	2189048	162233	P	19-Jul		25.40
Nohyaxche	2172106	162406	P	19-Jul		25.15
Crucero Oxa	2184313	177315	P	20-Jul		66.08
Kambul	2210879	302598	P	20-Jul		35.70
Carolina	2169035	284412	P	20-Jul		75.50
Leona Vicario	2320772	478779			06-Apr09	6.73
Cenote 7 bocas	2308483	495449			07-Apr09	5.40
Ranch de la dama y del caballero	2331652	490632			08-Apr09	9.18
Ranch la calandaria	2340314	490705			08-Apr09	9.11
El Delicios	2305327	476760			13-Apr09	12.30
Agua Azul	2306394	466128			13-Apr09	5.77
La granja	2300076	465719			14-Apr09	9.90
Victoria	2299043	470952			14-Apr09	10.58
Valladolid nueva	2316004	466370			14-Apr09	4.74
Chulutan	2274535	399668			15-Apr09	22.43
Felipe Carillo	2266554	409477			15-Apr09	19.76
Xalau	2286396	395166			15-Apr09	22.85
Santa Rosa	2266410	385745			16-Apr09	23.89
Chamul	2253724	388798			16-Apr09	23.92
San Juan	2257791	424286			16-Apr09	8.22
Camp. Hidalgo	2277620	430337			16-Apr09	22.76
Rancho el viejo	2349313	511993			20-Apr09	9.07
Solferino	2362074	455808			21-Apr09	10.44
San Eusebio	2366413	465038			21-Apr09	10.14
San Angel	2348368	454935			22-Apr09	7.82
Rancho san Juan	2346085	464437			22-Apr09	8.34
El Tintal	2310580	451711			23-Apr09	7.37
Nuevo Xcan	2307877	437487			23-Apr09	21.75
Kantanulikin	2325483	448345			23-Apr09	8.30
Esperanza	2319133	458937			23-Apr09	13.70
Aguakan Pozo 1B	2329198	496554			25-Apr09	10.44
Aguakan Pozo 3B	2328700	497195			25-Apr09	9.90
Aguakan Pozo 12	2323209	494420			25-Apr09	9.65
Aguakan Pozo 23a	2319761	488966			25-Apr09	9.24
Aguakan Pozo 23b	2319761	488966			25-Apr09	9.11

Aguakan vallarta	2306924	495710			25-Apr09	5.95
Pabalan	2293272	413680			26-Apr09	21.15
Estrella	2301048	423250			26-Apr09	21.02
Cenote el eden	2342432	483312			28-Apr09	5.12

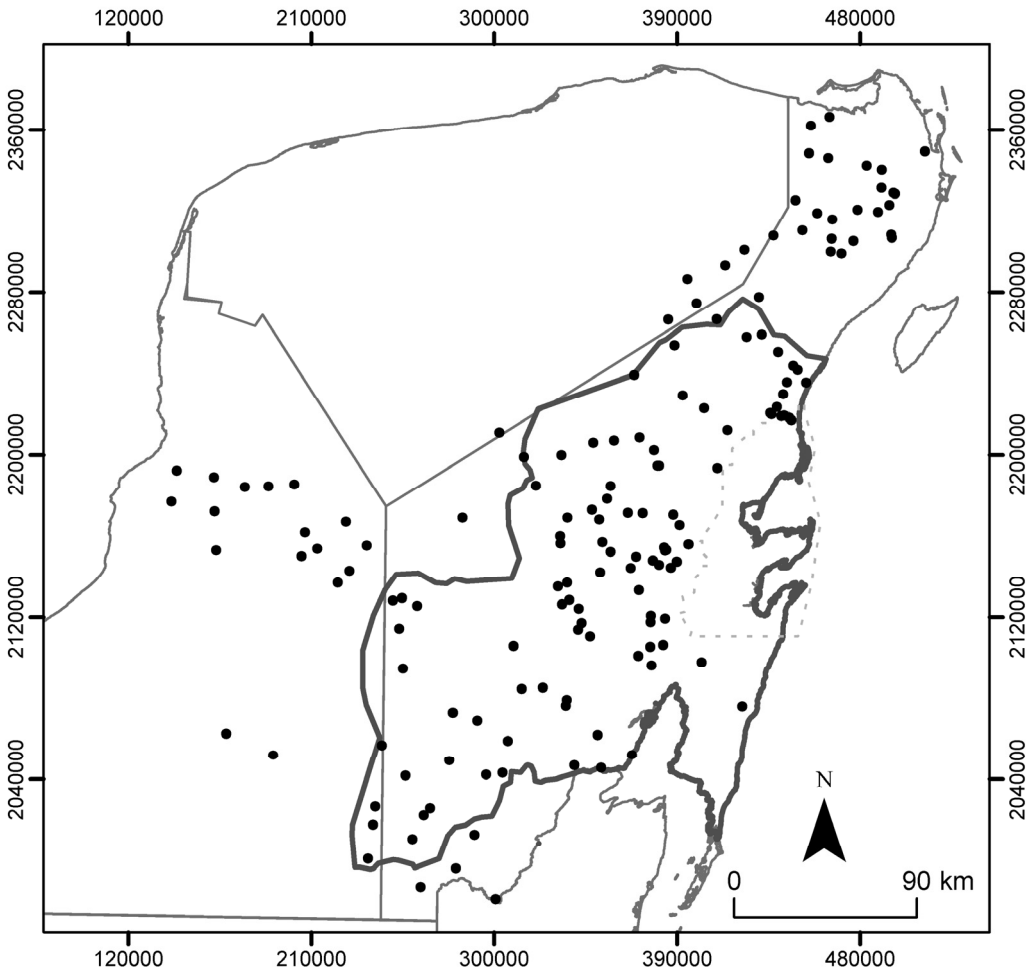

Fig. A6.1. Water level measurement points.

A6.2 GPS benchmarks

Elevations of GPS benchmarks at open spaces nearby the water level measurement sites. Benchmarks were also marked with paint in the field.

GPS measurements corresponding to the perched water level measurements from July 2007 were carried out by Chiara Fratini. GPS measurements corresponding to the sites north of the study area from April 2009 were carried out by Guillaume Charvet.

Location	Northing	Easting	Elevation of reference point at GPS benchmark (mamsl)
ASK Carillo	2165530.29	390614.04	18.10
Mariposa Tulum	2234528.53	450885.37	13.62
Bacalar	2066338.77	353465.20	16.26
Macario Gomez	2250444.93	439830.85	15.60
Chankah Veracruz	2155881.31	395648.41	5.63
Uhmay	2147267.76	389907.27	6.12
Xpichil	2178333.25	355594.37	22.41
Chunhuas	2171164.15	373073.24	15.15
San Andres	2145720.73	381162.60	6.41
Muyil	2220482.08	435844.86	5.37
Polyuc	2168998.47	336024.84	14.68
Nuevo Israel	2128291.53	336771.99	21.29
Las Panteras	2117135.32	342986.19	20.35
Los Divorciados	2110174.40	347023.06	33.05
Nuevo San Antonio	2170437.07	388121.87	8.73
Señor	2194780.54	381113.85	19.34
Tuzik	2202505.07	378621.66	19.78
San Jose Segundo	2208598.48	371608.71	21.59
Andres Quinta Roo	2117077.76	383997.46	11.52
Noh-Bec	2117476.24	376964.63	4.68
Polinkin	2120566.75	377073.88	9.75
Petcacab	2133133.23	371400.53	21.33
X-hacil	2144306.96	387020.57	6.67
Noh-Cah	2147856.05	378171.51	7.12
Mixtequilla	2144084.87	367154.46	16.22
Santa Maria Poniente	2142063.22	352205.85	10.16
Limones	2106314.48	383197.73	6.89
Chacchoben	2105304.48	376731.14	13.45
Rancho La Herradurra	2100902.04	370952.32	7.59
Pedro A. Santos	2096160.16	377380.88	9.49
Tepich	2239242.09	368945.63	23.24

Francisco I. Madero	2229167.16	392719.34	15.17
Chumpon	2212246.30	414667.54	7.88
Chunya	2222912.10	403573.57	15.09
San Luis	2172964.62	348141.79	23.99
Presidente Juarez	2136595.03	335842.68	25.32
Betania	2171390.35	365810.84	15.36
Tres Reyes	2193552.54	409797.62	7.38
Felipe Carrillo Puerto	2165592.82	391296.77	10.04
San Francisco Ake	2207264.17	358959.28	21.87
Dzoyola	2206336.47	348832.46	18.04
Javier Rojo Gomez	2199827.73	333162.24	24.94
Santa Isabel	2153126.65	384701.91	10.24
Laguna Ocom	2152767.76	384101.77	4.05
Chunkakah	2154335.99	383715.72	9.63
Reforma	2079186.16	335775.30	27.80
Altos de Sevilla	2085087.41	323979.22	69.18
Morocoy	2059103.01	306805.26	68.24
Rio Escondido	2084666.29	313658.13	58.83
Otillo Montaño	2105809.66	309560.73	49.36
Dzulá	2168249.80	351524.17	20.53
Laguna Kaná	2156931.26	353333.49	21.59
Yoactun	2152343.10	357358.85	22.00
Tulum federal plot	2235499.04	453583.19	2.57
Manuel Antonio May	2259023.39	431717.53	20.07
Centro Nocturno	2243802.33	447261.59	7.29
Cenote Azul	2062235.67	350866.27	16.08
Santa Elena	2045548.47	352714.16	1.66
Calderitas	2052211.91	367836.72	7.14
Ucum Qroo	2046782.50	339593.64	23.84
El Cedral	2069073.85	291758.09	88.98
Francisco Villa	2042999.44	304163.03	84.59
Nicholas Bravo	2042065.54	296126.16	105.19
Felipe Anjeles	2010501.92	259888.19	209.17
La Lucha	2025627.67	268553.63	179.86
Veinte de Noviembre	2041728.64	256347.09	200.39
Richardo Payro	2026620.46	241514.81	261.92
El Once	2000875.76	237965.56	266.27
Narciso Mendoza pozo	2017582.93	240426.60	241.89
Bel Ha	2094685.80	255190.06	138.05
José Maria Morelos	2184891.30	320642.61	23.35
Nuevo Becar chico	2072982.79	279730.84	96.73
Xkan-Ha	2114277.59	253373.51	129.42
Ucum Campeche	2129306.88	254665.22	105.29
Chanchen	2125429.25	262056.85	152.59
Xmejia	2127963.46	250245.68	3.86
Chunhuhub	2169034.74	284412.31	26.32
Surface water bodies			
Laguna Chichankanab	2198902.82	314565.40	3.86
Zoh Laguna	2056997.13	244806.72	259.80

Points outside the study area			
La Union	1981105.86	300777.24	10.66
Tòmas Garrido	1996078.41	281219.07	45.44
Tres Garantias	2012758.95	290295.88	149.58
OjoDeAgua	1986994.67	263863.31	74.05
Conhuas	2052115.49	191369.12	152.26
Costitucion	2062674.06	168167.78	82.26
Hopelchen_Petch_Base	2185554.92	201617.30	96.23
Pakchèn	2161783.50	206914.97	146.84
Dzibalchèn_Base	2153763.90	213062.10	164.54
Chencoh	2150063.23	205250.40	170.05
Kancabchèn	2136764.21	223131.29	156.56
Chiunchintok	2142792.52	228840.88	133.74
Ich-Ek_Base	2184542.14	189027.59	80.43
RamonCorona_Rancho_Base	2155270.62	237351.87	136.91
Iturbide	2167099.69	227165.63	119.51
Campeo Aleman	2192356.27	143844.98	12.67
Bolonchel Cahuich	2152921.74	163274.91	29.66
Uayamòn	2176952.92	141188.39	26.05
Tikinmul_Base	2189048.41	162233.43	27.61
Nohyaxche	2172106.29	162406.47	25.57
Crucero Oxa	2184313.38	177314.61	65.56
Kambul	2210878.54	302598.11	33.66
Carolina	2169034.74	284412.31	75.50
Leona Vicario	2320772.24	478779.44	5.79
Cenote 7 bocas	2308483.14	495448.97	5.76
Ranch de la dama y del caballero	2331652.04	490631.67	8.57
Ranch la calandaria	2340314.42	490705.30	8.37
El Delicios	2305327.35	476759.76	12.63
Agua Azul	2306393.87	466128.45	7.49
La granja	2300076.25	465719.37	11.68
Victoria	2299043.26	470952.39	10.57
Valladolid nueva	2316004.20	466369.79	3.71
Chulutan	2274534.55	399667.96	21.52
Felipe Carillo	2266553.74	409477.04	18.82
Xalau	2286395.77	395166.00	22.09
Santa Rosa	2266410.09	385745.18	22.05
Chamul	2253724.10	388798.15	21.92
San Juan	2257791.35	424285.84	7.45
Camp. Hidalgo	2277620.23	430336.55	22.03
Rancho el viejo	2349312.85	511993.06	8.31
Solferino	2362073.88	455808.07	9.94
San Eusebio	2366412.60	465038.05	8.39
San Angel	2348367.64	454934.93	7.46
Rancho san Juan	2346084.72	464437.28	7.82
El Tintal	2310579.98	451710.84	7.77
Nuevo Xcan	2307877.00	437487.26	21.08

Kantanulikin	2325483.28	448344.63	7.28
Esperanza	2319133.44	458936.52	13.82
Aguakan Pozo 1B	2329198.31	496553.87	9.92
Aguakan Pozo 3B	2328699.75	497194.65	9.48
Aguakan Pozo 12	2323208.91	494419.99	9.24
Aguakan Pozo 23a	2319760.71	488965.79	8.55
Aguakan Pozo 23b	2319760.71	488965.79	8.55
Aguakan vallarta	2306924.30	495709.69	5.61
Pabalan	2293271.54	413680.46	20.08
Estrella	2301048.40	423250.28	20.45
Cenote el eden	2342431.99	483311.56	6.64

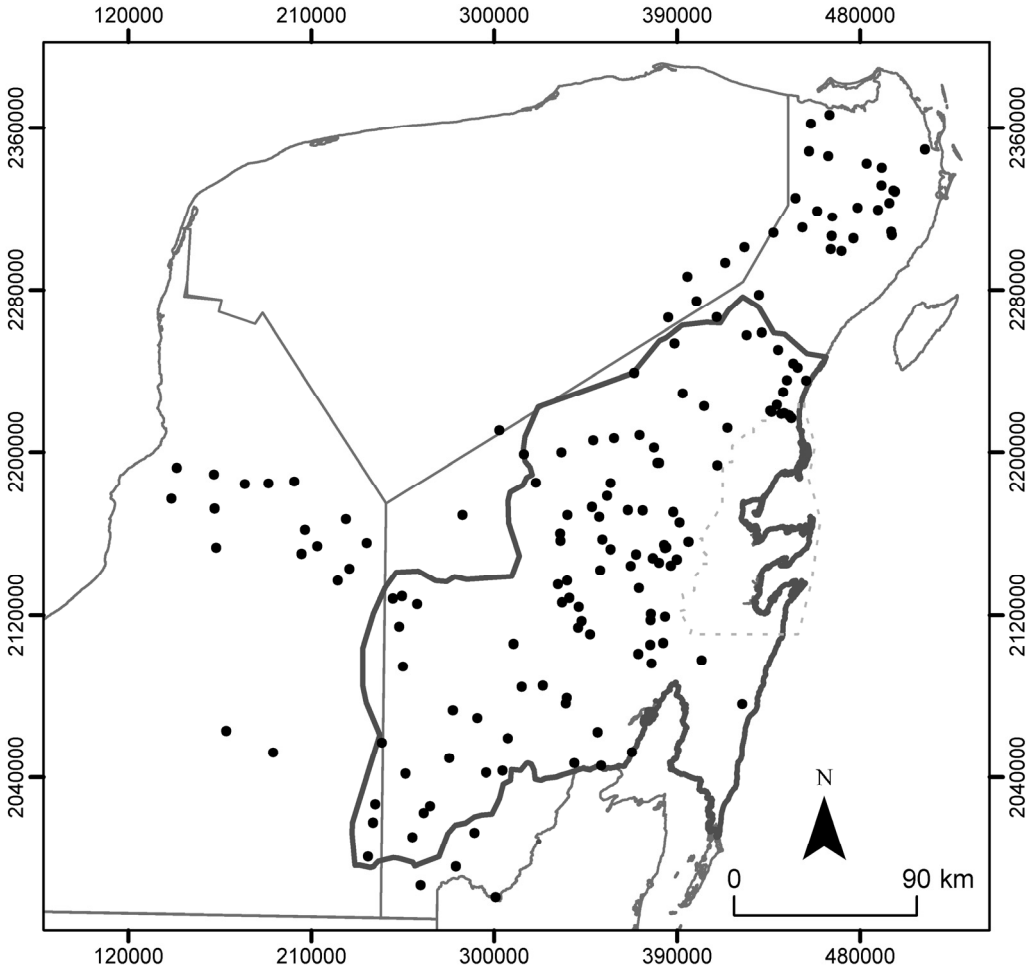

Fig. A6.2. GPS benchmarks.

A6.3 Water sampling sites

These data are also included as Electronic Supplement to Gondwe et al. (IV). The analysis run were: Ca^{2+}, Mg^{2+}, Sr^{2+}, K^{+}, Na^{+}, Ba^{2+}, SO_4^{2-}, Cl^{-}, NO_3^{-}, Br^{-}, HCO_3^{-}, $\delta^{18}O$.

Oxygen isotope analyses of water samples were kindly performed at Centre for Ice and Climate, Niels Bohr Institute, University of Copenhagen, Denmark. Sulfate and alkalinity analyses were kindly performed at CICY–CEA, Cancun, Mexico.

Location	Northing	Easting	Collect date
Groundwater			
Andres Quintana Roo	2119078	384045	24-Feb-08
Betania	2171991	364995	19-Feb-08
Caobas	2040402	278072	25-Feb-08
Dzula	2168188	351530	19-Feb-08
El Cedral	2069065	291628	23-Feb-08
Francisco Villa	2043887	305022	23-Feb-08
Las Panteras	2116954	343030	20-Feb-08
Limones	2103575	383133	20-Feb-08
Los Divorciados	2109676	346734	07-Feb-08
Mixtequilla	2144153	367118	18-Feb-08
Morocoy	2057464	308879	23-Feb-08
Naranjal Poniente	2141533	346663	18-Feb-08
Nicholas Bravo	2042505	296143	25-Feb-08
Noh Cah	2147855	378229	24-Feb-08
Nuevo Israel	2128250	337357	20-Feb-08
Otillo Montaño	2102587	307561	22-Feb-08
Pedro A. Santos	2096556	377217	20-Feb-08
Petcacab	2133494	371269	21-Feb-08
Polinkin	2120565	376854	21-Feb-08
Presidente Juarez	2137762	335917	20-Feb-08
Rancho Las Herraduras	2100867	370950	20-Feb-08
Reforma	2080887	334274	23-Feb-08
Rio Escondido	2088921	315400	22-Feb-08
San Luis	2172936	348052	19-Feb-08
Señor	2194275	380703	22-Feb-08
Ucum Q.Roo	2046238	339617	23-Feb-08
Xhacil	2144613	386587	18-Feb-08
Xkan-Ha	2114278	253374	27-Feb-08
Surface water			
Cenote Azul	2062367	350932	23-Feb-08
Narciso Mendoza	2017596	240428	26-Feb-08
Veinte de Noviembre	2041661	256369	26-Feb-08

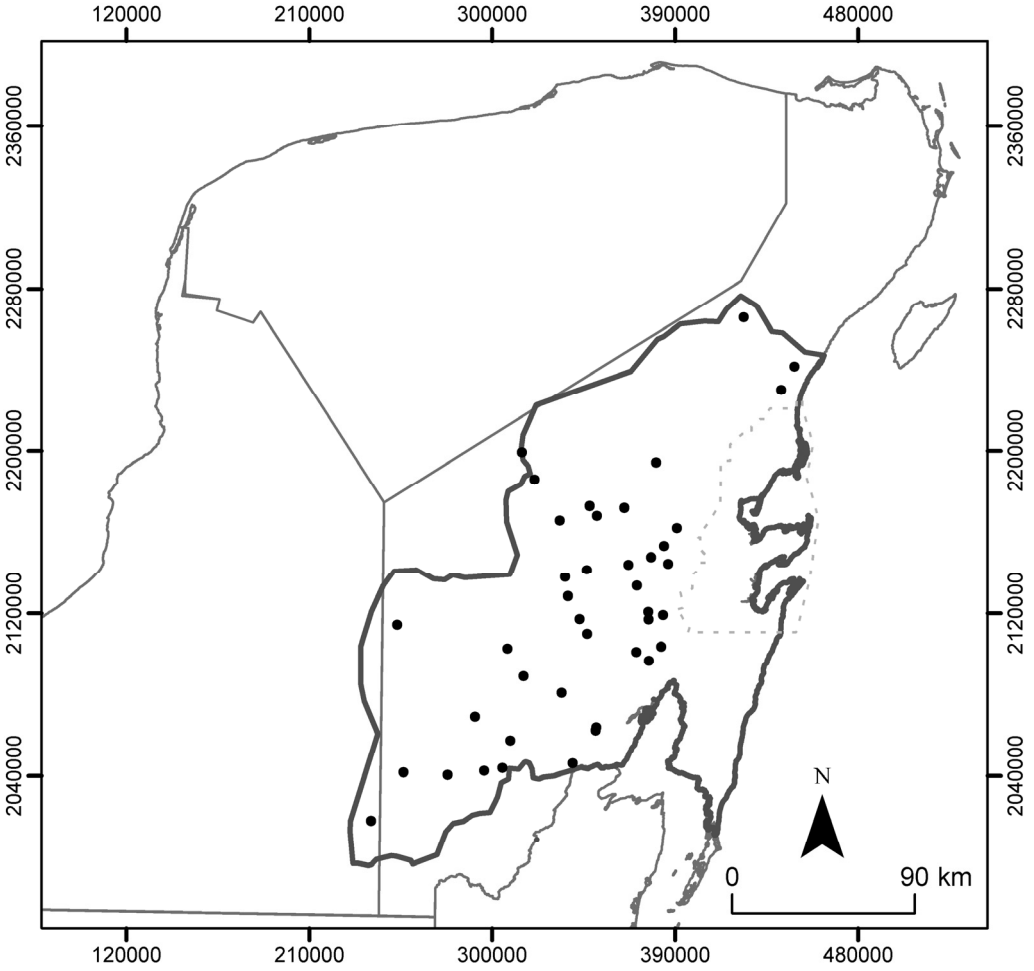

Fig. A6.3. Water sampling points.

A6.4 Time-domain EM measurements

Location	Northing	Easting	Collect date
Petcacab	2132856.48	371323.51	08-Mar-2007
Santa Maria Poniente	2142259.43	351003.55	09- Mar -2007
Chunhuas	2172005.95	373419.25	26- Mar -2007
Chunhuas	2172005.95	373419.25	28- Mar -2007
Uhmay	2146428.42	388542.65	29- Mar -2007
Andres Quintana Roo	2121908.04	383980.10	29-Mar-2007
Chumpon	2207223.85	420322.62	08-Apr-2007
Chumpon	2236617.00	454335.00	12- Apr -2007
Chumpon	2236231.20	454917.96	12- Apr -2007
Tulum airstrip	2237164.34	453513.25	12- Apr -2007
Muyil	2220496.25	435833.23	12- Apr -2007
Muyil	2220496.25	435833.23	15- Apr -2007
Macario Gomez	2250764.49	440307.24	15- Apr -2007
Centro Nocturno	2244101.04	447313.07	15- Apr -2007
Eden	2265885.56	473155.97	16- Apr -2007
Betania	2171406.39	365761.92	16- Apr -2007
Presidente Juarez	2136561.24	335946.37	16- Apr -2007
Manuel Antonio May	2258816.79	431917.09	17- Apr -2007
Tulum airstrip	2237164.34	453513.25	17- Apr -2007
Noh Cah	2147643.34	377737.96	19- Apr -2007
Mixtequilla	2143942.32	366940.15	19- Apr -2007
San Luis	2173347.12	348661.02	20- Apr -2007
Felipe Carrillo Puerto	2165534.72	386582.38	20- Apr -2007
Vigia Chico1	2173440.75	405328.02	22- Apr -2007
Vigia Chico2	2174981.54	407487.24	22- Apr -2007

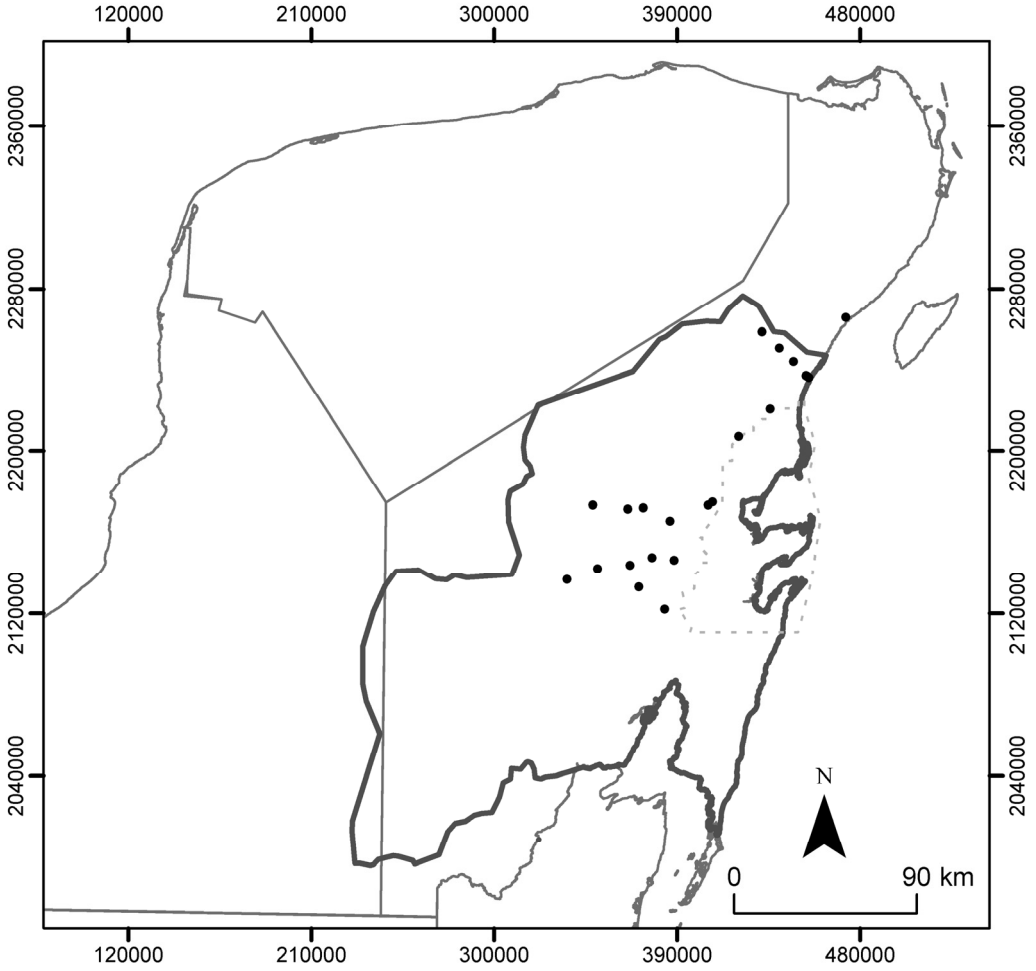

Fig. A6.4. Time-domain EM measurements.

A6.5 Borehole logging measurements

The following log types were carried out where possible: fluid temperature and fluid conductivity (F), natural gamma radiation (G), induction (I).

Location	Northing	Easting	Collect date	Type
Akumal 1	2261621	459155	31-Jan-08	F, G, I
Rancho Viejo	2244372	446092	31-Jan-08	F, G
Costa Maya km 30	2089897	409824	01-Feb-08	F, G, I
Costa Maya km 42	2081340	417453	01-Feb-08	F, I
X-pichil	2184785	357307	06-Feb-08	F, G, I
Felipe Carrillo Puerto	2165775	388591	07-Feb-08	F, G
Las Panteras	2113715	341417	07-Feb-08	F, G, I
Nuevo Israel	2126121	333379	08-Feb-08	F, G, I
Presidente Juarez	2134993	331399	08-Feb-08	F, G
Reforma	2076459	335318	11-Feb-08	F, G, I
Rio Escondido	2084621	313614	11-Feb-08	F, G, I
Morocoy	2059112	306809	12-Feb-08	F, G, I
Caobas	2041044	277498	12-Feb-08	G, I
Chankah Derepente	2144759	369928	14-Feb-08	F, G, I
Señor	2194778	380402	14-Feb-08	F, G, I
Chunhuhub	2159949	332456	15-Feb-08	F, G, I
Emiliano Zapata	2124021	341666	15-Feb-08	F, G, I
Nuevo Becar	2049273	278016	16-Feb-08	F, G, I

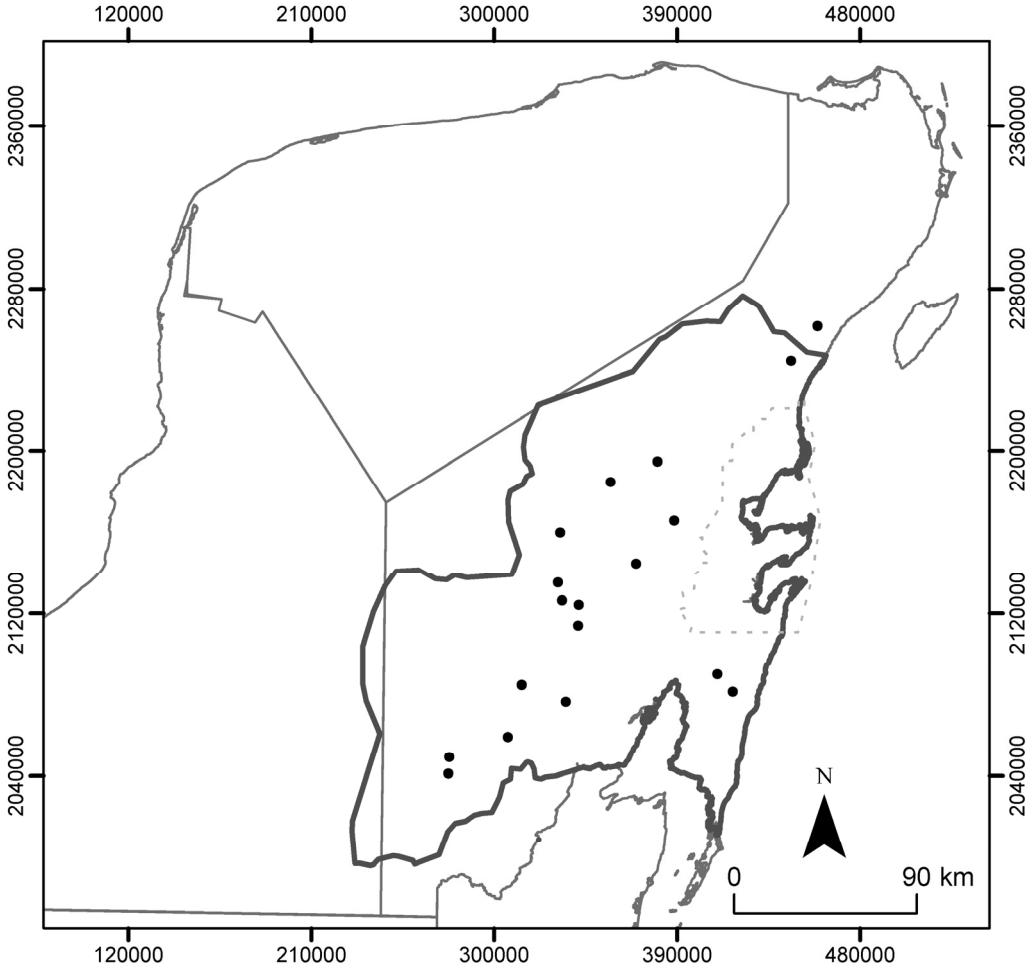

Fig. A6.5. Borehole logging measurements.

A6.6 Airborne EM transects

The locations of the airborne EM measurements are indicated on Fig. A6.6. The end points of the transects are given in the below table. The Holbox zone was flown with dense flight lines; 100 and 200 m line spacing. Across the inland structures, 5–6 parallel flight lines were flown, yielding transects ~1000 to 1500 m wide.

Location	Northing	Easting	Comment
Holbox zone	2243641	445969	Corner point 1 of area
	2239163	457019	Corner point 2 of area
	2235006	442700	Corner point 3 of area
	2231133	453395	Corner point 4 of area
Transect A	2137564	319720	
	2116502	340470	
Transect B	2101159	334463	
	2086877	353699	
Transect C	2148103	364053	
	2140434	373304	
Transect D	2093644	310300	
	2084971	319087	
Transect E	2076581	322658	
	2067454	330991	

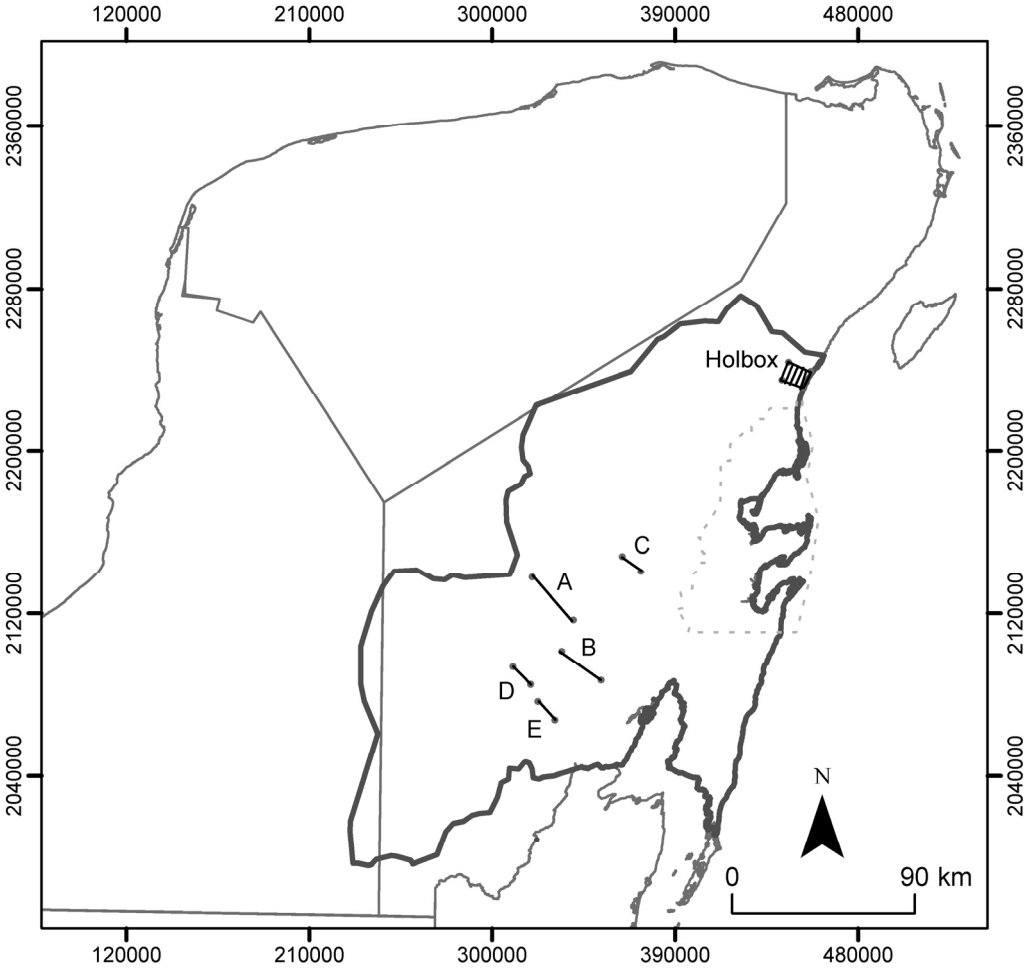

Fig. A6.6. Airborne EM measurements.

A6.7 Inventory of electronic data material

Inventory of electronic data material, available on DVD from the contact persons given in the beginning of this chapter. Folder names underlined and subfolders formatted with hanging indents. Brief descriptions also given. Airborne EM data is not given here; special permission to use these data must be obtained from Amigos de Sian Ka'an and Geological Survey of Austria.

FIELD_DATA

WaterLevels

Water level data, distributed in sub-folders according to the person who collected the data (Bibi, Chiara, Guillaume, ASK).

GPSData

GPS data, distributed in sub-folders according to the person who collected the data (Bibi, Chiara, Guillaume).

WaterSamples

Raw data in various files, including quality control data and methods used. Also all data collected in one spreadsheet given, as also presented in electronic supplement for Gondwe et al. IV.

TDEM

Raw TDEM data files and Excel-sheet with the processed data.

Logging

Raw logging data files as well as Excel-sheet and Word-document describing with the processed data

REMOTE_SENSING_DATA

Bibi_ET

TRMM monthly rainfall data covering the whole peninsula, 1999-2008, raw and adjusted according to the climate station data from CONAGUA. Excel sheet with the calculation of adjustment data also given.

All data used for producing the ET_a daily estimates for 2004-2008. I.e. ET_a calculated with the "triangle method" for cloud free pixels covering the whole peninsula, K_c, ET_{ref} (via Hargreaves, in folder PET), scripts for processing the data in ENVI-IDL. Method described in Gondwe et al. IV, Lerer (2008) and Stisen et al. (2008).

Structures

Shapefiles of structures outlined via visual inspection of satellite imagery. Used in the hydrological models.

Shapefiles of faults suggested in Gondwe et al. (I).

Landsat TriDecadal

Landsat TriDecadal imagery, used to outline the structures. See reference in Gondwe et al. IV for data source.

Landsat ETM+

Landsat imagery, used to outline the structures. See reference in Gondwe et al. IV for data source.

Interferograms

Georeferenced interferograms, subsets covering Sian Ka'an

Flooding_maps

Georeferenced_floodmaps

Landsat for flood verification The data used to compare classifications with. See Gondwe et al. (I) for data source.

An Excel-sheet with the no. of pixels in each flooding category is also given in this folder.

HYDROLOGICAL MODELLING

InputFiles

Input files used in hydrological models.

SteadyState_7ConceptModels

MIKE SHE files and result files for the 7 steady state models run. The results folders also include Excel-sheets comparing modelled and measured groundwater heads.

Examples also given of files used in particle tracking in separate particle tracking folder.

Transient_2ConceptModels

MIKE SHE files and result files for the 2 transient models run. Modelled interferograms and script for converting output to interferogram also given.

MonteCarloStackedResults

The stacked outputs of the MonteCarlo simulations.

ExampleMonteCarloScripts

Example of scripts used to generate the Monte Carlo simulations.

ExampleAutocalibrationScripts

Example of script used to autocalibrate the models using Matlab's nlinfit.

The Department of Environmental Engineering (DTU Environment) conducts science-based engineering research within four themes:
Water Resource Engineering, Urban Water Engineering,
Residual Resource Engineering and Environmental Chemistry & Microbiology.
Each theme hosts two to five research groups.

The department dates back to 1865, when Ludvig August Colding, the founder of the department, gave the first lecture on sanitary engineering as response to the cholera epidemics in Copenhagen in the late 1800s.

DTU Environment
Department of Environmental Engineering
Technical University of Denmark

Miljoevej, building 113
DK-2800 Kgs. Lyngby
Denmark

Phone: +45 4525 1600
Fax: +45 4593 2850
e-mail: reception@env.dtu.dk
www.env.dtu.dk

ISBN 978-87-91855-86-3